FACULDADE DE ENGENHARIA DA UNIVERSIDADE DO PORTO

4D Printing in the Development of a Composite Refugee Shelter

Carlos Manuel Martín Fernandes

Master's Degree Thesis in Mechanical Engineering

Supervisor: António Torres Marques

Second Supervisor: Púria Esfandiari

June 30, 2023

4D Printing in the Development of a Composite Refugee Shelter

Carlos Manuel Martín Fernandes

Master's Degree Thesis in Mechanical Engineering

June 30, 2023

Resumo

Desastres naturais e guerras continuam a aumentar o número de pessoas deslocadas a nível global. Isto, por sua vez, leva a uma necessidade crescente de soluções de abrigo de curto a médio prazo. A presente dissertação tem como objetivo contribuir para o desenvolvimento semi-produtos para um abrigo leve, estruturalmente estável e de autoassemblagem usando materiais compósitos de polímeros de memória de forma (SMPC) e tecnologia de impressão 4D, com base em vários trabalhos elaborados na Faculdade de Engenharia da Universidade do Porto. O foco desta pesquisa está em melhorar aspetos estruturais das soluções préviamente desenvolvidas, através do uso de filamentos compósitos de matriz polimérica com memória de forma. Para tal, é desenvolvido um sistema de extrusão de filamentos de matriz polimérica de Ácido Polilático (PLA) reforçados com fibra de carbono.

Para ter uma melhor compreensão do polímero usado no estudo, foram realizados testes de caracterização térmica. O teste de índice de fluidez em fusão (MFI) forneceu informações sobre a fluidez do PLA, enquanto a análise termogravimétrica (TGA) avaliou sua degradação térmica. Os resultados permitiram aprimorar a compreensão geral do comportamento e propriedades do mesmo. Um estudo numérico preliminar foi efetuado de modo a investigar o impacto de fenómenos como a queda de pressão e "die-swelling" no extrusor. A simulação, conduzida no software Ansys, forneceu distribuições de pressão, velocidade e taxa de deformação, que permitiram o cálculo analítico dos valores da queda de pressão e diâmetro máximo esperado à saída da fieira. Os resultados demonstraram uma baixa infuência por parte dos fenómenos em questão no processo de extrusão.

A instalação inicial de extrusão consistiu num cilindro liquefator onde as fibras de carbono se impregnavam com o PLA depositado, sendo depois extrudidas através de uma fieira cilíndrica. Contudo, esta configuração originou filamentos com geometria de secção transversal e diâmetro inconsistentes. De modo a aumentar a qualidade e consistência geométrica dos filamentos, um sistema de arrefecimento com água e um sistema motorizado responsável por puxar o filamento foram implementados na instalação.

As mudanças implementadas resultaram em melhorias significativas na qualidade dos filamentos. Análise por meio de imagens ampliadas com lupa confirmaram uma distribuição aprimorada das fibras e uma geometria de secção transversal melhorada. No contexto da impressão 3D, testes iniciais revelaram problemas ao nível da extrusão. De modo a superar as limitações, a produção foi retomada com um diâmetro de fieira intermédio aos dois valores previamente testados, permitindo o encaixe adequado nos elementos guiamento da impressora 3D. A substituição da fieira extrusora do equipamento de Fabrico Filamento Fundido (FFF) por uma de maior diâmetro potenciou a obtenção de material à saída do mesmo. Após um estudo térmico a temperatura de impressão adequada para o PLA em questão roundou os 190ºC, levando a filamentos de maior consistência geométrica. A impressão de provetes para ensaios mecânicos, por meio de equipamentos especializados, foi recomendada de modo a avaliar a performance dos filamentos compósitos e continuar a optimização da produção e processamento dos mesmos.

Abstract

Natural disasters and wars continue to increase the number of displaced people on a global level. This, in turn, leads to a growing need for short to medium term shelter solutions. The present dissertation aims to contribute to the development of semi-products for a lightweight, structurally stable and self-deploying shelter using shape memory polymer composites (SMPC) and 4D printing technology, building upon several works elaborated in the Faculty of Engineering of University of Porto (FEUP). The key objective is to improve the structural properties of the shelter solution by using SMPC filaments for 4D printing. To achieve this, a system capable of extruding reinforced composite filaments was developed and tested.

To better understand the polymer used in the study, thermal tests were conducted. The melt flow index (MFI) test provided insights into the utilized polymer's flowability, while the thermogravimetric analysis (TGA) test evaluated its thermal degradation. The results align with existing literature on Polylactic Acid (PLA) materials, enhancing the overall understanding of the material's behavior and properties.

A preliminary numerical simulation was performed before conducting experimental work to investigate the impact of die-swelling and pressure drop phenomena in the extruder machine. The simulation yielded results for shear rate, pressure, and velocity fields, allowing for the analysis of pressure drop and die-swell in the extruder die. The findings indicated that these phenomena had minimal influence on the extrusion process, and the values obtained were in line with existing literature.

The initial extrusion installation consisted of a cylindrical liquefier barrel where the carbon fibers impregnated with the deposited PLA. The mixture would then be extruded through a die, with the desired cross section. However, this setup faced challenges such as inconsistent cross-sectional geometry and filament diameter. In response to these issues, a water cooling system was incorporated to facilitate rapid filament consolidation at the extruder exit, ensuring the desired circular cross-sectional geometry within the die. Additionally, a motorized filament pulling system was also integrated to achieve a more consistent filament diameter and explore different pulling speeds for fine-tuning filament properties.

The implemented changes resulted in significant improvements in the quality of the filament samples compared to the original setup. These improvements were validated through magnifying glass imaging, which confirmed enhanced fiber distribution and cross-sectional geometry. In the context of 3D printing, initial tests revealed extrusion problems with the previously produced filaments. Consequently, production resumed with an intermediate die diameter that allowed proper fitting in the 3D printing device's guiding elements. Replacing the extrusion die of the Fused Deposition Modeling equipment with a larger diameter facilitated material output from the printer. After conducting a thermal study, the PLA's appropriate printing temperature was determined to be 190°C, granting improved geometric consistency to the printed material. Printing test specimens for mechanical testing using specialized equipment was recommended to evaluate the performance of the composite filaments and further optimize the filament production and processing methods.

Agradecimentos

Primeiramente, gostaria de agradecer ao Professor António Torres Marques, não só por toda a disponibilidade em partilhar o seu conhecimento comigo mas também pelo próximo acompanhamento do desenvolvimento desta mesma dissertação.

De seguida, gostaria também de expressar a minha gratidão ao engenheiro Púria Esfandiari e a toda a equipa do Laboratório de Materiais Compósitos do ISEP, em especial ao Prof. João Francisco Silva, à Rita Carreiras e ao Manuel Soares. Sem o seu conhecimento, disponibilade e boa disposição o avanço experimental do projeto não teria sido possível.

O desenvolvimento da componente numérica da dissertação foi concretizável devido ao conhecimento partilhado e disponibilidade do Professor Alexandre Afonso e do Tomás Schuller e, como tal, os meus agradecimentos e votos de sucesso futuro para ambos.

Queria também agradecer à Ana Gomes da ARCP do UPTEC, à D. Emilia do laboratório materialográfico da FEUP e à Ana Pais do LDPS por terem disponibilizado os seus equipamentos e conhecimento no decorrer dos testes experimentais da dissertação.

À FEUP e a todos os docentes e colegas envolvidos na minha formação académica, um agradecimento por terem feito parte deste percurso memorável.

Aos meus pais, um enorme obrigado por me terem criado e me terem dado a melhor companhia e exemplo possível na forma da minha irmã. Estarei eternamente grato por tudo o que fizeram e continuam a fazer por mim.

Por último, mas não menos importante, um grande agradecimento a todos os meus grandes amigos e amigas, que tornaram dias aparentemente cinzentos em memórias que levarei para o resto da minha vida.

Carlos Manuel Martín Fernandes

"We can easily forgive a child who is afraid of the dark; the real tragedy of life is when men are afraid of the light"

Plato

Contents

List of Figures

List of Tables

Abbreviation List

AM	Additive Manufacturing
ARCP	Associação Rede de Competência em Polímeros
CAD	Computer Aided Design
DMA	Dynamic Mechanical Analysis
ETFE	Ethylene Tetrafluoroethylene
HDPE	High Density PolyEthylene
IDP	Internaly Displaced People
IOM	International Organization for Migration
IRFC	International Federation of Red Cross and Red Crescent societies
ISEP	Instituto Superior de Engenharia do Porto
FDM	Fused Deposition Modeling
FFF	Fused Filament Fabrication
GF	Glass Fiber
HDT	Heat Deflection temperature
LDPE	Low Density PolyEthylene
LDPS	Laboratório de Desenvolvimento de Produtos e Serviços
MFI	Melt FLow Index
NIF	Near InfraRed
NGO	Non-Governmental Organization
PLA	Polylactic Acid
SLA	StereoLithography
SLS	Selective Laser Sintering
SMM	Shape Memory Material
SMA	Shape Memory Alloy
SME	Shape Memory Effect
SMH	Shape Memory Hybrid
SMP	Shape Memory Polymer
SMPC	Shape Memory Polymer Composite
STL	Standard Triangle Language
TGA	Thermogravimetric Analysis
TPU	Thermoplastic Polyurethane
UNHCR	United Nations High Commissioner for Refugees
UMAT	User MATerial
UPTEC	Parque de Ciência e Tecnologia da Universidade do Porto
UV	Ultraviolet

Symbol List

E	Young's modulus - Pa
f'_c	Compressive strength - Pa
R_f	Shape Fixity Ratio - %
R_r	Shape Recovery Ratio - %
T_t	Transition temperature - ºC
σ	Tensile strength - Pa
σ_y	Yield strength - Pa
ν	Poisson's ratio
S	von Mises stress - Pa
τ	Shear stress - Pa
$\dot{\gamma}$	Shear rate - $\frac{1}{s}$
ϕ	Material fluidity constant
m	Material flow exponent
ΔP_{x_υ}	Pressure drop at section x- Pa
ΔP_υ	Total pressure drop - Pa
υ	Extrudate entry velocity - m/s
β	Extruder-tip diameter transition angle - º
D_x	Section x diameter - m
L_x	Section x length - m
D	Maximum die-swell induced diameter - m
D_c	Extruder tip diameter - m
N_1	First normal stress difference - Pa
n	Local flow curve slope
M_w	Mean weight of the extruded MFI samples

Chapter 1

Introduction

1.1 Context and Objectives

With the recent increase in armed conflict around the world and the recurrence of natural disasters, the number of forcibly displaced people worldwide is showing rapid growth. Over the last decade, conflict and violence have catapulted the number of Internally Displaced People (IDP) to about 58 million and the number of refugees to 26 million [48]. This number approximately reaches the 100 million mark if the data for asylum seekers and stateless people is taken into account, as seen in Figure 1.1. As high as this number may seem, the reality is that this might be a low estimate in relation to the real numbers, as the data for the most recent conflict in Ukraine and earthquake in Turkey/Syria is still not available.

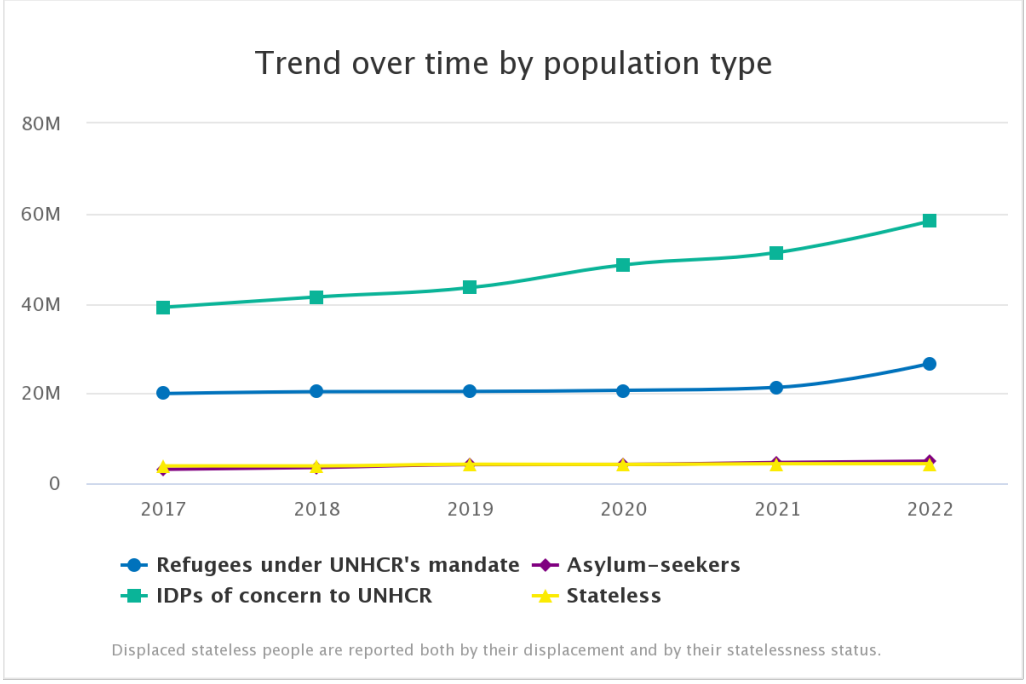

Figure 1.1: Forcibly Displaced People over recent years [1]

As the presented data indicates, the need for a first response shelter solution with fast and easy assembly characteristics is more evident than ever.

Emergency shelters are essential facilities designed to provide temporary housing and support for people who have been displaced from their homes due to the aforementioned crises. These shelters offer a safe and secure environment where individuals and families can seek refuge, receive medical care, and access food, water, and other basic necessities.

The theme of the present thesis stands as a continuation of a plethora of previous dissertations with the same goal: the development of an easily transportable and fast assembling shelter solution for crisis situations. While its predecessors managed very interesting and notable developments, namely in the shelter design and deployability, some issues were still left unanswered.

This work aims to build upon the groundwork laid out by the previous FEUP students, hoping to improve some of its structural shortcomings with the use of Shape Memory Polymer Composites (SMPCs), in order to reach a shelter construction capable of providing a temporary home for the displaced people.

1.2 Dissertation Structure

The contents of this dissertation are divided in 5 chapters:

Chapter 1 introduces the theme, contextualizing the subject of the dissertation and setting its objectives. It also establishes the thesis' structure and reports the advancements achieved in the previous works developed at FEUP.

Chapter 2 exhibits the state of the art of several areas of interest regarding the theme of the dissertation. Firsly, emergency shelters are reviewed in **section 2.1**, referencing the main Non-Governmental Organizations (NGOs) involved in supplying them, as well as mentioning the restrictions they impose on the development of such structures. **Section 2.2** overviews the most relevant Additive Manufacturing techniques currently used. Naturally, this also entails a brief summary of prominent terms like Shape Memory Materials (SMMs) and their nuances, shedding a brighter light on SMPCs. This chapter also addresses several noteworthy research works in the field of self-deployable structures, drawing inspiration for the upcoming design process of the shelter. A brief summary of the applications of fiber reinforced filaments in 3D printing is also made, along with a theoretical introduction to relevant aspects related to the flow characterization of melt material within the extruder setup.

Chapter 3 describes the experimental component of the dissertation. The chapter proposes the development of an innovative extrusion installation with the goal of producing composite filaments capable of being utilized in current 3D printing technology. The performed tests are explained in detail and the results are presented and briefly discussed.

Chapter 4 further elaborates on the obtained results and discusses their validity and physical meaning. It also briefly summarizes the progress made with the present research work.

Chapter 5 draws some final remarks while also prospecting future works.

1.3 Previous Works

The present section has the goal of highlighting the main takeaways from previous dissertations developed at FEUP about the creation of an emergency shelter. The collection of previous related works amounts to a total of 4 theses, which will be presented in chronological order.

1.3.1 "4D Structures for Rapid Construction of a Shelter in Crisis Situations"

Being the first installation of various soon to follow works regarding the development of a shelter for crisis situations, this dissertation proposed the creation of a structure that managed to deploy autonomously under the presence of temperature stimulus, taking full advantage of the 4D printing technology. [2]

This self-deployment could be achieved through the use of 3D printed smart materials such as the Shape Memory Polymer named Polylactid Acid (PLA).

After thorough research on both the design restrictions and the most suited materials for the shelter, the author managed to reach a solution that managed very respectable shape deformability and recoverability. The shelter suffered many design iterations and culminated on the solution seen in Figure 1.2.

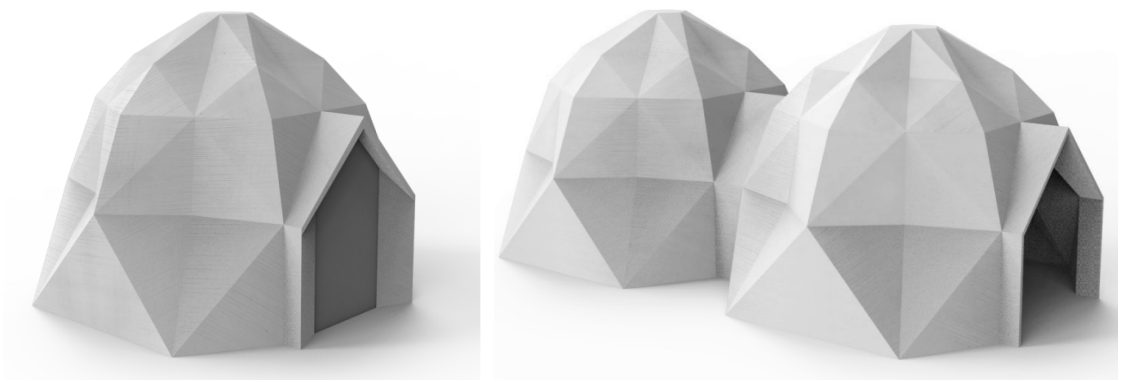

(a) shelter model with door (b) shelter modules connected

Figure 1.2: Final shelter design [2].

This shelter construction allowed for the expansion of living space by connecting two shelter units consecutively, although this could only be achieved through the addition of another door on the back side of the shelter, as seen in Figure 1.2b.

The model was also experimentally validated in terms of its shape fixity and recoverability. The results are shown in Figure 1.3. Both the 1:40 and 1:20 models managed to properly fold in order to correctly fit in transportation pallet sizes.

Overall, the dissertation accomplished the creation of a self-deployable structure while complying with many of the imposed restrictions on shelter design. This particular shelter construction managed to successfully validate the following requisites:

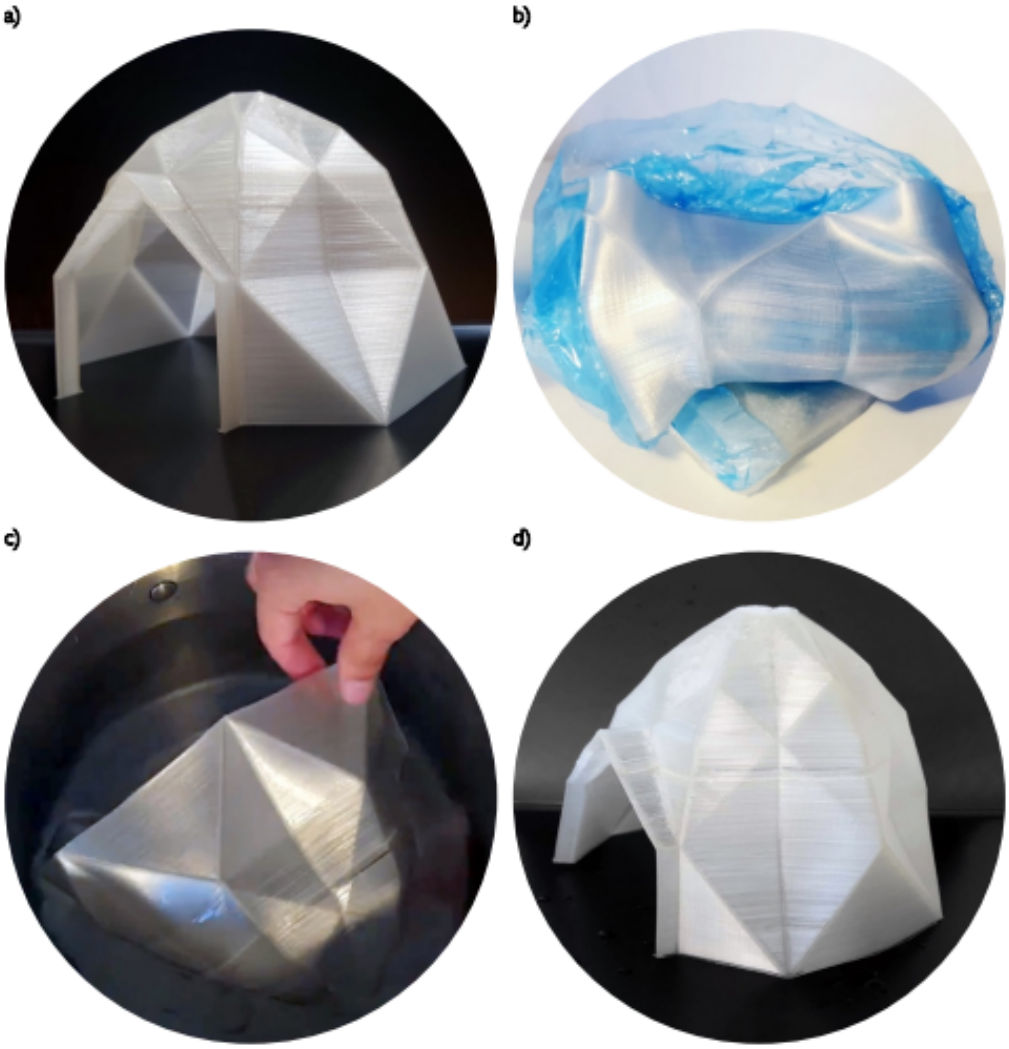

Figure 1.3: Validation of the 1:20 scale shelter model. [2]

- Grant a minimum of 3.5 m^2 living space per person and at least 2m height.
- Modularity and adaptability to fit shipping sizes in pallets (120x110 cm^2).
- Support family shelter over common one.
- Consider the lifetime, recyclability and sustainability of the material, maximizing its lifespan.
- Weigh less than 50kg.
- Provide assistance and material for IDPs to build on their own.

Although the research performed by L. A. C. Henriques [2] achieved interesting results, it lacked depth in regards to the structural viability of the shelter. Throughout the documented work

no geological and external climate factors were taken into account. Besides, no numerical simulations or practical experiments were conducted in order to assess the degree of both structural stability and durability of the developed solution. Another compromising aspect was that the cost for building a singular shelter unit with the technology used in the production of the 1:40 and 1:20 scale models (Fused Deposition Modeling) floated around the 10691€ mark. Even though this value could be reduced to 2256€ with the use of Fused Granular Fabrication (FGF), it would still be way higher than the benchmark for current solutions, which hovers around 280€. Given the previously referred factors the author recommended, among other things, the following developments for the research:

- Analyze and characterize the mechanical properties of the material (SMP filament and SMP pellets);
- Test the models for several climate conditions, as well as UV test and fire retardant test;
- Estimate the durability of the shelter;
- Improvement of the material properties in terms of specific strength, stiffness and toughness that can be achieved using composite materials;
- Study the possible effect of creep or relaxation in the shape memory process;
- Simulate the process of shape memory effect from a designed concept, in order to predict the shape that the concept should be printed and, later on, folded and restored;
- Consider the possibility of developing a composite material from SMP matrix, reducing the weight and cost of the developed structure;
- Determine how to hold the structure to the different types of soil;
- Study the attachment of the door to the rest of the structure;

1.3.2 "Structural Analysis of a Temporary Shelter with Shape Memory Effect"

Following the developments accomplished in the previously presented dissertation, this particular work attempts to overcome some of its structural shortcomings. It intends to do so by testing the previously used material (DiAPLEX MM45-20 SMP) while keeping the same shelter design, as well as studying the influence of several printing parameters in the shelter's mechanical properties.

After gathering data on the mechanical performance of the Shape Memory Material used in the shelter construction developed in 1.3.1, the obtained values were implemented in numerical simulations with the intention of validating the design in question. A couple of simplifications were assumed for the simulations, namely the consideration of isotropy for the used materials' properties and the consideration of exclusively static loads. The loads applied in the simulation were calculated according to the Eurocode: overload, self weight, wind and snow [3].

As expected, the DiAPLEX MM45-20 Shape Memory Polymer left much to be desired in terms of mechanical performance, so various solutions were pondered by the author.

The first consisted in simulating the behaviour of a shelter composed of Glass Fiber Reinforced DiAPLEX MM45-20 (GFR DiAPLEX MM45-20). The material's properties that stemmed from the reinforcement were an elastic modulus of 20 GPa and a density of 1900 kg/m^3.

Table 1.3.1 exhibits the results obtained for the stock and reinforced shape memory polymer, for section thicknesses of 1.5, 4.5 and 15 mm.

Table 1.1: Simulation results for stock and GFR DiAPLEX MM45-20 [3]

Material	Section Thickness [mm]	Maximum Displacement [mm]	Mass [kg]
DiAPLEX MM45-20	1.5	59210	50.4
	4.5	2318	151
	15	80.55	504
GFR DiAPLEX MM45-20	1.5	5921	79.9
	4.5	231.8	240
	15	8.055	799

As seen in table 1.1, the maximum displacements obtained for the DiAPLEX MM45-20 SMP were too high for it to be considered a viable material for the shelter, obtaining values as high as 80.55 mm for a substantially high 15 mm section thickness, with a mass over 500 kg. Similarly, the GFRP was shown to be incapable of complying with the structural requirements of the shelter, as it presented a respectable 8.055 mm maximum displacement but, in turn, had a weight of around 800 kg. This made the transportation of the retracted construction very unlikely if not impossible altogether.

With the unviability of both of the two previous materials, the author suggested the implementation of structural components to the shelter design, in the form of SMP pillars connected to the door of the model and also reinforcement bars along the whole structure, resembeling a skeleton construction. The results are shown in table 1.2

Table 1.2: Simulation results of the structurally reinforced solutions [3]

Material	Section Thickness [mm]	Maximum Displacement [mm]
GRF DiAPLEX MM45-20 + pillars	1.5	956
	4.5	35.35
	15	4.493
GRF DiAPLEX MM45-20 + pillars + bars	1.5	942.4
	4.5	35.77

*Note: The added mass resulting from the sole addition of the pillars can be dismissed, as it relatively low in value when compared to the entire structure. As so, the mass values are equal to the ones presented in table 1.1. Contrarily, the implementation of the skeleton adds around 20 kg of weight.

While the results shared in table 1.2 managed a slight reduction in maximum displacement, it came at the cost of an increase in weight, making this solution, yet again, not viable.

Therefore, one final suggestion was made in attempts of finding an optimal compromise between structural rigidity and weight. Such suggestion consisted in using a sandwich structure constituted out of two SMP sheets and a hexagonal core between them. Thus, numerical simulations were performed and results were registered. This solution managed, with a material with an Elastic Modulus of 20 MPa and sheet and core thickness values of 1.5 mm and 30 mm, respectively, to obtain a **maximum displacement of 4.460 mm**. To further validate the solution, the shape memory effect of the sandwich material was experimentally verified, as shown in figure 1.4.

Finally, a sensitivity analysis on the influence of the thickness of the sheets and core on both the maximum displacement and mass of the shelter was performed and the following conclusions were discussed:

- The parameter height of core shows the smallest sensitivity, which means a small change in this parameter does not cause big differences on the structure's stiffness.
- Due to the core's geometry, it is impossible to have the same thickness values for the core and sheets. Additionally, the influence of these parameters with respect to the total mass must also be taken into account. With that being said, the parameter that shows the least influence in the mass value is the height of the core.
- Increasing the parameters thickness of core and height of core on the same proportion translates as an equal increase in mass. However, in this case, varying the height of core results in better performance (since it is a bigger variation). Furthermore, despite this result, the variation of thickness of sheets leads to lower mass.

Overall, this work managed to propose a satisfying solution to the structural issues present in the model developed in 1.3.1. Nevertheless, more accurate simulations and a scale prototype model were yet to be tested experimentally. In addition, the increase of stiffness of the structure implied an increase in weight and, consequentially, in cost. This ultimately meant that the shelter still lacked the ideal weight and price to compete with modern day solutions.

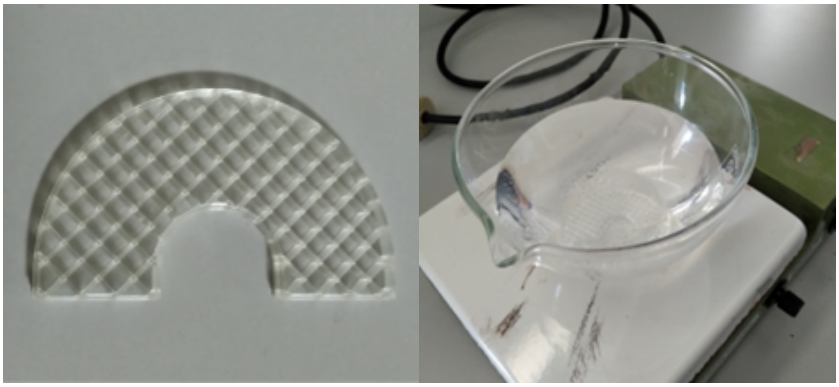

(a) Printed part.

(b) Water heating and submersion of the part.

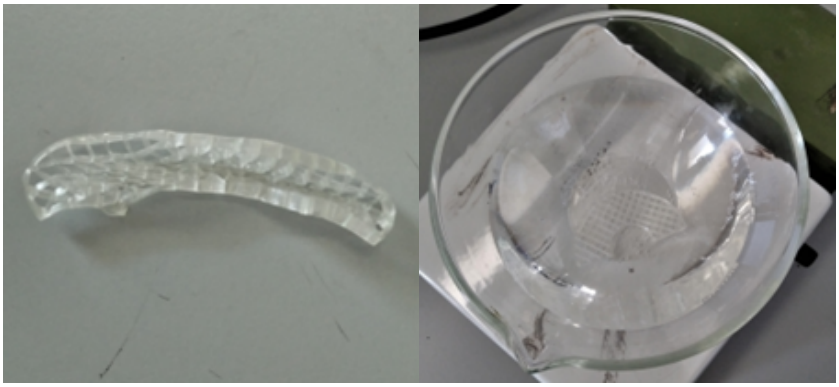

(c) Deformation imposed on the part.

(d) Re-submersion of the part and return to its initial shape.

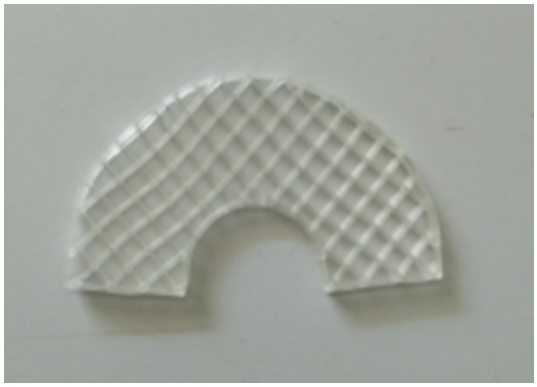

(e) Final part.

Figure 1.4: Validation of Shape Memory Effect by way of practical experimentation [3].

1.3.3 "Development of an emergency shelter using 4d printing"

This dissertation aimed to compile the structural requirements for the shelter and improve some of its aspects, namely on the structural, economical, assembly and transportation fronts, while accounting for the progress accomplished by the two previously presented works.

Before suggesting innovations and improvements, the author first reported on the influence of various printing parameters on the overall quality of the 3D printed samples, hoping to use the gathered knowledge on upcoming experimental procedures [4].

As mentioned earlier, this dissertation had intentions of reaching a lighter and more economical solution, which led to the search of alternative materials to the already tested commercially available SMPs. Thus, various alternatives were considered, namely the conception of new materials by way of extrusion. Inspired by the compiled literature, a new material consisting of a blend of Thermoplastic Polyurethane (TPU) and PLA was developed. The idea was to combine the shape memory and structural abilities of the PLA with the flexibility of the TPU to obtain a simultaneously somewhat rigid and flexible material. The possibility of combining PLA with recycled TPU, in order to benefit economically and in terms of sustainability, was also studied.

Before initiating experimental procedures, the author of the dissertation set out to improve the shelter design, emphasizing on the mechanisms that led to its deployment which, as it stood, consisted in submerging the contracted shelter in hot water. After proposing different designs for the shelter, the solution depicted in figure 1.5a was selected. The design made use of a hole placed on the top of the construction from which the placed hot water would flow to the remainder of the shelter, through the cavities present in its walls. In order to gain sensibility in regards to this deployment method, a simple structure with irregular cavities was developed and tested. This structure can be seen in figure 1.5b. Figure 1.6 portrays the result of this initial experiment.

(a) shelter model (b) shelter modules connected

Figure 1.5: Shelter and experimental deployment test prototype [4].

Figure 1.6: Deployment test result. [4]

As seen figure 1.6, the structure started to delaminate and to yield in a certain direction. This ultimately led to the rejection of this idea, as it failed to produce the intended deployment effect.

Although the thought of deployment concept didn't work, the shape memory effect of the structure could still be evaluated. As such, the model in question was submerged in water at 100ºC, acquiring the morphology shown in figure 1.7a. Afterwards, the model was deformed, taking a more elongated form (figure 1.7b). Finally, the prototype was re-submerged in water at 100ºC and begun recovering its initial shape, as seen in figure 1.7c. Figure 1.7 details the various steps completed in the experimental procedure.

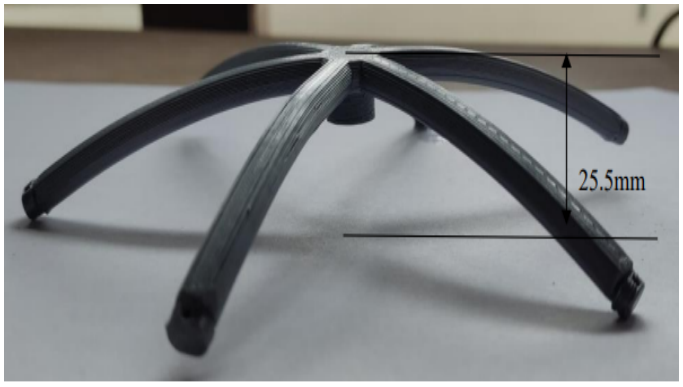

(a) prototype's natural warp,after contact with hot water

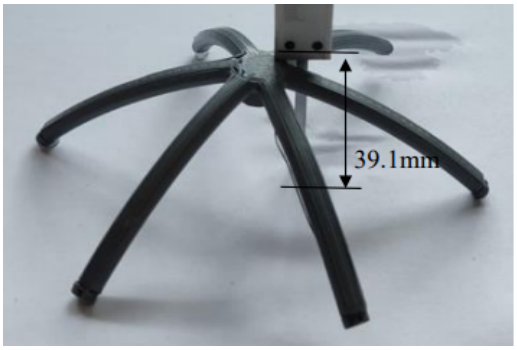

(b) elongated prototype (temporary state)

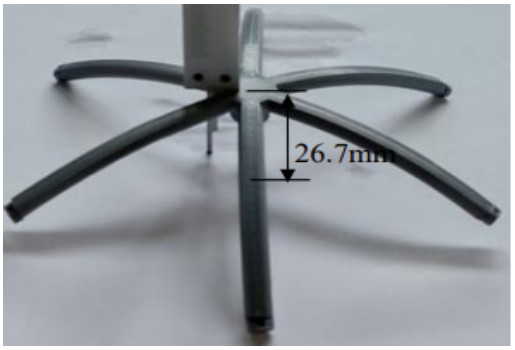

(c) contracted prototype

Figure 1.7: Experimental deployment test [4].

The research then proceeded by commencing its experimental component, in which a list of four candidate materials was submitted to several tests. That list was comprised by:

- PLA
- DiAPLEX MM45-20
- TPU/PLA
- TPU/PLA (recycled)

The tests aimed to mechanically characterize the materials in question, with emphasis on their shape memory performance and their stress and strain properties. Accordingly, four specimens were printed for each of the materials and subjected to shape fixity and recovery tests, followed by tensile tests.

Table 1.3 summarizes the results obtained for both SME and tensile tests of all four materials. The obtained parameters in these tests were the material's density, shape fixity ratio (R_f), shape recovery ratio (R_r), Young's Modulus, Yield strength (σ_y) and Poisson's Ratio (ν). Note that the results appear as the mean values for all four specimens of each material.

Table 1.3: SME and Mechanical properties of the four tested materials [4]

Material	Properties					
	Density [g/cm^3]	R_f (%)	R_r (%)	Young's Modulus [MPa]	σ_y [MPa]	Poisson's Ratio (ν)
PLA	1.177	100	87.81	834.87	47.97	0.28
DiAPLEX MM45-20	1.117	95.17	61.01	618.61	34.44	0.28
TPU/PLA	0.926	82.68	76.46	391.80	18.66	0.28
TPU/PLA (Recycled)	1.102	100	80.63	661.95	33.23	0.28

Having completed the practical experiments and acquired data on the materials to use in the hypothetical manufacturing of the shelter, the research gathers all the requisites to move towards a numerical analysis. However, before running simulation on *Abaqus*®, a prior structural study was conducted using the EN EUROCODE, in order to determine the loads applied to the shelter's numerical model [4].

What followed was the execution of the numerous numerical simulations, attending to four different design variants of the shelter model, varying in terms of wall thickness (t), printing perimeters and (d) infill percentage (i). Having run the simulations, results were finally obtained, and some conclusions were reached:

- The maximum displacements obtained were far above the 11.43 mm recommended value. This outcome, besides the obvious structural limitations of the used material, could very well have been caused by the usage of the experimentally obtained elastic moduli, which were quite inferior to the ones found in the literature.
- Even though the displacement values were high, the materials' yield limit was never surpassed. The usage of sandwich structured materials was, yet again, considered a very plausible solution to tackle the verified structural issues.

- In printing, the expansion of the piece's perimeters has a significant impact on the equivalent Young's modulus, but the overall mass also grows significantly. The equivalent Young's modulus decreases as thickness increases, but the shelter's rigidity increases significantly without substantially adding to its weight. It was discovered that decreasing the infill of the piece might raise the shelter's rigidity without increasing the weight of the shelter (assuming the wall thickness was increased). Despite the simulations performed, all of these variables could still be changed to further optimize the parameter combination.

- Comparing the four different materials, it was possible to observe how the parameters density and Young's modulus affect both the total weight and stiffness of the shelter. As expected, it was the PLA which, despite being heavier, showed better resistance to the applied loads. It was followed by TPU/PLA (recycled), DiAPLEX MM45-20 and TPU/PLA, which registered the highest deformations. What this last mixture lacked in terms of structural performance, it made up for with an interesting low density, allowing for a lightweight shelter construction. The TPU and recycled PLA mixture was yet again second best in terms of lightness, followed by the DiAPLEX MM45-20 and lastly the PLA.

1.3.4 "Finite element analysis of shape memory polymers"

This dissertation, elaborated simultaneously with the one previously registered in 1.3.3, focused on achieving more reliable and truthful results through numerical simulation. This, in turn, entailed an accurate description of the complex thermomechanical behaviour of SMPs.

Consequently, the research attempted to develop a constitutive model capable of capable of modeling the behavior of polymers with shape memory sensitive to temperature variation. This model assumed the presence of two distinct phases, amorphous and crystalline. The shape memory cycle was simulated through the implementation of a User-defined material model in an *Abaqus*® subroutine [5].

Initially, simple single element uniaxial and biaxial test simulations were performed and later compared with experimental results from the literature. The obtained results were in accordance with the researched constitutive theory, showing the presence of a crystalline (with a higher Young's Modulus) and rubbery phase (with a lower Young's Modulus) for temperatures below and above T_g, respectively.

Subsequently, similar numerical tests were conducted for a Polyurethane based SMP and compared with an experimental work found in the literature. The results and their direct comparison appear in the following figure.

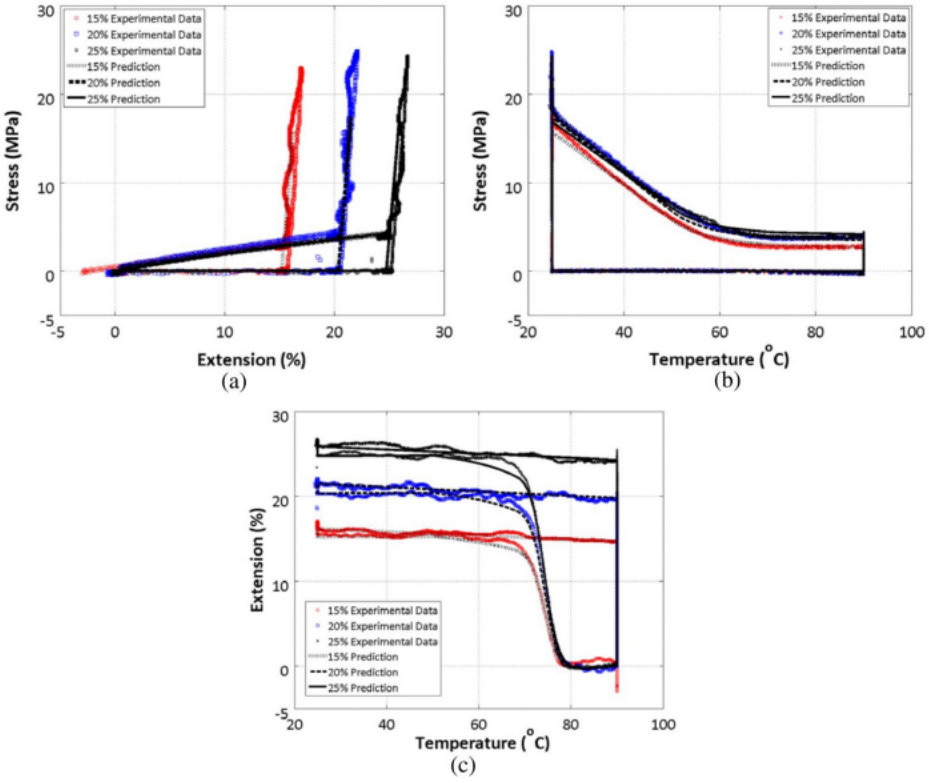

Figure 1.8: Comparison of experimental and simulation results [5].

The following tests sought to perform simulations for more complex geometries. As such, three different structure morphologies were tested in regards to their shape memory behaviour: a flower-shaped structure made of two types of styrene-based SMPs (Figure 1.9), a hexagon structure to test a possible application to a refugee shelter (Figure 1.10), and a cube (Figure 1.11).

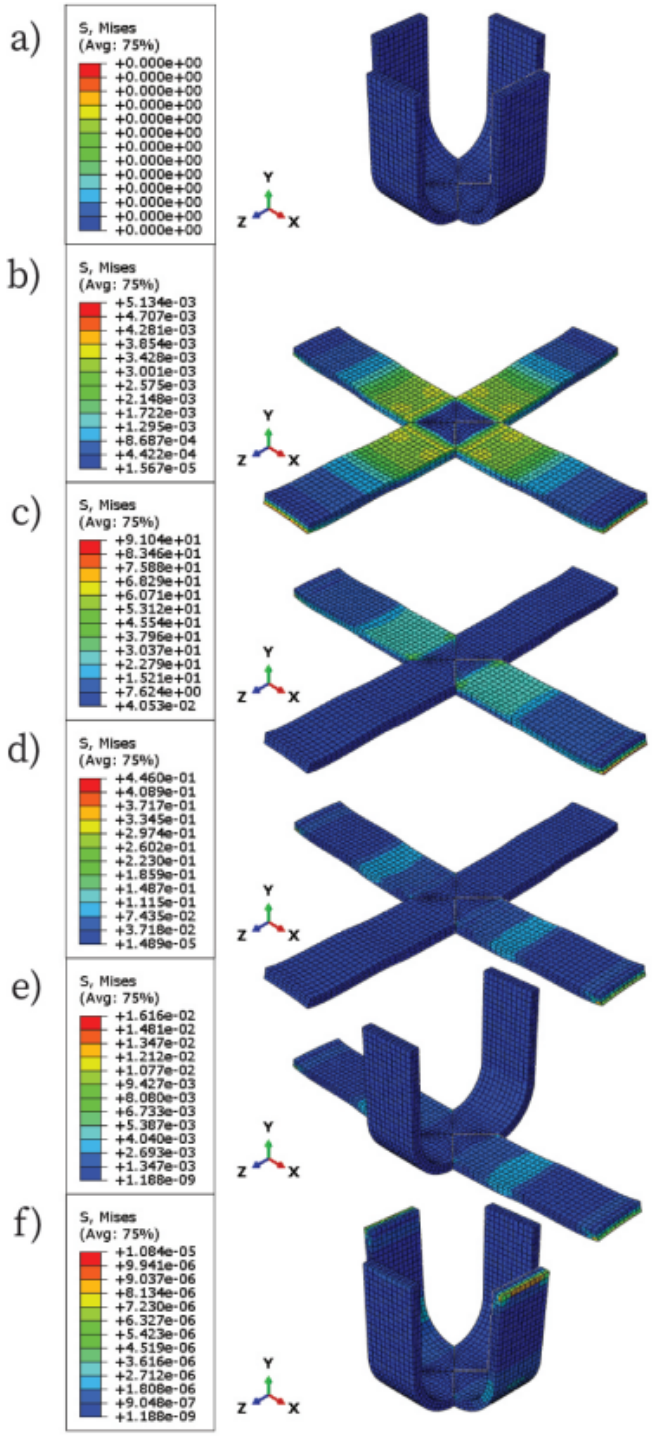

Figure 1.9: von Mises Stress evolution during a flower structure's Shape Memory cycle [5].

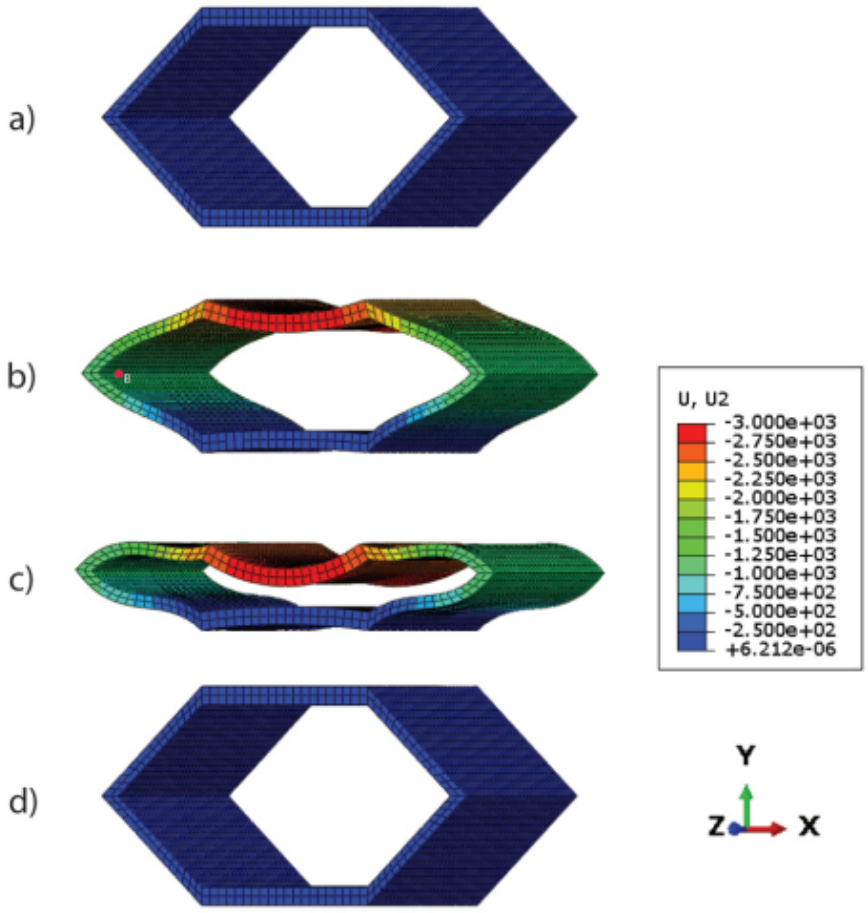

Figure 1.10: Deformation evolution during Shape Memory cycle of an hexagonal structure. (a) Initial shape, (b) during folding, (c) fixed state, and (d) deployment complete [5].

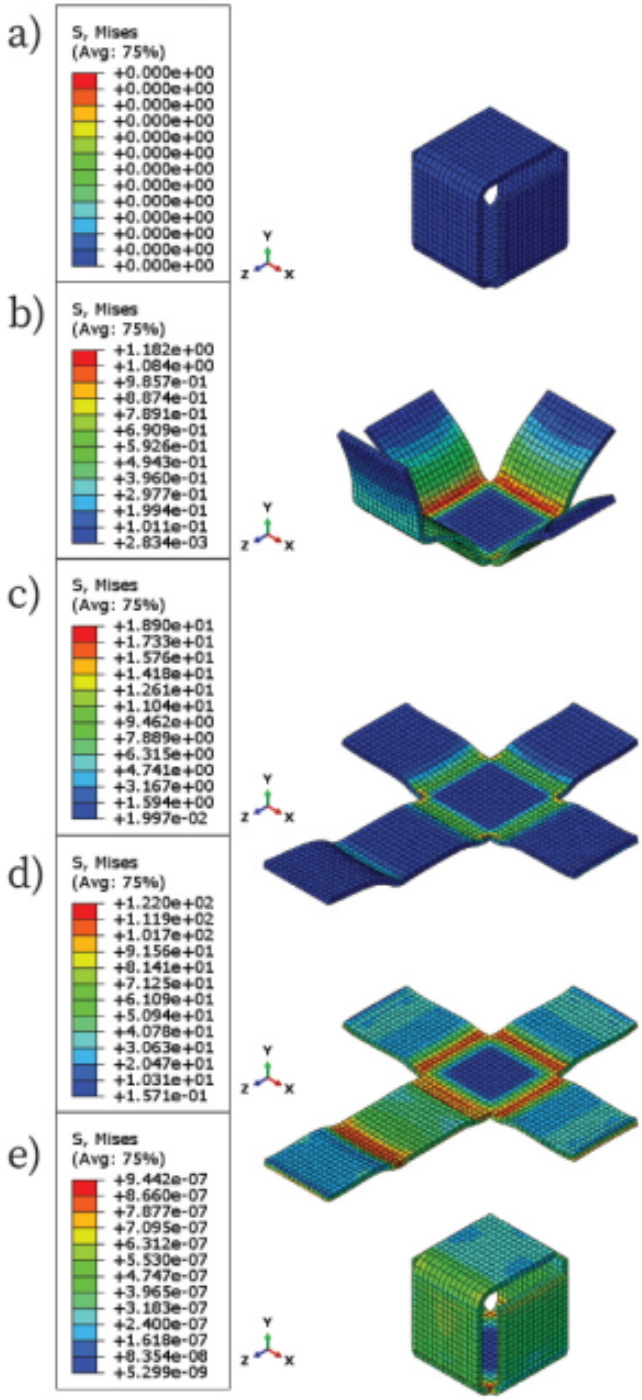

Figure 1.11: Von Mises Stress evolution during a cube's Shape Memory cycle [5].

Overall, this work managed to present a constitutive model that, when implemented in a UMAT subroutine managed to successfully emulate the complicated thermomechanical behaviour of Shape Memory Polymers, doing so with less parameters than the ones found in the literature. Nevertheless, the model could be improved in order encompass a wider range of materials, such as anisotropic and hyperelastic materials [5].

Chapter 2

State of the Art

Shelters play a major role in the stabilization of post crises situations, immediately offering a safe and protected environment to the victims of such tragedies. In the aftermath of disasters like earthquakes, hurricanes, floods and armed conflict, the time interval between the happening of the calamity and the arrival of food, supplies and shelter is of great importance to the preservation of human life. Humanitarian organizations such as the International Organization for Migration (IOM), the UNHCR, the Sphere Association and the International Federation of Red Cross and Red Crescent operate with the goal of providing the displaced people with essential goods and adequate shelter and settlement, along with the ensuring basic human rights.

2.1 Shelters

2.1.1 Shelter Requirements

A shelter is defined as a habitable covered living space able to provide a secure and healthy living environment with privacy and dignity. This means that beyond its "protection from the elements" functions, a shelter must also provide safety and security for people and possessions and help to preserve or rebuild family unity.

In 2016, the Sphere Association published the *The Sphere Handbook*, which contains ethical, legal and practical guides for humanitarian response, and has turned into one of the most referenced humanitarian resources in the world. Although different types of catastrophes may require different shelter characteristics, this document clearly states three essential guidelines for shelters [1]:

- Minimum 3.5 m^2 covered living space per person in tropical or warm climates, excluding cooking facilities or kitchen (it is assumed that cooking will take place outside).
- Minimum height of 2m at the highest point.
- Minimum 4.5 m^2 to 5.5 m^2 covered living space per person in cold climates, including kitchen facilities as more time will be spent inside the shelter (cooking, eating, and livelihoods). 2m ceilings to reduce the heated space.

Furthermore, according to the UN Refugee Agency (UNHCR), the minimum requirements for the construction of a shelter are:

- Guarantee the minimum of 3.5 m^2 living space per person and the height should be at least 2m at the highest point;
- Protect against environmental issues, such as hazards zones or severe weather, and guarantee privacy, security and protection of belongings;
- Consider the lifetime of the material (at least two years in most challenging conditions), recyclability and sustainability;
- Adapt the shelter solutions according to climate conditions, cultural and geographic context, and also with the local skills and materials;
- Supply the minimum materials required, blankets, mats and tarpaulin;
- Shelter design should be, if possible, flexible to fit its occupants' individual needs;
- If possible, provide assistance and materials for IDPs to build a shelter independently;

Shelters may also be classified as to their longevity of use and their housing capabilities. To that end, shelter constructions can be labeled as **emergency shelters**, **temporary shelters**, **temporary houses** and **permanent houses**. The first two solutions are meant for short term use, in time spans ranging from a few days to a maximum of a few weeks. The two remaining shelter subtypes constitute long term solutions for the displaced people, granting shelter for periods of time between six months up to three years in the case of temporary houses, and permanently in the case of permanent houses.

The shelter to be developed in this work, just like the ones previously developed in the aforementioned FEUP dissertations, aims to form a hybrid solution between temporary shelter and temporary housing, due to its disassemblability, upgradability, reusability, recyclabilty and relocation potential. Since it doesn't provide all main aspects of a traditional house, such as a toilet, kitchen or ventilation, this nomenclature isn't suited for this particular construction [49; 50].

Figure 2.1 helps to illustrate the categorical placement of the prospective shelter.

Recalling one of the previously stated requirements for the construction of a shelter, it is recommended that the IDP use locally acquired materials. Moreover, the displaced people are incentivized to build their own shelters. Although this may be beneficial for the recovery of the local economy, it also means that the quality of the shelter directly depends on the available materials [51]. Additionally, more often than not, the victims of the priorly stated calamities don't possess the required skills to correctly assemble a shelter on their own. Counterintuitively, this approach also negatively conditions the time it takes to build the shelter.

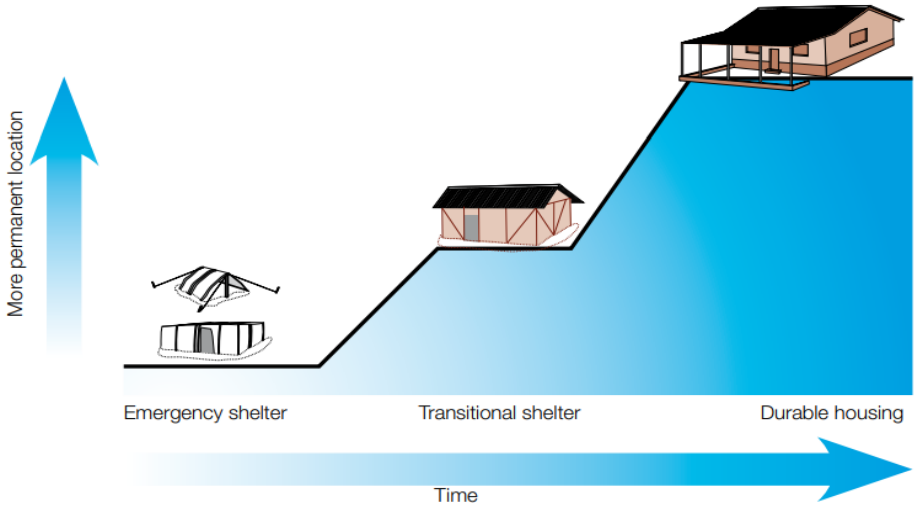

Figure 2.1: Shelter types [6].

2.1.2 Current Shelter Solutions

Having established the main requirements for the construction of an emergency/transitional shelter, currently available solutions will be studied and described in order to gain a general idea on the benefits and disadvantages inherent to each shelter morphology.

Some of most noteworthy shelter solutions in current use are:

1. **Tarpaulin and rope shelter kit** - this is the most commonly used shelter solution, mostly due to its assembly's simplicity and quickness. It isn't a viable solution in the long run because of its vulnerability. The most widely distributed shelter kit is provided by the IFRC and it is constituted by a collection of tools (rope, handsaw, nails, hoe, shovel, machete, shears, tie wire, claw hammer and woven sack) and two plastic tarpaulins (made of HDPE black fibers fabric laminated on both sides with LDPE coating) [7]. Figure 2.2 depicts both the IFRC shelter kit (left) and the shelter after assembly (right).

(a) IFRC shelter kit (b) assembled IFRC shelter

Figure 2.2: IFRC tarpaulin shelter solution [7].

2. **Tents** - Structures composed of a rigid frame with a flexible plastic or cotton cover. They are easily manufactured and transportable and generally offer a more feasible solution than the previous tarpaulin shelters. Figure 2.3 shows a UNHCR standardized framed family tent. This construction is adaptable to all climate conditions, fire retardant, waterproof, UV stabilised and can simultaneously house a total of 5 people [8].

Figure 2.3: UNHCR family tent [8].

3. **Designnobis' "Tentative"** - A compact individual cell-like structure, Tentative by Designnobis, is a deployable emergency shelter with a height of 2.5 m, allowing for the housing of a family of two adults and two children. The framework is supported by an aluminum frame and is made of quilted, weather-resistant fabrics with insulating perlite sandwiched between layers. The roof possesses the ability of collecting water, and also provides excellent lighting and ventilation. The floor is made of recyclable heat insulating boards that are raised off the ground by legs to retain heat [9]. The shelter in question and its interior are illustrated in figures 2.4a and 2.4b, respectively.

(a) Designnobis' "Tentative" shelter (b) shelter interior with human for scale purposes

Figure 2.4: Designnobis' "Tentative" shelter [9].

4. **Sky Shelter.zip** - A concept created by polish designers, this foldable skyscraper constitutes a mobile, zipped and solar powered shelter solution that is easily transportable and deployable. The vertical stacking of all the necessary functions in a post disaster scenario is probably the main feature of this construction, as it greaty reduces the total area occupied by the victims of such disasters. This allows for a shelter setup closer to the affected populations' homes, making it especially important in densely populated areas. Additionally, this solution takes advantage of its large surface area by incorporating a network of small perovskite solar cells into its Ethylene Tetrafluoroethylene (ETFE) foil based nanomaterial walls, giving it the ability of producing clean energy. Similarly, the ballon residing of top of the structure is shaped in such a way that it allows the flow of water through its hollow centre, where it is cleansed by specialized filters and stored for future use [10].

(a) Skyshelter.zip in an emergency scenario.

(b) Skyshelter.zip interior plant.

Figure 2.5: Skyshelter.zip shelter solution [10].

5. **TornadoPod** - This shelter, developed with the intent of protecting up to six people from a tornado scenario, makes use of both metals and composites to reach a solution capable of withstanding the high velocity winds and the subsequent destructive force associated with this phenomenon. As seen in Figure 2.6, the base is threaded so it acts as an anchor on 5400 kg of concrete, and the exterior is a domed steel cage with a 9.5 mm thick ballistic shield composed of multiple layers of woven glass fabrics and *Innegra Technologies* composite fabrics [11].

Figure 2.6: TornadoPod [11].

6. **IKEA- Better Shelter** - This shelter (Figure 2.7), developed by the leading furniture company worldwide IKEA, can accommodate 5 people. The construction possesses a solar-paneled roof and interior insulation. Its low budget doesn't compromise the overall quality of the shelter, as it offers security, insulation, and durability.

Figure 2.7: IKEA - Better Shelter [12].

7. **Life Cube** - this shelter is designed to be an on-site maneuverable shipping container capable of rapid deployment into an emergency response shelter. It has an air beam canopy that is made with a weather-resistant and fire retardant material. Each unit of the *Life Cube* is supplied in the form of rugged cube-shaped container and can be air-dropped or delivered on a pick-up or flatbed truck. This shelter can house up to 5 people for 5 days with food and water without any assistance and it comes with a self-sufficient power system, Global Positioning System, water filtration devices, propane cook top, first aid kits, ready-to-eat meals (MREs) and a wide variety of essential survival supplies [13].

Figure 2.8: Lifecube on-field assembly [13].

2.2 Additive Manufacturing

As briefly mentioned in 1.2, a general overview of the most common Additive Manufacturing (AM) techniques will be made in the present chapter. This review will then be followed by a short explanation of the concept of 4D printing, which naturally directs the focus to Shape Memory Materials (SMMs), more specifically Shape Memory Polymer Composites, as they represent the biggest probability of success in achieving a viable and functional self-deploying shelter construction.

2.2.1 3D Printing

Additive Manufacturing, commonly known as 3D Printing, is a technology that has undergone nearly forty years of developments since its first appearance, allowing users to create complex geometries otherwise impossible using traditional manufacturing methods. The distinction between said traditional methods and additive manufacturing lies in the fact that 3D printing functions by adding material layer by layer, instead of removing it like in traditional processes.

After its emergence, in the 20^{th} century, the integration of this technology in "mainstream" industry was quite slow, due to the high prices attached to both printing devices and materials. But after continuously larger investments in 3D printing, which led to several competitive solutions and overall price reductions, the technology was ready to be industrialized and was widely adopted in various fields. Some of these fields include fashion jewellery, polymer printed textiles, robotics and automation, tissue and scaffolds, electronics, soft medical devices and end-use products [52].

In large scale industries related to the education, aerospace, automotive and medical fields, AM is mainly used in rapid prototyping, using a vast range of raw materials, from (mainly) polymers, ceramics, metal alloys and glasses. More recently, the upsurge of composite usage has potentiated the application of 3D printing in the civil and construction industry, allowing for the creation of structures similar to the shelter to be developed in this sequence of works.

As the name implies and as previously mentioned, AM consists in adding material until the desired shape is achieved. Generally speaking, the 3D printing process starts with the designing of a CAD model that is then converted into an STL file via CAD software. STL files represent the object through its surface made with a set of triangles. After obtaining the STL file, it is uploaded in a “slicer” software in order to get a slicing model, represented by a G-code that contains all the printing process parameters, such as printing speed, layer thickness, infill deposition, temperature and support structures. Finally, the printing of a component can be achieved by simply uploading the G-code into a 3D printer and running the system. This process is vaguely illustrated in figure 2.9.

Additive Manufacturing includes a broad range of technologies, namely material extrusion, vat photopolymerization, powder bed fusion, material jetting, binder jetting, sheet lamination process, and directed energy deposition. For simplicity’s sake, this research will highlight and overview only the three most common methods: **FDM** (figure 2.10a), which falls under the material exclusion category of AM processes; **StereoLithography (SLA)** (figure 2.10b), which constitutes

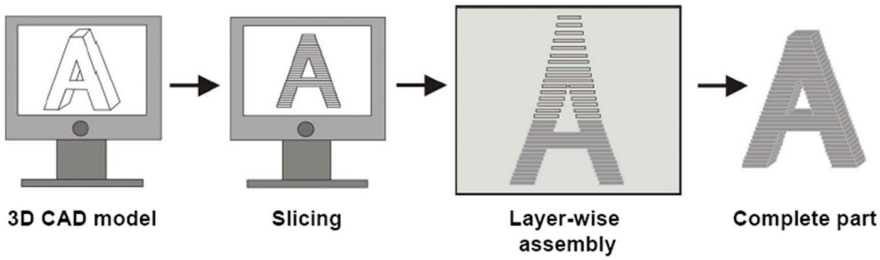

Figure 2.9: Additive Manufacturing process steps [14].

a vat photopolymerization technique; and **Selective Laser Sintering (SLS)** (figure 2.10c), which represents a Powder bed fusion AM method.

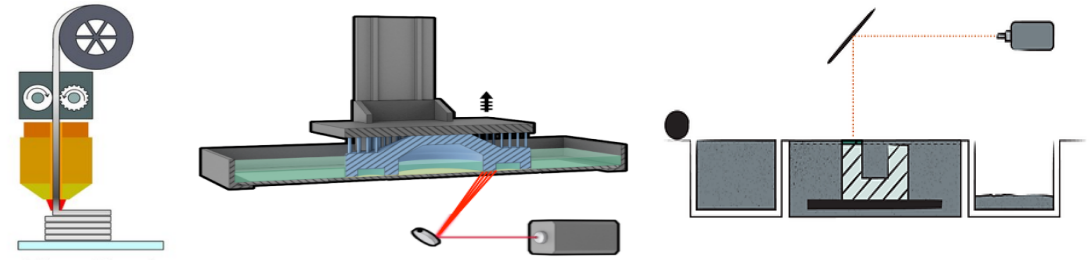

(a) FDM [53]. (b) SLA [54]. (c) SLS [55].

Figure 2.10: AM techniques.

Each technology has its own unique advantages and disadvantages and follows its own set of rules and restrictions, catering more towards certain applications with specific geometric requirements than others. The key is in understanding what type of AM method better suits a determined design, in order to obtain the best possible dimensional accuracy.

The dimensional accuracy and overall quality of the manufactured components is also dependant in the intrinsic design of said components and in the materials used in the production process. Quality of the raw material (or filament in the case of FDM), thermal contraction, quality of the machine, machine calibration, quality of resin and post-processing , can also positively or negatively affect the dimensional accuracy of the obtained parts [56].

Table 2.1 reviews the aforementioned Additive Manufacturing methods and compares them between themselves.

In short, conventional 3D-printing technologies focus on fabricating static structures, which cannot meet all the demands of dynamic functions needed for applications such as the one intended in this work.

AM Technology	Fused Deposition Modeling (FDM)	StereoLithographic Aparatus (SLA)	Selective Laser Sintering (SLS)
Description	Process in which material is selectively extruded through an orifice or nozzle.	Process in which a liquid photopolymer is selectively cured by (ultraviolet) light.	Process in which thermal energy selectively fuses regions of a powder bed.
Typical Materials	Pellets or filaments of thermoplastic polymers (PLA, TPU), composites and highly filled polymers with metals or ceramics.	UV-curable photopolymer resins (with various fillers)	Plastics, metals, ceramics, sand, but mostly (nylon) powders.
Advantages	Inexpensive equipment. Wide range of materials, easy to use. Possibility of producing in small or large scale and manufacturing multimaterial parts.	High level of accuracy and complexity. Accomodates large building areas. Smooth surface finhishing.	High complexity level. Powder acts as a support structure. Wide range of available materials.
Disadvantages	Low speed and accuracy. Property anisotropy. Need for support structures and rougher surface limited by nozzle radius	Limited to photoresins only and liquid monomers can be harmful. Subject to material creeping after curing and long post-processing needed. Expensive equipment and possible need for support structures.	Expensive equipment. Requires special powders that are costly, can be harmful and can age fast. Need for post-processing

Table 2.1: Main AM techniques overview [47].

2.2.2 4D Printing

The demand for dynamically controlable shapes triggered the appearance of a research branch originated from 3D printing which utilized smart materials that could respond to external stimuli, adding the dimmension of time to Additive Manufacturing. This branch introduced by Skylar Tibbits [57] was later named **4D printing** and basically consisted in the 3D printing of structures that displayed targeted shape or property transformation under a given external stimulus.

Research in 4D printing is closely related to 3D printing, meaning that advancements achieved in the latter will correspond to developments in the former. At the embryonic state that this technology finds itself in, most research focuses on the shape changing ability of the 4D printed structures, namely in bending, twisting and elongating. The many research topics in current 4D printing fall into one of the following three categories: development of equipment, deformation mechanisms, and mathematical modeling, as shown in figure 2.11.

This technology showed great promise in the creation of dynamic structures with diverse shapes, properties, or functionality, achieving multi-functionality, self-assembly, and self-repair. 4D printing envisioned the achievement of structures with incredibly complex shapes while also reducing their overall volume, facilitating their transportation and assembly. Such benefits are of crucial importance for reaching a functional self-deployable structure like the shelter construction which stands as the end goal of this dissertation.

Even though 4D printing has the potential of solving many real world problems in the future, there are still plenty of challenges this technology is yet to overcome. One of the most notable challenges is related to the limitations in 3D printing, which still hasn't successfully addressed one of its main issues in the form of the need for support structures. The technology also lacks the ability to simultaneously print different material groups, as well as competitive speeds and price when compared to other more conventional manufacturing methods and with 3D printing itself.

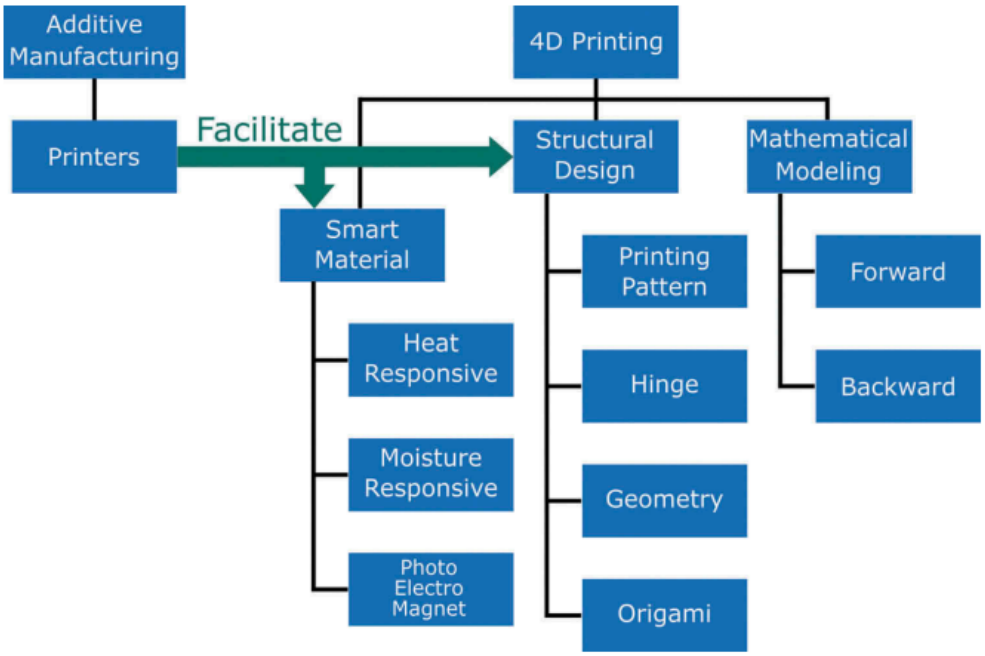

Figure 2.11: 4D printing research paths [15].

Another major challenge stems from the clash between the desired mechanical material properties and the intended shape or property transformation. To obtain the desired shape of the printed part, certain ratios of polymer are required, which can end up hindering the mechanical performance of the component.

Other challenges come in the form of slow and inaccurate actuation, limited material availability and lack of control over intermediate states of deformation.

2.2.3 Shape Memory Materials

Smart or Shape Memory materials are materials capable of returning to its original shape after deformation, by responding to a certain external stimulus such as temperature, light, humidity or electricity. In short they are materials that possess Shape Memory Effect and are of extreme importance in 4D printing, as it is them that basically allow the shape shifting mechanism to occur. Smart materials can be classified as to the nature of their primary material family [58]:

- Shape Memory Alloys (SMAs).
- Shape Memory Polymers (SMPs).
- Shape Memory Hybrids (SMHs).
- Shape Memory Ceramics (SMCs).
- Shape Memory Gels (SMGs).

The most adequate, and therefore studied and used smart materials for Additive Manufacturing are SMAs and SMPs, with the latter outdoing the former in terms of and overall development and suitability towards AM. This preference of SMPs over SMAs stems mainly from the polymers' better mechanical property tunability as well as their lower cost, density, higher elastic deformations and higher biocompatibility. As such, the focus of this research will be SMPs and their applications in 4D printing.

2.2.3.1 Shape Memory Polymers (SMP)

Shape Memory Polymers are, as the name implies, polymeric materials that are capable of recovering their original shape from a significant and seemingly plastic deformation, when exposed to a specific stimulus. These materials can also be classified according to the type of stimulus that activates their Shape Memory Effect. To that end, five main classes arise [15]:

- **Thermo-responsive SMP** - As their denomination suggests, this subclass of materials initiates or "reverses" its deformation when stimulated with a temperature value that falls within a programmed range for a given material. This programmed temperature being the transition temperature (T_t) of the polymer in question. The Shape Memory cycle of a thermo-responsive SMP will be described further ahead in this subchapter.
- **Moisture responsive SMP** - Shape Memory Polymers that trigger their SME when in contact with a certain level of solvent or moisture. These usually appear in the form of hydrogels, which are highly hidrophilic materials able to expand to 200% of their original volume. Beyond their hydrophily, hydrogels also show great printability and biocompatibility, making them a viable resource in many applications that involve contact with water/moisture, namely in the human body.

- **Photo-responsive SMP** - Materials that absorb light (which unlike heat and moisture is an indirect stimulus) as heat, triggering their deformation. The heat absorption rate is be determined by the colour of the joint responsible for absorbing the light power. This type of deformation activation mechanism has proven quite useful for long-range and outer space applications, as concentrated light can be shone even in locations that lack an atmosphere.

- **Electro-responsive SMP** - Also an indirect stimulus, electricity can be used to trigger deformation in 4D printing. It does so by applying either electric current or voltage to specific polymers (generally containing metallic electric conductive elements) in order to generate heat. These materials have shown great potential in areas like soft robotics and artificial muscles.

- **Magneto-responsive SMP** - 4D printed materials that respond to magnetic fields. This can be achieved by incorporating magnetic nanoparticles in a polymeric material, although the intended effect will only take place if the structure is lightweight enough to be affected by the magnetic field.

Similarly to previous dissertations developed on the same topic at FEUP, the research will particularly focus on thermo-responsive materials, as they appear to be the most solid choice for the deformation triggering mechanism in a chaotic post disaster scenario. This is mostly caused by the uncontrollability or scarcity of the remaining mentioned stimuli like water/moisture, light, electricity and magnetic fields.

As such, the understanding of a thermomechanical Shape Memory cycle of a thermo-responsive material is of considerable relevance. This process is divided in three stages [59; 60]:

1. **Heating and shaping** - After heating it to at least its transition temperature (T_t), the material is deformed into its desired shape under external load.

2. **Cooling and fixing** - While maintaning the external load and decreasing the temperature, the sample adopts a more rigid state and immobilizes the polymer chains, fixing the deformation. This results in an unaltered shape upon unloading.

3. **Reheating** - The initial shape can then be reinstated by increasing the temperature to a value superior than T_t, finalizing the shape memory cycle.

Figure 2.12 visually depicts the main steps of the shape memory cycle of a shape memory material.

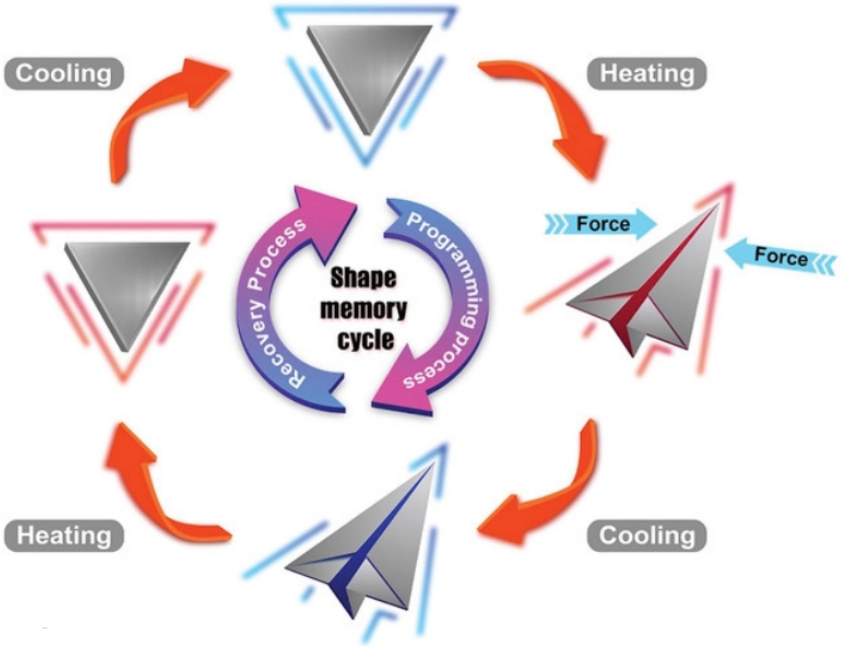

Figure 2.12: Shape Memory Cycle of a SMM [16].

To get a better grasp of the inner mechanics at play in this process, one must first gain more detailed knowledge regarding the physical and chemical intricacies of SMPs.

These materials shift between a hard and brittle glassy state and a soft and more ductile rubbery state, when their temperature values lie below and above the transition temperature, respectively. The hard glassy state possesses restricted chain mobility with a higher Young's Modulus, while the soft rubbery state shows greater chain mobility (and consequently elasticity) at the cost of a lower Young's Modulus. It is this rearrangement in polymeric chains that causes the SME to take place (figure 2.13) [61].

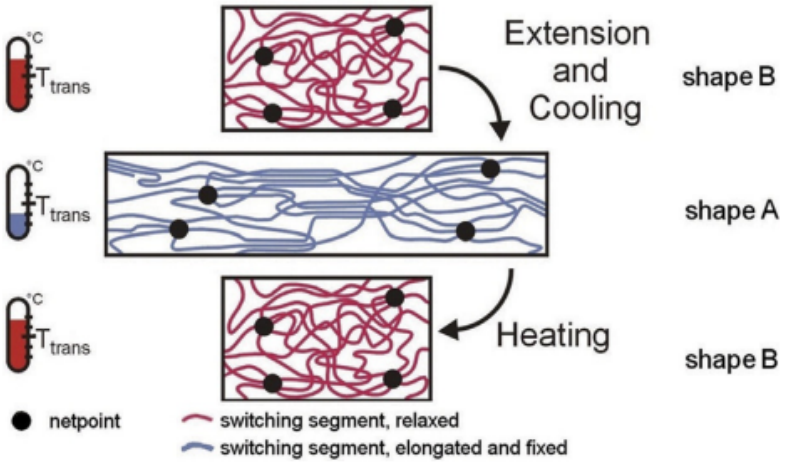

Figure 2.13: Illustration of the thermally induced shape memory effect at a molecular level [17].

Shape Memory Polymers are copolymers constituted by hard and soft segments. The hard segments store strain energy during deformation that can then be released through the monomer cross links, which provide the required elasticity and mechanical strength to revert the material back to its original form when heated above T_t. Conversely, the soft segments maintain the shape of the printed components when they sit below the transition temperature. The initial shape's segment chains undergo reorientation when stress is applied. After deformation, the part is cooled, and the soft segments vitrify to form a new segment chain arrangement. This ensures that the new shape will remain fixed until the sample is reheated. As a result, the soft segments become weaker and are unable to support the new segment chain configuration. Entropy causes the stored strain energy to be released, which in itself causes the shape memory effect to be activated. It is energetically advantageous for the material to return to its disordered conformation [61; 62].

The previous explanation was made in light of the micromechanical theorem of phase transformation (theoretical) constitutive model for SMPs. This theorem states that the material gradually switches between a glassy state at lower temperatures and a rubbery state at higher temperatures. Besides the previously mentioned constitutive model, the linear viscoelastic theory is also a common approach when trying to describe SMPs' behaviour. The lack, both in depth and in quantity of viable constitutive models for these materials is holding their development back, as it hinders the implementation of simulations that mimic shape memory behaviour. As such, most models still rely on empirical parameters mostly based on experimental results [62].

2.2.3.2 Shape Memory Polymer Composites (SMPC)

As presented in section 1.3, where an overview of the previous FEUP dissertation works on the same theme was made, it was verified that all of them had selected SMPs as the shelter's material of choice. Although those choices were made under different circumstances, the overall consensus was that these materials, besides offering good printability, also offered great shape fixability and recoverability at a reasonable price. However, SMPs showed some drawbacks in terms of their structural reliability, being, in most cases, unable to withstand the required imposed loads on the shelter construction as well as producing low recovery forces.

To combat these structural shortcomings the authors suggested a series of possible solutions. Perhaps the most promising of those suggestions was the use of fiber reinforced SMPs, also known as **Shape Memory Polymer Composites**.

These are basically composites with a shape memory polymer matrix reinforced with either (long or short) fibers, nanoparticles or nanostructures. SMPCs manage to enhance six aptitudes of pristine SMPs: structural performance, shape memory effect, shape memory performance, long term behaviour, stimulus method and value addition [17]. Figure 2.14 encapsulates the priorly exposed information on shape memory polymer composites.

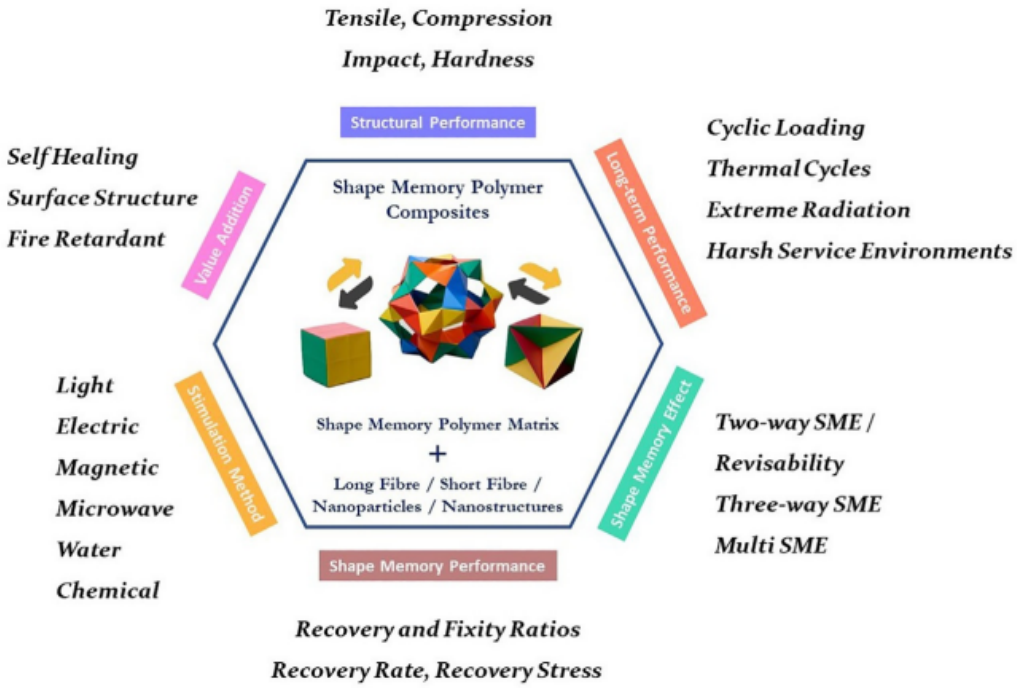

Figure 2.14: SMPCs' capabilities and significance [17].

Reinforced Shape Memory Polymer Composites have the ability to operate in unusual and extreme service environments such as in body fluids, extreme temperatures and radiation, and under cyclic loads and thermal cycles. This ultimately expands the opportunities of use of these materials in numerous smart applications in the most diverse areas. Said applications range from both non-invasive (adaptive components for orthosis and fracture fixators) and invasive (bone scaffolds, oclusion devices, vascular tents) biomedical devices, self-healing structures, textile fabrics, and aerospace and space components (hinges, trusses, booms, antennas, optical reflectors, and morphing skins).

As a subject of study, SMPCs have been around for nearly forty years, and recent developments in both experimental and numerical fronts have proven the applicability of SMPCs for micro- to large-scale engineering projects.

2.2.4 Case Studies

The present section will exhibit various noteworthy 4D printing application cases. As the material of choice for the shelter construction is a SMPC, yet to be defined, special attention will be given to cases which meddled with this specific class of composites. Another subject of interest in this research is the development of self-deployable structures, and as such several cases will be observed in a more attentive fashion. To exemplify the aforementioned versatility and wide applicability of 4D printing, several applications in areas like aerospace, biomedicine and soft actuators will also be briefly mentioned.

2.2.4.1 Medical Applications

The following figure presents a collection of 4D printing applications in the medical field. This technology has allowed for the creation of dynamic medical devices that further enhance the already reliable personalized medical care provided by 3D printing.

In the medical field, 4D printed proved to be useful in the production of **targeted drug delivery devices**, **stents** and **splints**.

Targeted drug delivery devices ensure the delivery of medication to specific intended areas of the body, when a certain stimulative condition is met. Figures 2.15 (a), (b) and (e) are examples of devices responsible for drug containment and release [15].

4D printing also allows for a quick fabrication of customized patient-specific stents. In turn, the shape memory abilities of the printed stents allow for minimal surgical invasion of the implants (as seen in figures 2.15 (c) and (d)) by first printing the stent with the desired dimensions and then compressing it to reduce its overall volume. After stabilizing at body temperature, the stent will return to its original intended shape [15].

One of the more crucial aspects regarding biomedical devices such as splints is geometry, as the fit on the subject greatly impacts the proper functioning of said gadget. 4D printing could combat the difficulties of splints in accompanying the subject's growth, as the shape memory properties in these devices provide the necessary tension and compression conditions for their adequate growth in accordance with the subject. The external airway splints, nerve guidance conduits and biomedical scaffolds present on figures 2.15 (e), (f) and (g), respectively, constitute some examples of 4D printed splints.

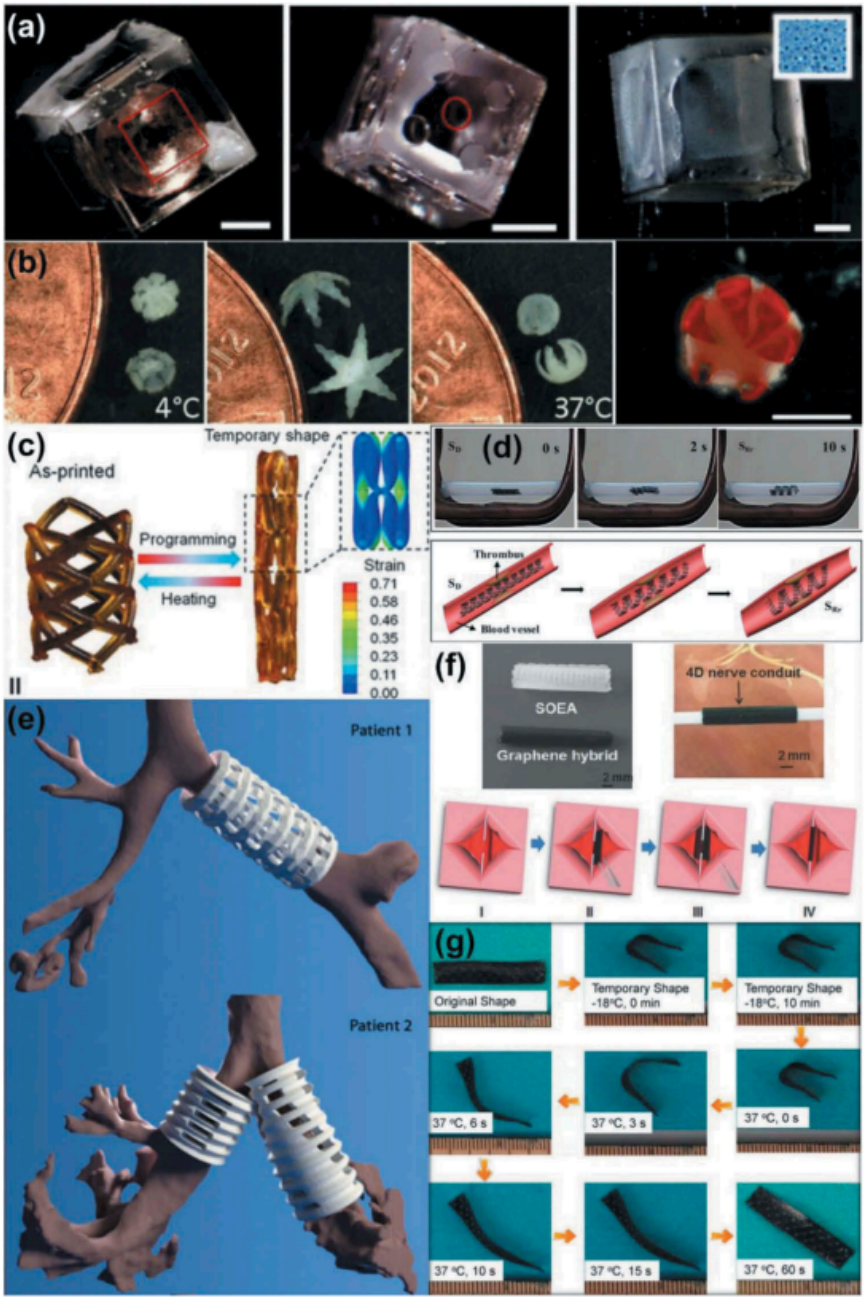

Figure 2.15: 4D printed medical devices. (a) Drug delivery polymer containers obtained through photolythography, with different patterned porous faces outlined in red [18]. (b) Shape Changing demonstration of a thermo-responsive theragripper. The rightmost image shows the device gripping a lump of cells [19]. (c) 4D printed stent [20]. (d) 4D printed magnetic stent [21]. (e) Surgically implanted 4D printed air-way splints [22]. (f) 4D printed nerve guidance conduit [23]. (g) Shape Memory demonstration of a 4D printed scaffold structure [24].

2.2.4.2 Soft Robotics

Soft robotics is a branch of robotics that emerged due to the necessity of equipment capable of organic operations mimicking, for example, the grip of a human hand. This branch makes use of soft materials like special elastomers to fulfil the aforementioned functions, assuring a soft and non-damaging interaction between the robots and their environment [15].

This soft interaction between the printed actuator and the environment is somewhat of a double-edged sword, because although it allows the the former's shape changing process to occur without damaging the object it is interacting with, it also compromises the maximum gripping/actuation strength. As research on different SMMs and actuator designs moves forward, it is expected that a better comprehension on the trade-off between shape memory properties and actuation force is reached, in hopes of achieving widely functional soft actuators.

Most applications in soft robotics materialize in the form of shape changing actuators (figure 2.16) and hydraulic or pneumatic actuators (figure 2.17).

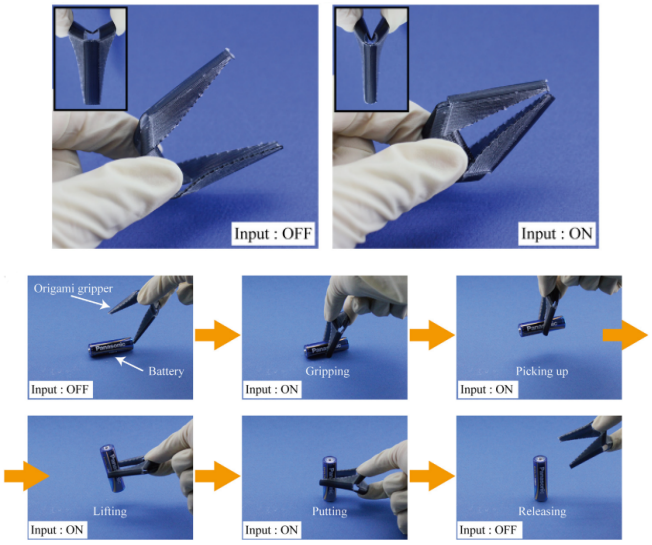

Figure 2.16: 4D printed origami gripper and its shape memory demonstration [25].

Figure 2.17: Pneumatic soft actuator - Artificial muscle [26].

2.2.4.3 Self-Deployable Structures

Self-deployable structures have recently transitioned from a conceptual stage to a practical stage. One of the main reasons for this is the emergence of smart materials and 4D printing, which enabled self-assembly through the manifestation of the SME of said materials on carefully designed localized swelling or shrinking areas.

The present subchapter will briefly overview recent representative applications of self-deployable or self-construction structures developed using 4D printing and SMPs/SMPCs [15].

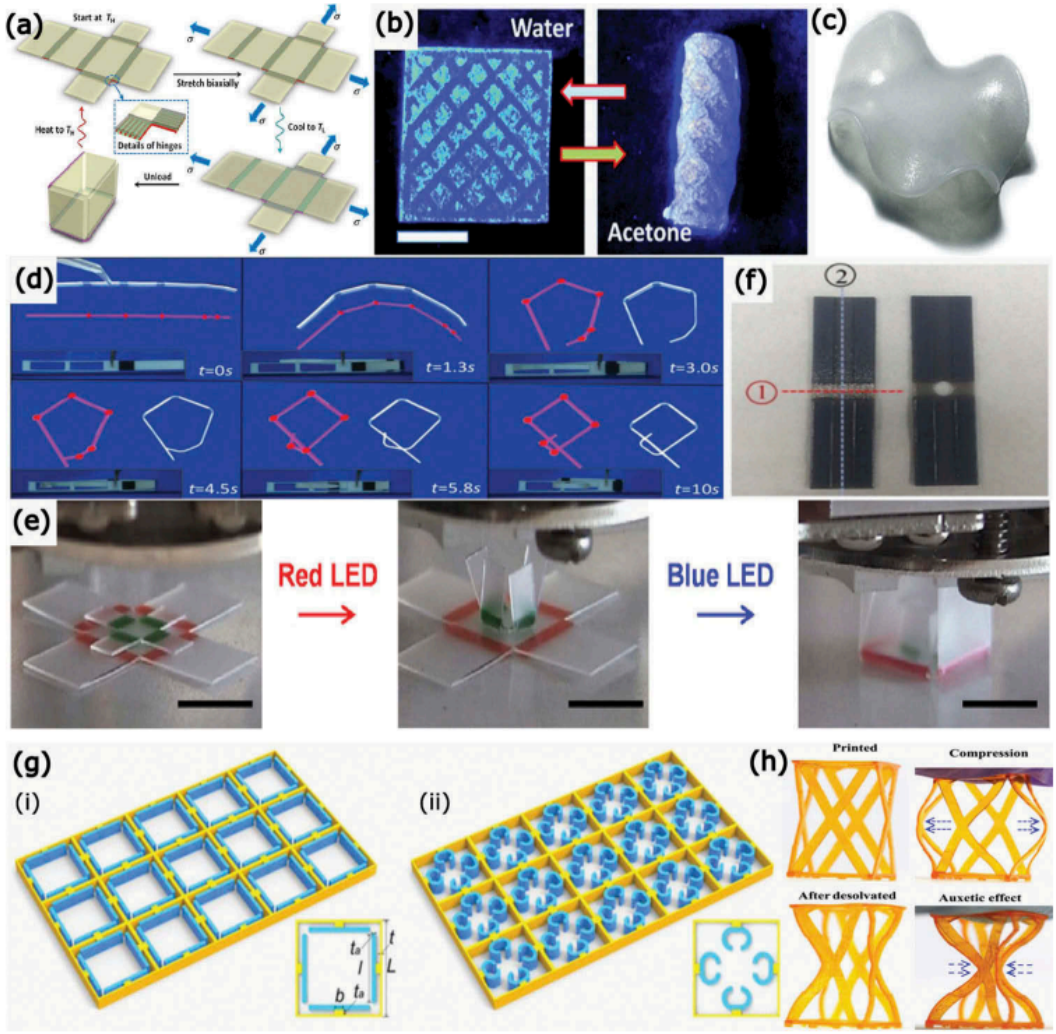

Figure 2.18: 4D printed self-deplolyable structures. (a) Self folding cubic container made with SMPs [27]. (b) Smart polymer self-rolling tube container actuated by acetone [28]. (c) Complex curved geometry deformed from a flat state, printed using hydrogels with a gradient distribution [29]. (d) Self-lockable sequentially folded stipe structure, where the joint are printed with different combined SMPs [30]. (e) Self nested cubic boxes with different coloured SMP joints [31]. (f) Cross folding test specimens with (right) and without (left) stress release hole [32]. (g) Concept design of a material with a tunable lattice structure which possibilitates bondgap control [33]. (h) Multi-functional scaffold structure with adjustable Poisson's ratio [34].

The following content will focus on smart applications involving the use of SMPCs. As hinted earlier, SMPCs are expected to be given the utmost attention in the field of smart materials, due to their enhanced mechanical properties, wide range of stimuli, large recoverable stresses and strains, biocompatibility, biodegradability, customizable transition temperature and multifunctional nature. This set of advantages allows for applications ranging from micro- to large-scale in areas such as the construction, biomedical and smart textile industries, as well as in self-healing applications.

Currently, most research in smart applications using SMPCs is directed towards the development of deployable structures like hinges, trusses, antennas, solar arrays and even habitats, for use in the aerospace and space industries [35].

The following list compiles some notable SMPC applications and comments on each case's achievements and possible improvements.

1. **Deployable Space Habitat Structure**

   Herath et al. [35] managed the creation of a carbon fiber reinforced SMPC self-deployable structure that managed near 98% shape recovery when stimulated by both heat and near infrared radiation. The structure also achieved a volume reduction of almost three times in its programmed state (figure 2.19), whilst managing a very respectable mechanical performance.

   The material used in this application was a styrene based SMP reinforced with 0º/90º woven carbon fiber, manufactured via prepreg layup with subsequent vacuum bagging curing. The obtained SMPC sheets were then cut into specimens in order to gather the material's mechanical properties (table 2.2) and shape memory behaviour (figures 2.21).

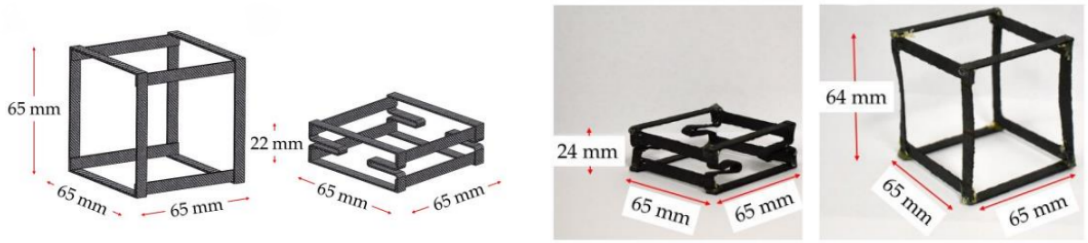

(a) Concept deployable cube in its deployed (left) and contracted (right) state.

(b) Real deployable cube model contracted (left) and deployed (right).

Figure 2.19: Self-deployable cube structure [35].

Figure 2.20: Shape recovery sequence of the deployable cube structure [35].

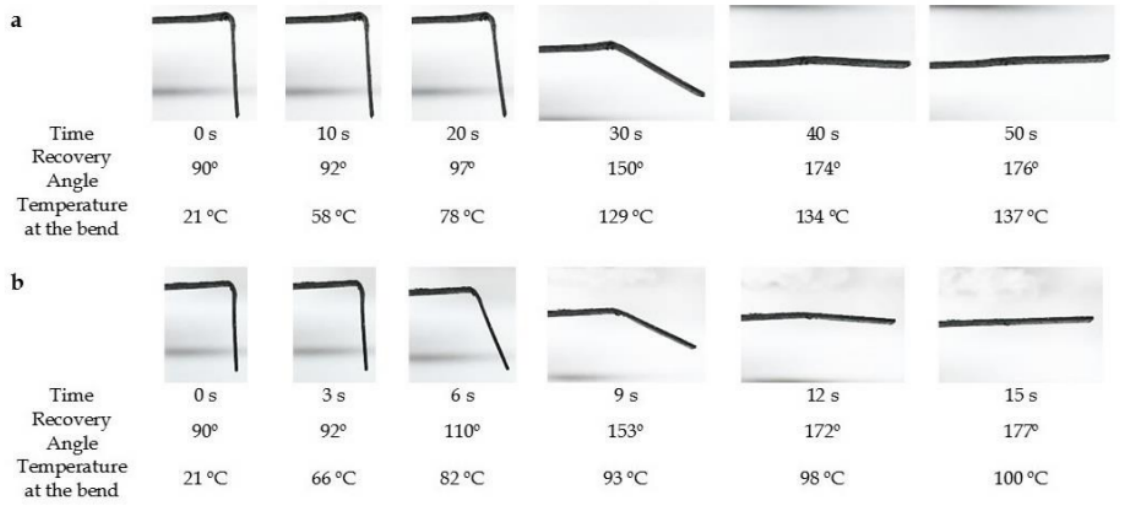

Figure 2.21: Shape Memory behaviour of a 90º bent SMPC segment (a) Stimulated with an 808nm NIR radiation (b) Stimulated with heated air. [35].

	Tensile strength (σ)	Young's Modulus (E)	Compressive Strength (f'_c)	T_t	Shape Fixity Ratio (R_f)	Shape Recovery Ratio (R_r)
Styrene based SMP 0º/90º woven carcbon fiber	517 MPa	42 GPa	120 MPa	98ºC	100 %	98 %

Table 2.2: Deployable Cube's SMPC Mechanical and Shape Memory properties [35]

Although the developed self-deployable structure managed impressive shape memory behaviour and multi-stimuli activation, it only managed to do so in a somewhat lengthy time of approximately 18 minutes, all the while not actually achieving a full reinstatement of its initial shape. This last setback was caused by stresses developed in the structural members, so further investigation on the constrained stress strain recovery of the model would be recommended.

In conclusion, the reviewed work showed that SMPCs can be used in the elaboration of functional self-deployable space habitats, and thus constitutes a good "role model" for the intended final product of this dissertation.

2. **SMPC Cubic Deployable Support Structure**

   In this study, F. Li et al [36] developed a cubic deployable support structure consisting of 4 dependent spacial cages. Each of the cages are composed of 12 three-longeron SMPC truss booms and their respective end connections, as shown in figure 2.22.

   Figure 2.23 lists the components that make up the cubic deployable structure. The three longeron deployable laminate unit stands as the main modular entity of the structure and it is composed of one extendable central bracket, arc-shaped deployable laminates, and connectors.

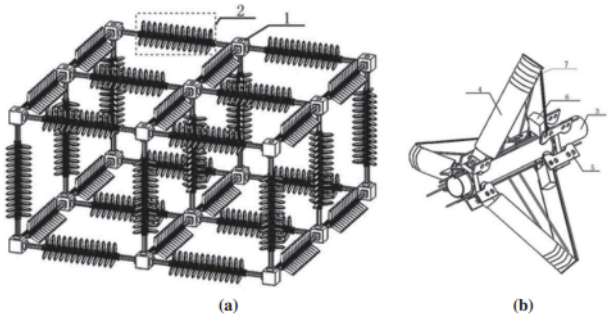

Figure 2.22: (a) Cubic Deployable Support Structure Concept. (b) Three Longeron Deployable Laminates Unit. 1 – end connection, 2 – three-longeron SMPC truss boom, 3 – extendable central bracket, 4 – arc-shaped deployable laminate, 5, 6 – connectors, 7 – resistor heater [36].

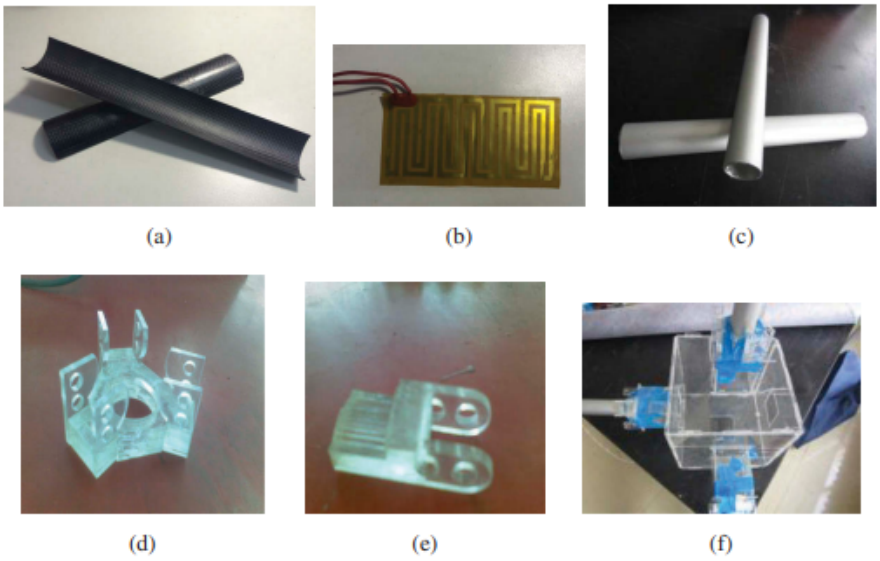

Figure 2.23: Cubic Structure's main components (a) arc-shaped deployable laminate, (b) resistor heater, (c) extendable central bracket, (d, e) connectors, (f) end connection. [36].

The primary material choice for this work, more specifically for the deployable laminates, was a type of carbon fiber-reinforced epoxy-based SMPC, fabricated via hand molding where the reinforcement consisted of four plies of plain carbon fabric.

After a Dynamic Mechanical Analysis (DMA) was carried with the intent of obataining basic thermo-mechanical properties of the SMPC, the results showed a transition temperature of 100ºC and a storage modulus of 7 GPa at 20ºC.

The shape recovery stimulus used for this work was heat provided by the resistors placed on the inside surface of the arc-shaped deployable laminates.

As for the deployment method itself, it can occur in two distinct ways. The first consist in the simultaneous deployment of all the SMPC truss booms in all three orthotropic directions (figure 2.24). The second involves deploying all the truss booms in a given direction at the

same time, and when that action is carried out the deployment in a different direction can begin. This process is repeated until full deployment is reached.

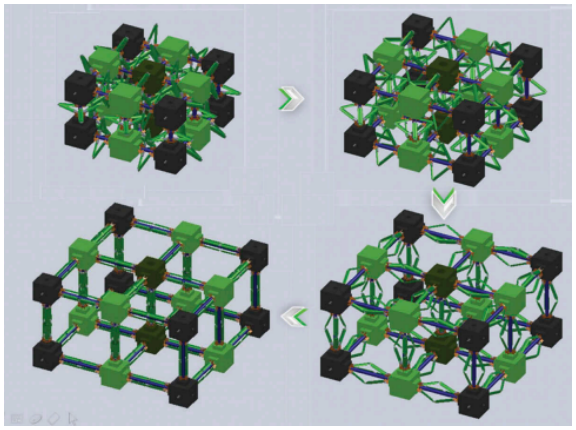

Figure 2.24: Cubic Structure's simultaneous deployment in all three orthotropic directions [36].

The deployment process was also evaluated with respect to its most favourable direction, as seen in figure 2.25. The direction which saw the fastest deployment time was direction (c), with 420s. The average deploying time was 465s, and this value accounts for the average load-bearing force of each three longeron deployable laminate unit of 8,37N, although this value isn't to fully trusted given the rough experimenting conditions.

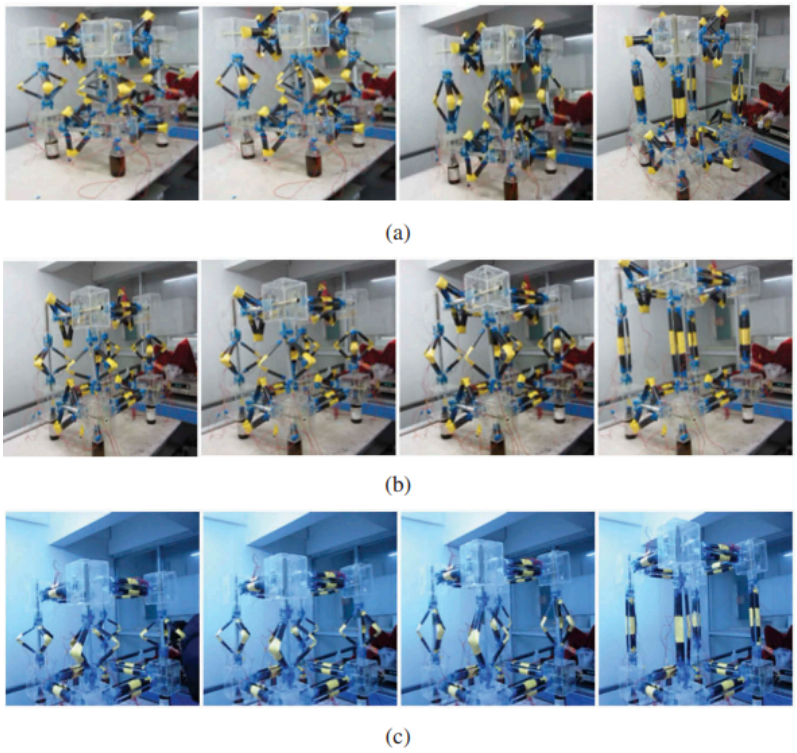

Figure 2.25: Cubic Structure's recovery tests in three different directions (a), (b) and (c) [36].

An experiment attempting to determine the maximum three-longeron deployable laminates unit bending recovery force was also performed, and it resulted in a maximum vertical load of 8,5 N.

All in all, this study introduced a cubic support structure that managed to autonomously deploy (all be it with the aid of the heat resistors) without the need for any complex mechanical devices, though the maximum recovery force and deployment time still need improvement. This research also cements itself as one of the explorations of SMPCs in large-scale deployment applications, setting a staple for more advanced models to come in the future.

3. **Autonomous Programmable Actuator and Shape Reconfigurable Structures Using Bistability and Shape Memory Polymers**

   The following work, made reality by Chen et al. [37] sought to implement the bistability principle with the goal of crating a self-deployable structure. To that end, a bistable 4D printed programmable actuator was designed and tested.

   This bistable actuator (figure 2.26) would be activated via change in the surrounding temperature and would integrate a shape memory polymer strip (SMS) as the temperature controllable energy source and a bistable mechanism as the linear actuator and force amplifier, as seen on figures 2.29 and 2.28, respectively.

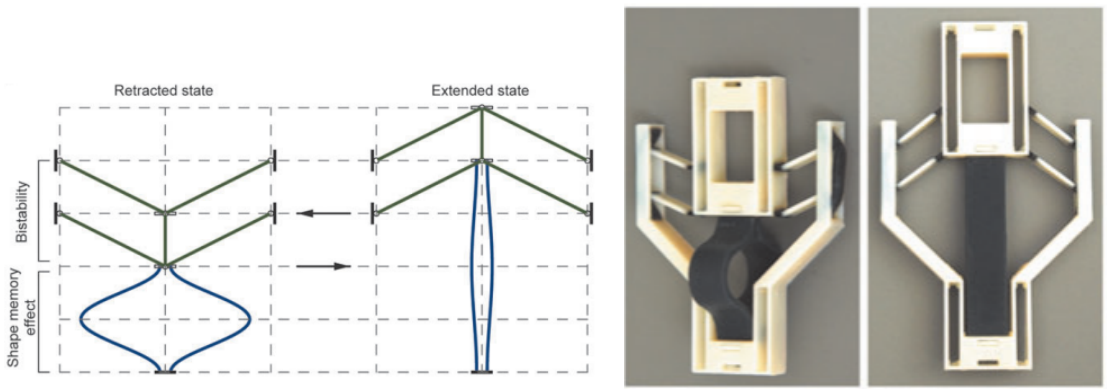

(a) Bistable actuator schematic activation. (b) Unit actuator activation demonstration.

Figure 2.26: Bistable Actuator Unit [37].

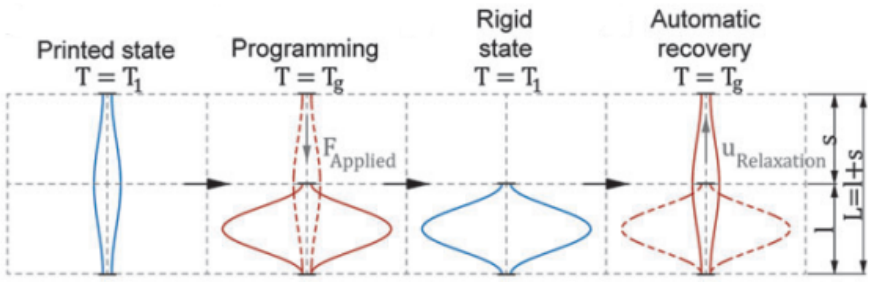

Figure 2.27: Bistable actuator unit working scheme [37].

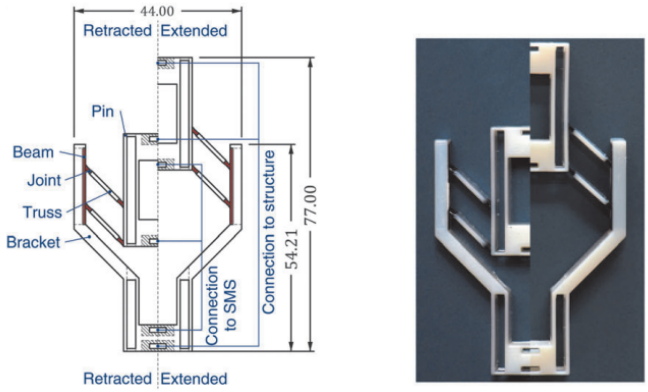

(a) (b)

Figure 2.28: Bistable Mechanism concept (a) and specimen (b) [37].

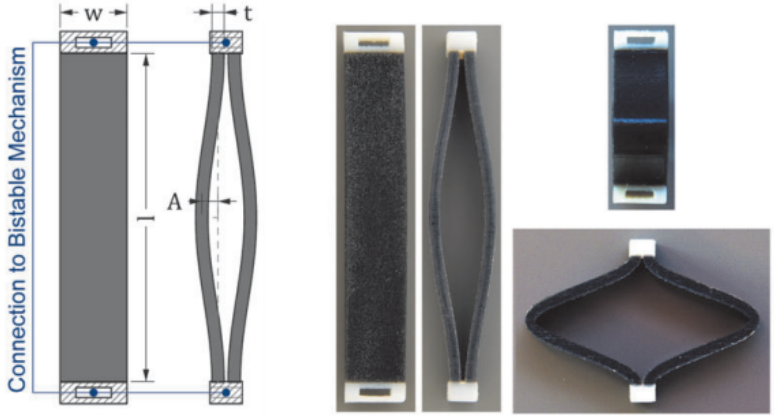

(a) (b)

Figure 2.29: Shape Memory Strip (SMS) concept design (a) and specimen (b) [37].

The bistable unit actuator makes use of the previously explained Shape Memory Effect provided by the SMP to either expand or contract under temperature change, enabling autonomous deployment and shape reconfiguration. The materials experimented for the Shape Memory Strips of the actuators were a few special Shape Memory Thermoset resins, such as the PolyJet Photopolymer Agilus30 and the Rubber-Like Digital Material FLX9895, obtained through a multimaterial inkjet technology which selectively deposited photoreactive liquid resins of different stiffness and transition temperatures.

The actuator is also designed to to be assembled into larger deployable and geometrically reconfigurable structures, like the ones present on figure 2.30. The structures initially seen in the image time lapse correspond to 2D designs that deploy into 3D layouts as the teperature increases. This is one of the main requirements for the shelter solution to be developed in this work, as it allows for easy transportation due to the low volume of the contracted design.

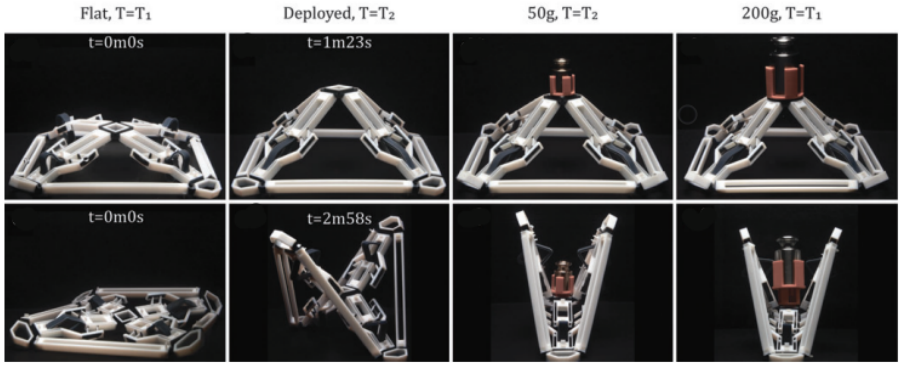

Figure 2.30: Geometrically reconfigurable structures showing shape recovery and load-bearing capabilities, along with their respective deployment times. T_1=22ºC, T_2=40ºC [37].

Though the maximum additional weight which the structures managed to hold was an underwhelming 200g (and the self-weight of the structure was neglected due to the low density of the materials used - 1175 kg/m^3), the replacement of the used SMP for another SMP with higher elastic strength, or even for a SMPC should improve the load-bearing capabilities by a large margin.

There is also the possibility of creating structures capable of sequential activation, by tailoring each SMP to a distinct activation time (basically means using SMPs with different transition temperatures or different SMPs altogether). This feat is demonstrated on figure 2.31.

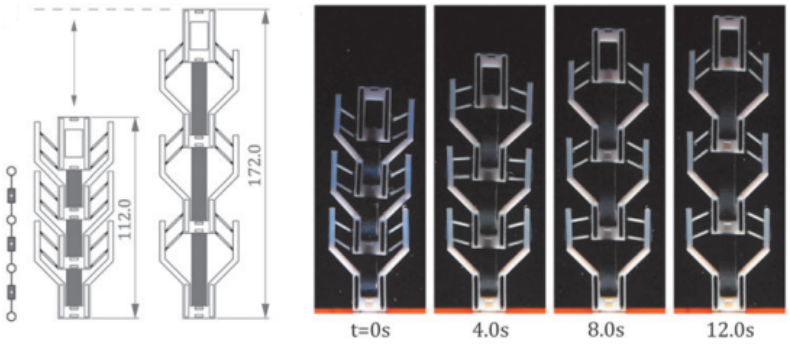

Figure 2.31: Sequential activation of multiple bistable unit actuators [37].

This particular application showed the potential benefits that the combination of materials capable of manifesting Shape Memory Effect and mechanical bistability can have across various engineering fields. Though there were some constraints regarding the fabrication method of the Shape Memory Strips, as well as a poor structural performance, these could most definitely be mitigated and improved with further research on a technological level and with the simple replacement of the used materials with ones with higher structural prowess. The work performed by Chen et al. also opens up the oportunity for gathering the obtained

experimental results in hopes of refining and developing algorithms to generate and optimize large-scale reconfigurable structures.

2.2.5 Fiber Reinforced Filaments for 3D Printing

With the increasing notoriety of composite materials in recent times, it didn't take long for their implementation in 3D printing technology. The introduction of composite filaments has significantly expanded the capabilities of 3D printing, enabling the fabrication of parts with enhanced mechanical strength, improved heat resistance, superior durability, and unique functionalities. By combining traditional thermoplastic matrices with reinforcing fibers, particles, or additives, composite filaments offer a wide range of material options and applications.

Composite filaments leverage a diverse range of matrix materials such as polylactic acid (PLA), acrylonitrile butadiene styrene (ABS), nylon, polyether ether ketone (PEEK), and others, which provide the desired mechanical, thermal, and chemical properties required for specific applications. As for the reinforcement of the polymeric matrix materials, synthetic fibers such as carbon fibers, glass fibers, and aramid fibers are usually preferred. These fibers are incorporated into composite filaments to enhance the strength, stiffness, and impact resistance of the printed parts. Additionally, particles and additives like metal powders, ceramics, graphene, and carbon nanotubes can be included to provide unique properties like electrical conductivity, thermal management, or magnetic behavior.

Regarding the production of composite filaments, various techniques are employed, including melt compounding, solution blending, and in-situ polymerization. Melt compounding (see figure 2.32), which stands as the most commonly used method, involves the extrusion of a thermoplastic matrix with reinforcing materials. The overall filament quality is directly correlated with the control parameters during filament manufacturing, and can be validated by observing the filament's geometry and fiber distribution, among other things.

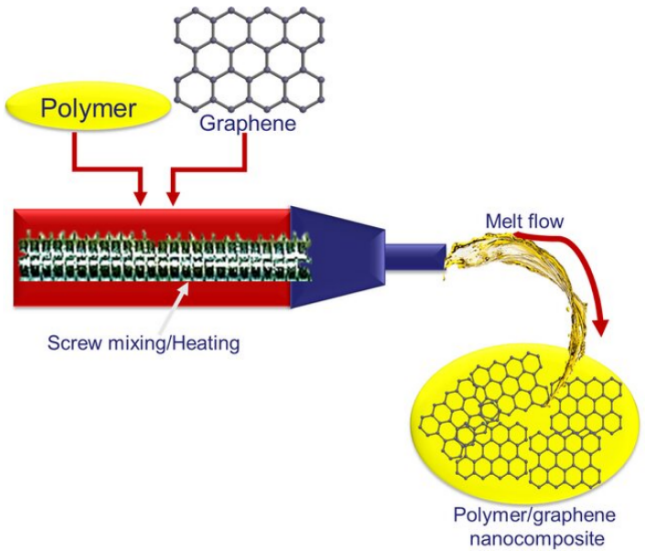

Figure 2.32: Melt compounding set-up of polymer/graphene nanocomposite. [38].

The implementation of composite filaments in 3D printing technology didn't come without its difficulties. Though previously mentioned printing methods such as fused filament fabrication

(FFF), selective laser sintering (SLS), and digital light processing (DLP) are compatible with composite filaments, certain considerations regarding nozzle wear, filament breakage, and print defects need to be addressed when printing with these filaments. The integration of composite filaments in 3D printing has unlocked new possibilities across numerous industries. Aerospace, automotive, consumer products and medical sectors have seen remarkable advancements. Some examples include include the production of lightweight and high-strength aerospace components [63], customized medical implants with tailored properties [64; 65], functional durable prototypes for product development [66], and tooling applications with improved wear resistance [67].

While significant progress has been made in the field of 3D printing with composite filaments, many challenges still remain. These include optimizing filament composition, developing robust printing guidelines, and addressing interfacial adhesion between the matrix and reinforcements. Future research should focus on advancing composite filament manufacturing techniques, exploring new reinforcement material alternatives, and developing reliable multi-material printing systems.

2.2.6 Extrusion Process Flow Characterization

In an endeavor to optimize time efficiency and mitigate potential incidents during the installation of the aforementioned extrusion equipment, a numerical simulation was employed. This simulation aimed to emulate the desired effects by employing numerical methods to forecast the die-swelling phenomenon observed at the extruder's outlet and the pressure drop encountered around the die-air interface of the extrusion apparatus.

Die-swelling refers to the phenomenon where the diameter of an extruded polymer or composite filament expands upon exiting the die, and it can occur due to various factors, such as elastic recovery, molecular relaxation, viscous dissipation and wall slip.

The resulting simulation outcomes were subsequently compared against findings derived from analytical models documented in existing literature, followed by evaluation and potential validation. It should be noted that the methodologies in question solely assess the flow characteristics of the molten polymer, excluding the reinforcing fibers, and merely serve as an initial indication of the ideal flow parameters for the extrusion process.

Analyzing the dynamics of a polymer extrudate presents a challenging task due to the intricate nature of unsteady movement exhibited by the viscous molten fluid, along with other influential factors such as fluid compressibility, the nature of contact between the melting flow and the extrusion chamber's walls, and alterations in the physical state of the molten material. Furthermore, the non-linear dependencies of a polymeric material's properties on temperature and shear rate bring additional difficulties to the modeling process. Consequently, a number of assumptions were employed to simplify both the analytical and numerical models, facilitating expedited acquisition of results. Thermoplastic materials such as PLA exhibit shear thinning behaviour, i.e., the viscosity decreases when the shear rate increases. This opens up the possibility of using more complex models such as the Bird Carreau law and the Cross law, which account for yield stress, though various works have demonstrated that a simpler model in the form of a power law manages to obtain results in conformity with their experimental counterpart for the modeling of generalized Newtonian fluids. As such, the adopted model culminated in a steady-state problem featuring a Power Law based mathematical model for the modeling of a generalized Newtonian fluid. Accordingly, the power law states:

$$\tau = \left(\frac{\dot{\gamma}}{\phi}\right)^{\frac{1}{m}} \tag{2.1}$$

where τ is the shear stress, $\dot{\gamma}$ is the shear rate, and ϕ and m are material constants and correspond to the fluidity and flow exponent, respectively. This flow exponent (m) is responsible for encapsulating the general flow characteristics of a given material, as it reflects the deviation of said material from Newtonian behaviour.

According to [39], three distinct extruder regions can be identified, as seen in figure 2.33. The first region (I) encapsulates the whole of the extruder's region up until its conic feature, which by

itself constitutes region II of the liquefier. Region III corresponds to the volume comprised by the shaped die of the extruder.

Performing a momentum flux balance on a fluid element and applying the Power Law to each of the previously specified regions, it is possible to determine the total presssure drop on the extruder apparatus:

$$\Delta P_{1_\upsilon} = 2L_1 \left(\frac{\upsilon}{\phi}\right)^{\frac{1}{m}} \left(\frac{m+3}{(D_1/2)^{m+1}}\right)^{\frac{1}{m}} \tag{2.2}$$

$$\Delta P_{2_\upsilon} = \left(\frac{2\cdot m}{3\cdot tan(\beta/2)}\right)\left(\frac{1}{D_2^{3/m}} - \frac{1}{D_1^{3/m}}\right)\left(\left(\frac{D_1}{2}\right)^2 (m+3)\cdot 2^{m+3}\right)^{1/m} \tag{2.3}$$

$$\Delta P_{3_\upsilon} = 2L_2 \left(\frac{\upsilon}{\phi}\right)^{\frac{1}{m}} \left(\frac{(m+3)+(D_1/2)^2}{(D_2/2)^{m+3}}\right)^{\frac{1}{m}} \tag{2.4}$$

where D_1 and L_1 correspond to the diameter and length of the extruder (section I) and D_2 and L_2 represent the diameter and length of the nozzle tip (section III). β stands as the convergence angle of the extruder-tip diameter transition, and υ is the velocity of the material at the entrance of the liquefier.

The total pressure drop can then be computed by adding the three pressure drop values for each section of the extruder device.

$$\Delta P_\upsilon = \Delta P_{1_\upsilon} + \Delta P_{2_\upsilon} + \Delta P_{3_\upsilon} \tag{2.5}$$

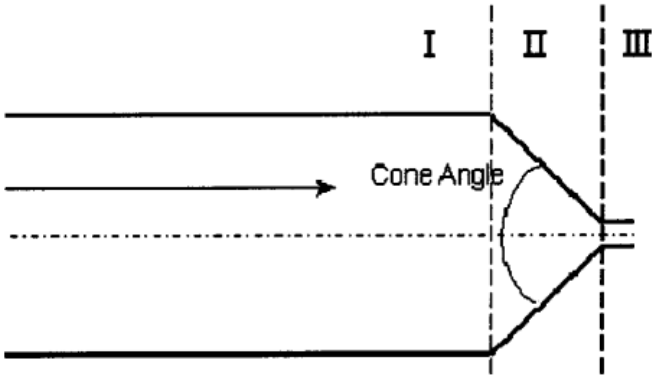

Figure 2.33: Regional decomposition of an Extruder apparatus [39].

The previously hinted at relation between shear stress and die-swell comes in the form of the following expression, according to [68]:

$$\frac{D}{D_c} = \left[1 + \frac{1}{2}\left(\frac{N_1}{2\tau}\right)_w^2\right]^{1/6} \tag{2.6}$$

with D being the maximum die-swell induced diameter and D_c the die tip diameter. N_1 corresponds to the First Normal stress difference or, to put it simply, the first component of the normal stress tensor, which can be calculated using equation 2.7 [69]. τ represents the local shear stress value at the extruder's exit, which can naturally be obtained via the priorly presented Power Law-based expression (equation 3.2).

$$N_1(\dot{\gamma}) = 2|\tau|\sqrt{1-n^2}n^{-1.4} \tag{2.7}$$

This expression is commonly known as the Sharma-McKinley Equation, where N_1, $\dot{\gamma}$, τ represent the previous enumerated parameters, while n stands as the local slope of the flow curve, and can be denoted as:

$$n = \frac{dln\tau}{dln\dot{\gamma}} \tag{2.8}$$

According to the presented information, the numerical simulation took place and is registered and explained with detail on section 3.2.1 of the upcoming experimental chapter 3.

Chapter 3

Experimental Tests

This chapter will register the experimental trials performed, necessary to not only corroborate the previously explored theoretical concepts, but also to validate the acquired materials' properties by comparing them with results present in the literature.

Efforts will also be made with the goal of developing a functional filament extruder machine with the available resources at both FEUP and ISEP.

As priorly mentioned, this research attempts to use SMPCs in order to mitigate the formerly appointed shortcomings. The materials acquired for the completion of such a task, having in mind the geographical and monetary limitations at place, ended up being:

- **Polylactic Acid (PLA)** as the polymeric matrix to the composite material, acquired from Smartfil (Smart Materials 3D);
- **Carbon Fiber (CF)** as the reinforcement fiber material to the composite material, acquired from Teijin Tenax;

Both the polymeric matrix and reinforcement fiber materials' data sheets are presented in Appendices A and B, respectively.

As such, the present chapter will be divided in 3 parts, which will report on the experiments involving the characterization of the acquired polymer, the setup and development of the filament extruder installation and the conception and production of the CF reinforced Shape Memory Polymer Composite filaments.

3.1 PLA

Polylactid Acid, also known as PLA, is a biodegradable polymer commonly used in 3D, and by extension 4D printing applications. It stands as a linear aliphatic thermoplastic polyester derived from fully renewable sources such as corn and wheat, which grants it high biocompatibility, high stiffness and UV stability, making it the most used biopolymer in current biomedical, textile and food packaging applications. PLA, however, also suffers some shortcomings regarding its brittleness and low temperature resistance, justifying the need for combining it with reinforced materials,

such as natural or synthetic fibers [70]. Generally, natural fibers are more sustainable and environmental friendly, but lack the strength that synthetic fibers possess and are also tougher to disperse in the polymer matrix.

The PLA samples obtained for the following experiments were purchased from Smartfil - by Smart Materials 3D, Jaén, Spain. Some of the material's most relevant physical, mechanical and thermal properties were noted on the PLA's technical data sheet, and are exhibited on table 3.1. Additional printing data parameters, along with the data already presented are also present in Appendix A. Though more reliable materials were available for the task at hand, PLA stood as an economic option that better suited the experimentative nature of the performed tests.

Polylactid Acid (PLA)	Value		Unit	Standard
Physical Properties				
Density	1.24		g/cm^3	ASTM D792
Mechanical Properties	XY plane	ZX plane		
Tensile Strength	55.5	43.8	MPa	ISO 527
Tensile Modulus	4.6	3.130	GPa	ISO 527
Flexural Strength	107	18	MPa	ISO 178
Flexural Modulus	3.12	2.5	GPa	ISO 178
Elongation at max. Stress	1	1.4	%	ISO 527
Elongation at break (traction)	1.1	1.4	%	ISO 527
Elongation at break (bending)	5.2	1.8	%	ISO 178
Impact strength (Charpy impact test)	17.5	7.0	kJ/m^2	ISO 179
Hardness	85		Shore D	ISO 7619-1
Thermal Properties				
Glass Transition Temperature	60		ºC	ISO 11357
VICAT B (50 N 50ºC/h)	59		ºC	ISO 306
HDT B (0.45 MPa)	60		ºC	ISO 75

Table 3.1: Smartfil's PLA physical, mechanical and thermal properties

VICAT and HDT are experimental tests which output the Vicat softening point and the heat deflection temperature, respectively.

The former test determines the softening point for materials with no definite melting point, such as thermoplastic polymers. In the B variant of the VICAT test, the temperature at which the specimen is penetrated to a depth of 1 mm by a flat-ended needle with a 1 mm^2 circular or square cross-section is registered, and the applied load is 50 N with a heating rate of 50ºC/h.

The HDT test establishes the heat deflection temperature, which corresponds to the temperature at which a polymer or plastic sample deforms under a specified load. In the case of the HDT B test, the corresponding load is 0.45 MPa and the temperature is increased at 2 °C/min until the specimen deflects 0.25 mm [71]

To obtain a more complete characterization of the polymer, there are still properties that must be registered, namely regarding the thermal behaviour of this particular PLA. As such, a set of

experimental tests were realized with the intent of securing important parameters for the better characterization of the material to be used.

3.1.1 Melt Flow Index (MFI) test

In recent years, the demand for thermoplastic polymers in granular form has increased, steadily becoming the go to base material form in the production of plastic products. As such, tight physical and chemical testing of these materials is necessary so that they can be used for their intended applications.

One of any thermoplastic's most important physical properties is its Melt Flow Rate (or Melt Flow Index or Melt Index), as every processing technique that uses these materials entails the flow of melt polymer. Melt Flow Index is a measure for a melted plastic's flowability. This property is obtained through a test that requires specific equipment (MFI tester), whose working principle is based on material extrusion, and is calculated as the mass of the material in grams flowing per 10 minutes (g/10min) [72].

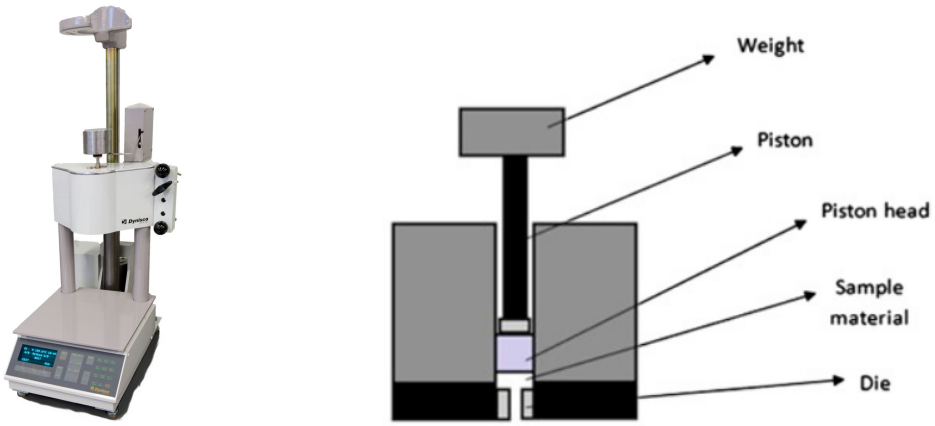

(a) (b)

Figure 3.1: MFI Tester machine. (a) Dynisco LMI 4000 [40]. (b) Basic construction of a melt flow tester [41].

The test was performed at the laboratory of composite materials at ISEP, which provided all the necessary testing equipment. The MFI tester model used was the one seen in figure 3.1a. Figure 3.1b also shows the basic construction of a MFI tester machine. This equipment consists of a cylindrical barrel wrapped and surrounded by a heater coil, which itself has an outer layer of insulation material to restrict the heat losses. The heater is automatically controlled by a process control box. The system also garners a standard weight applied through the piston, a piston head and dies to deposit the materials.

As for the test itself, it acted in accordance with the ASTM D1238 standard, following a prescribed set of steps:

1. Programming the tester machine with the adequate temperature and set time.

2. Preparing 2 samples of 7g of the PLA material.

3. Letting the test run for 10 minutes and then collect the melt material extruded from 15 to 15 seconds.

4. Registering the weight of the obtained extruded samples and calculating the MFI of the material.

After registering the weights of the obtained extruded samples, a mean value for the weight was obtained. This value was then interpolated to match the weight of the PLA after 10 minutes of extrusion, following the simple formula shown below:

$$MFI = \frac{M_w[g] \cdot \frac{600}{15}[s]}{10[min]} \tag{3.1}$$

With M_w corresponding to the mean weight of the samples extruded every 15 seconds.

The experimental value obtained for the M_w **was 0.3681g, which led to an MFI value of 14.72 g/10 min**.

As seen in figure 3.2, the obtained value for the MFI is within the range of studied PLA materials present on the database, and isn't far off of the average 12.6 g/10min value.

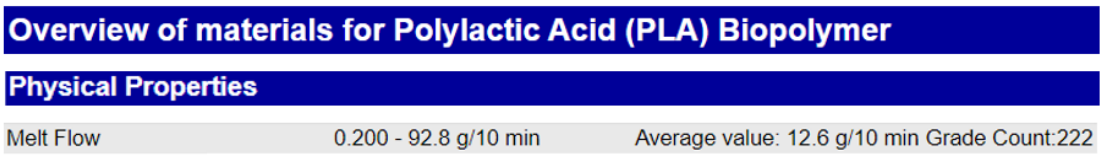

Figure 3.2: Melt Flow Index overview for PLA biopolymers [42].

3.1.2 Thermogravimetric Analysis (TGA)

It is also important to evaluate the acquired polymer's performance and consistency when subjected to temperature change. Thermogravimetric analysis or thermal gravimetric analysis (TGA) is a method which observes the material's physical and chemical changes as a result of an increase in temperature, and stands as an indication of a material's thermal stability. The method in question basically consists in the measurement of weight loss in a user-defined heating process, and provides insight about physical phenomena such as phase changes and absortion as well as chemical phenomena including thermal decomposition and oxidation reactions. The main parameter to be determined with this test, though, is the material's degradation temperature, which corresponds to the highest weight loss drop seen in the weight percentage per temperature curve [73].

This specific test is conducted on a device known as the thermogravimetric analyzer, which continuously measures the mass of a sample while the temperature is changed over time. Mass, temperature and time are the three basic parameters to be registered by these instruments, though more recent equipment also manages to measure other parameters such as moisture, volatiles and ash [74].

The test was conducted by credited workers at ARCP, an UPTEC branch. The samples consisted of the acquired PLA's pellets, which had to be cut in order to reduce their weight and be processed by the thermogravimetric analyzer. This instrument consists of a precision balance with a sample pan located inside a furnace with programmable control temperature. As for the procedure followed, the analyzer can be operated in three ways [75]:

- **Isothermal or static thermogravimetry**: in this technique, the temperature is kept constant and the sample's weight is recorded as a function of time.
- **Quasistatic thermogravimetry**: in this technique, the sample temperature is raised in sequential steps separated by isothermal intervals, during which the sample mass reaches stability before the start of the next temperature ramp.
- **Dynamic thermogravimetry**: in this technique, the sample is heated in an environment which changes its temperature in a linear manner.

The experiment was carried out under a predetermined set of conditions, which are listed below:

- Number of samples: 3
- Initial temperature: 20ºC
- Final temperature: 450ºC
- Heating rate: 10ºC/min
- Mass of each sample: 15mg

- Air atmosphere

This particular quasistatic thermogravimetry culminated in the determination of a mass % vs temperature curve for the acquired PLA, which is displayed in figure 3.3.

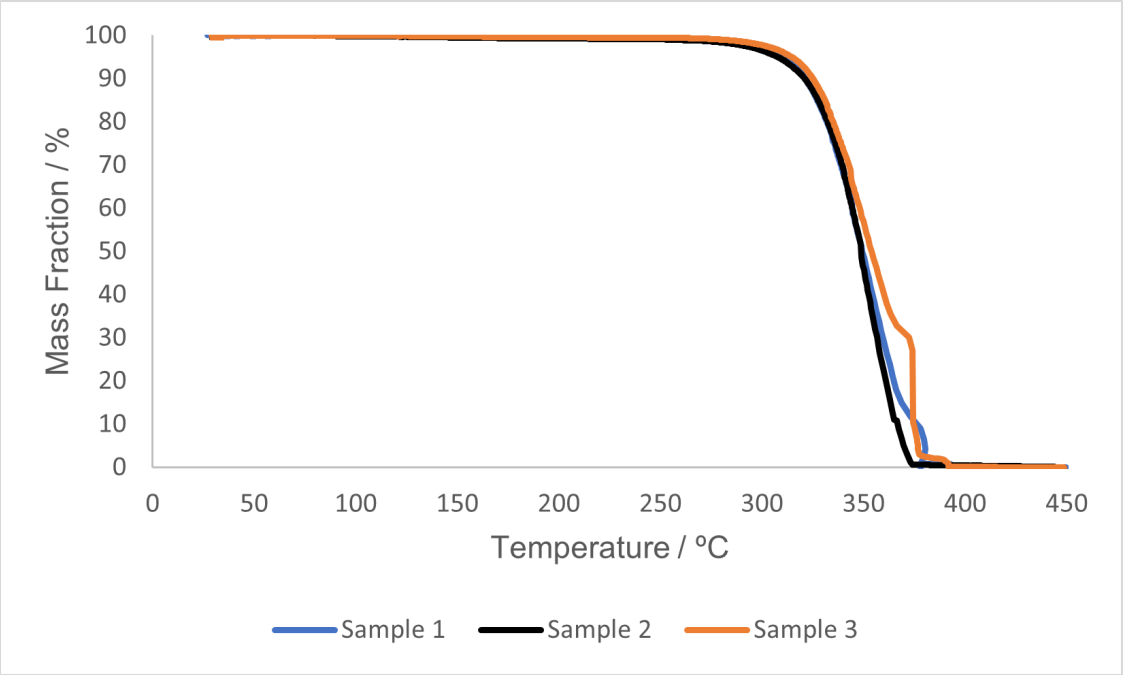

Figure 3.3: Mass fraction vs Temperature plot of the provided PLA samples.

As seen, the thermal degradation for this particular PLA begins at approximately 325ºC and leads to a mass loss of 100% by the time the temperature nears 380ºC. This value is within the range of degradation temperatures found in the literature for similar PLA polymers.

3.2 Filament Extruder development

The present section attempts to describe and register all the theorycrafting and advancements related to the development of an innovative reinforced SMP filament extruder setup. This setup, unlike the ones common in current usage, simultaneously resembles melt compound and pultrusion setups, in the sense that the reinforcement fibers are pulled through a shaped die immediately after impregnating with the polymer under the adequate temperature.

The main part of the setup is, unsurprisingly, the extruder itself, and it is shown in figure 3.4a. It consists of an aluminium cylindrical barrel through which the fibers impregnate with the polymer and at the end of its course end up coming out of a die with a central hole diameter of 2 mm (figure 3.4b) into the pulling system, where the filaments would then be rolled and stored.

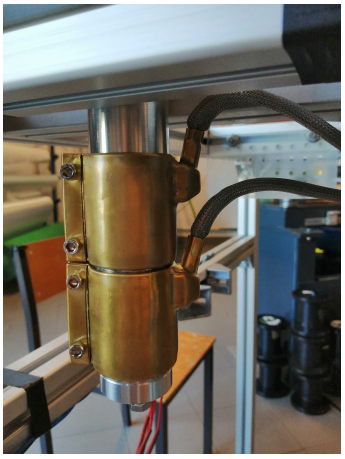

(a) Extruder with resistors.

(b) Cylindrical die.

Figure 3.4: Extrusion machine components.

3.2.1 Extrusion Process Numerical Simulation

Building upon the knowledge gathered on 2.2.6, this subsection seeks to complete the analytical and numerical models in order to gauge the impact of die-swelling and pressure drop phenomena in the extruder's performance.

The priorly introduced expressions, 2.2 to 2.5, rely on the assumption that the flow inside the liquefier is isothermal at a temperature T equal to the deposition temperature. As previously mentioned, material parameters like m and ϕ are needed for the completion of both numerical and analytical models. With the impossibility of performing rheological tests on the acquired PLA, the rheological parameters used were adapted from [76]. In this particular work, a simple Power Law based model (3.2) was employed for the modeling of PLA, which was assumed as a generalized Newtonian fluid.

$$\tau = k\dot{\gamma}^n \tag{3.2}$$

The material parameters gathered from the performed rheological tests in [76], for a temperature of 190 ºC, were:

- k = 4.22E + 08 [Pa]
- n = 0.91

These values would then be implemented in the numerical model with the goal of outputting the necessary shear stress values for the analytical calculation of the die-swell on the extruder tip. Additionally, the pressure drop values can be analytically obtained using equations 2.2 to 2.5.

With the analytical and numerical models established, the commencement of the simulations was imminent. The numerical problem was executed using the student version of the commercially available software *Ansys* ®. An Ansys Workbench Polyflow analysis system module was used and the simulation followed a prescribed set of steps, as outlined below:

1. **Definition of the extruder geometry** - The Ansys SpaceClaim workspace was utilized for this task. To accomplish this, the original design blueprints developed at ISEP were recreated within the aforementioned workspace, accounting for all three spatial dimensions. Consequently, two distinct variations of the extruder geometry were examined. The differentiating factor between these two geometry models resided solely in the presence or absence of an extended volume intended to simulate the air surrounding the extrudate at the die exit, as depicted in figures 3.5a and 3.5b.

   The comparison of results obtained from both models would provide insights into the significance of incorporating the aforementioned feature in the numerical model. Various "air chamber" dimensions were also experimented with in the model design, but ultimately proved to be indifferent to the overall numerical results of the simulation.

(a) (b)

Figure 3.5: Extrudate geometry in Ansys SpaceClaim. (a) air neglecting model. (b) air considering model.

2. **Mesh generation** - After importing the geometric model into Ansys meshing, the extruder part began its meshing procedure. Initially, a linear tetrahedral element uniform mesh, with an element size of approximately 1mm was implemented on the piece. The extrudate area which contacted with the die, being the most relevant for this simulation, received special attention and was refined with a local sizing of the elements, which had an approximate length of 0.25mm. Additionally, mesh inflation was also accounted for and applied in areas near the die lips and the geometry boundaries, in an attempt to increase the mesh quality and subsequently improve the accuracy and reliability of the obtained results. This mesh inflation technique adds additional layers of elements near the boundaries of the geometry by successively refining the mesh elements as they approach the boundary. In turn, this refinement ensures that the mesh resolution is higher near the region of interest, allowing for a more realistic capturing of boundary layer phenomena such as velocity profiles, shear rates, and pressure gradients. The mesh that resulted from the above specified steps is presented in figure 3.6.

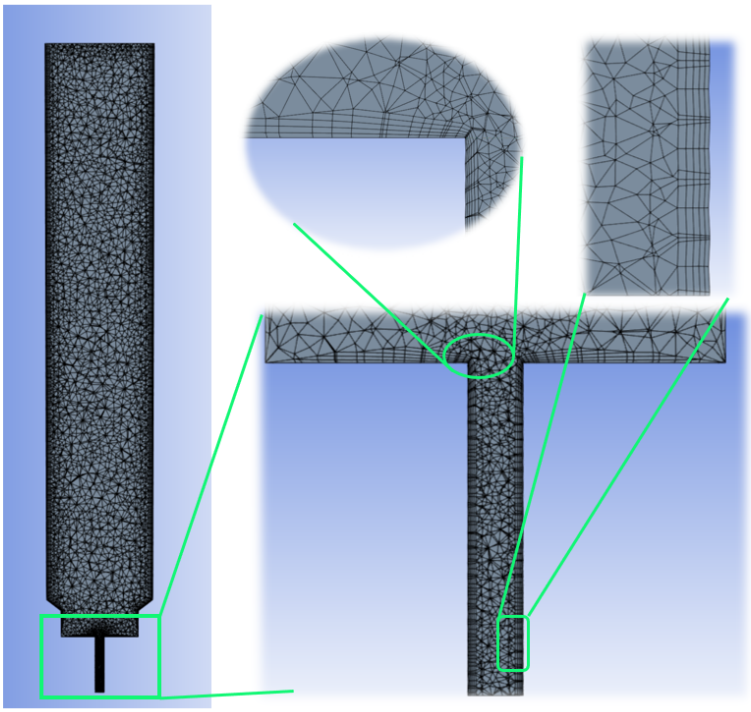

Figure 3.6: Detailed view of the extrudate geometry's final mesh.

3. **Numerical model setup and solution** - The previously defined steady-state finite element problem was manually imported into a polydata component system in Ansys. A sub-task was created where the domain, material data, flow boundary conditions and interpolation options were specified in accordance with the established mathematical model. The following list attempts to briefly summarize the most relevant simplifications and assumptions implemented in the numerical model:

    - The model consisted of a 3 dimensional, steady-state, isothermal finite element analysis involving a generalized Newtonian fluid;
    - The material (PLA in this instance) would flow vertically and downwards, and the flow would be fully developed. Inertia effects were neglected and gravity effects were applied in negative direction the corresponding Y axis;
    - The polymer flow would be characterized by a Power Law expression, so material data was filled out according to the previously listed parameters obtained in [76]. This data consisted of the density and shear-rate dependence of viscosity;
    - A zero wall velocity boundary condition was assumed for the wall contacting areas of the extrudate geometry. Given the similar operating temperature and nozzle diameters of both the MFI test and the projected extruder device, an mass inflow rate of about 15g per 10 minutes, or roughly 0.0245 g/s was assumed for the inlet of the liquefier device.

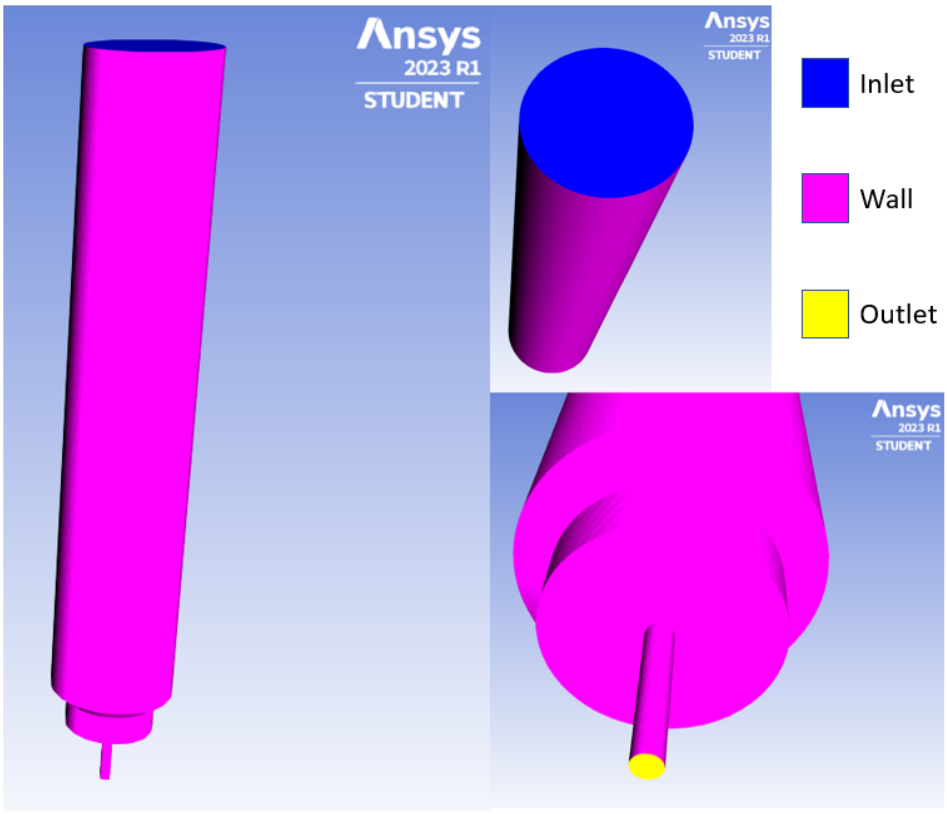

Figure 3.7: Numerical model's geometry sections, with their respective labeling.

Having established all the required parameters, the numerical model was then solved and results were obtained and will hereon be presented.

4. **Results** - After running the numerical simulation, results were obtained and analyzed. Particular emphasis was given to the velocity and shear rate distribution along the die nozzle area of the extrudate geometry, as it was this particular set of values that would aid the analytical prediction of both the die-swell and pressure drop phenomena. Appropriately, the local shear-rate and velocity numerical results are depicted in figures 3.8a and 3.8b, respectively. The formerly hypothesized inclusion of the "air chamber" in the simulation was ultimately proven to be pointless, as results with and without the aforementioned feature were very similar. As such, only the results obtained for the "airless" model are displayed.

   As seen, the area of emphasis for the performed simulation lies in the extrudate zone that would be in contact with the die. The results show a shear stress value nearing 3000 s^{-1}, and a maximum velocity of 3.6 m/s on the central line of the die nozzle.

   As previously delineated, these values will allow for the analytical acquiring of the estimated die-swell felt at the exit of the extruder and total pressure drop along said apparatus. Both parameters' calculation process was conducted as follows:

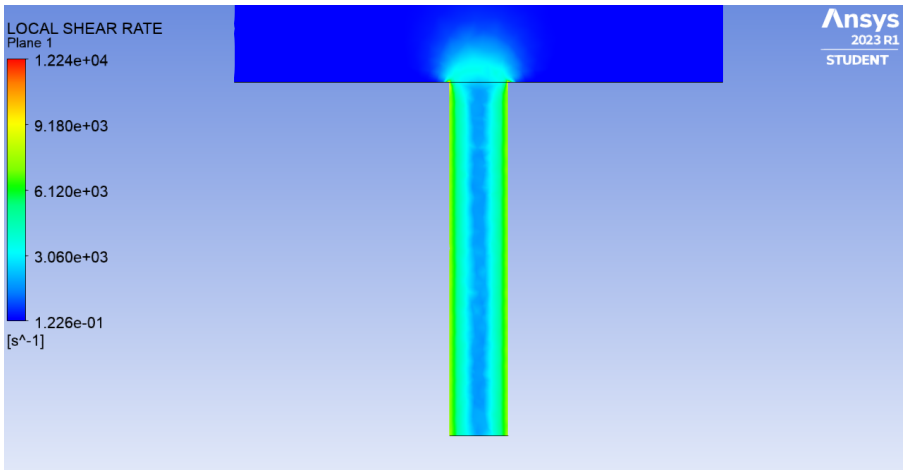

(a) Local shear-rate contour.

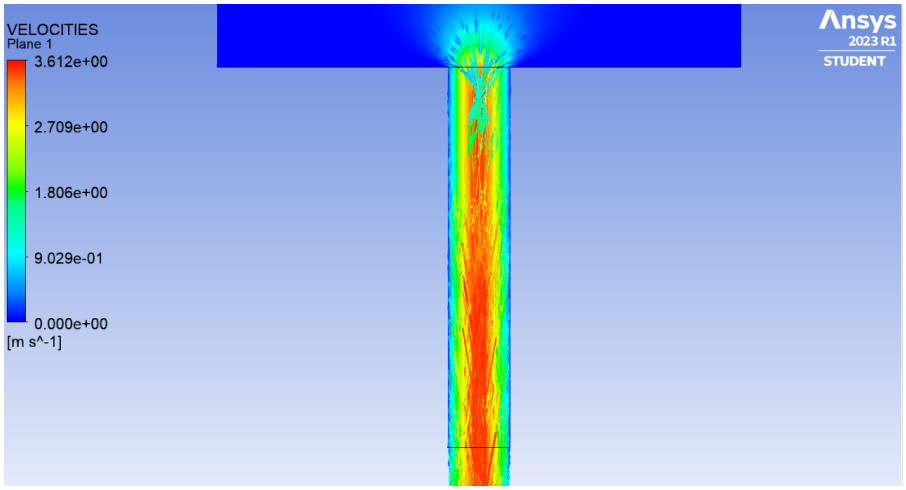

(b) velocity contour and vectors.

Figure 3.8: Numerical results obtained through Ansys Polyflow.

- **Die-swell Computation**

  The calculation of die-swell, specifically the ratio between the maximum swollen diameter and the nominal die nozzle diameter, can be accomplished by obtaining the first normal stress difference (N_1) and the shear stress (τ) at the extruder's exit, as indicated by the previously introduced equation 2.6. To determine N_1, both the shear stress and the slope (n) of the local viscosity versus shear rate curve are necessary. Hence, by selecting the local shear rate values along the extruder's exit (refer to figure 3.8a), an interval ranging from 1000 to 3000 s^{-1} is obtained. The corresponding shear stress values can be obtained through the experimental data gathered in [43], which provides the necessary linkage between the aforementioned shear rate and shear stress, as illustrated in the figure.

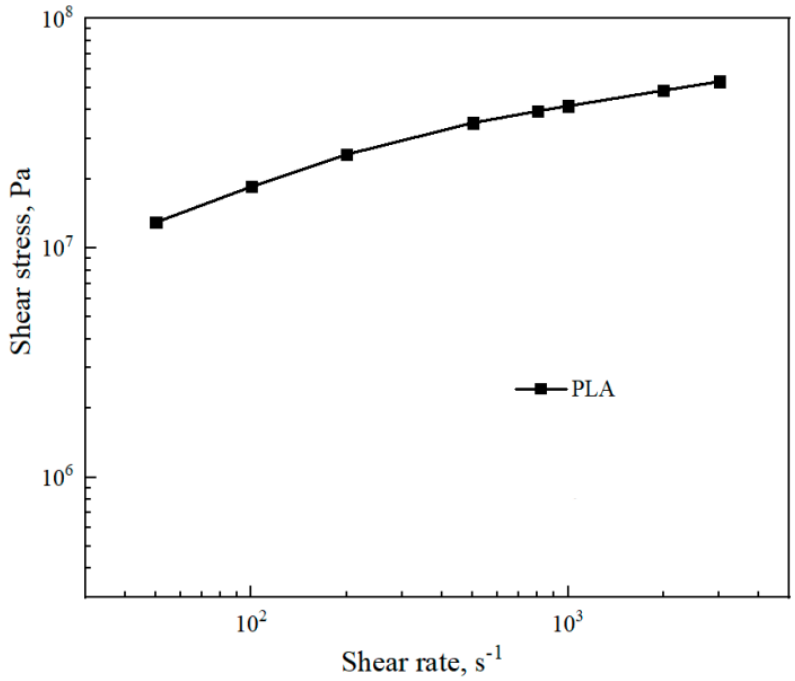

Figure 3.9: Shear stress (τ) vs shear-rate ($\dot{\gamma}$) logarithmic curve [43].

The local slope value (n) for the priorly mentioned interval can be determined and equals **0.325**. Additionally, assuming a mean shear-rate value of 2000 s^{-1} at the extruder exit, which is perfectly in line with the simulation results, a corresponding value of **5x**10^7 **Pa** is obtained. Inputting the two values on the Sharma-McKinley equation (2.7), a first normal stress difference of approximately **456 MPa** is obtained.

Substituting the expression parameters on 2.6 with their respective calculated values, a diameter "**D**" of 3mm was obtained, which meant that the extrudate would theoretically **swell an additional 1mm in diameter**.

- **Pressure drop calculation**

  The computation of the total pressure drop on the extruder can be obtained through equations 2.2 to 2.5, as previously shown. Subsequently, to reach any of the specified regions' pressure drop values, parameters such as m, ϕ and υ are needed.

  m can be obtained by direct correlation with the Power law based expression 3.2, where m is the equivalent of $1/n$, which translates to a value of 1.099.

  Similarly, relating expressions 2.1) and 3.2, a ϕ value of 3.17 x 10^{-10}

  As formerly referred, υ corresponds to the material velocity at the entrance of the liquefier, and can be obtained through the mass inflow of the extruder, which was previously deemed to have a value 0.0245 g/s. Furthermore, the inlet area of the liquefier, which possesses an inner wall diameter of 25 mm is 0.00049 m^2, or 490 mm^2. This ultimately leads to a inlet velocity of 4.03 x 10^{-5}.

  These parameters, along with the remaining geometric ones necessary to successfully calculate the pressure drop values for each of the extruder sections, are displayed on the following table:

Parameter	m	ϕ	υ [m/s]	D_1 [mm]	L_1 [mm]	D_2 [mm]	L_2 [mm]	β [°]
Value	1.099	3.317 E-10	4.03 E-5	25	147	2	10	50

Table 3.2: Material and geometric parameters needed for the pressure drop computation.

Uploading the values from table 3.2 into the each of the previously specified sections' pressure drop expressions (2.2 to 2.4),the following set of values is obtained:

$\Delta P_{1\upsilon}$ = 42380.94 Pa

$\Delta P_{2\upsilon}$ = 602235.75 Pa

$\Delta P_{3\upsilon}$ = 1532804.73 Pa

And, as such:

ΔP_{υ} = 2177421.42 Pa or 2.177 MPa

Though pressure drop is highly influenced by both the geometry of the extruder (particularly its nozzle diameter) and the flowing parameters of the extruded material, which means that every combination of different liquefier and material would theoretically lead to distinct pressure drops, the obtained value in this instance is in line with ones found in the literature [77; 78]. Generally, lower nozzle diameters and higher angles near the extruder tip lead to higher pressure drops, and vice-versa. For optimal flowing conditions, the pressure drop should be as low as possible.

Regardless of the obtained pressure drop's lack of significant negative impact in the extrusion process, further extruder and die geometry optimization would ultimately lead to lower pressure drops at the extruder's exit, and consequently to optimal material flowing conditions.

3.2.2 Setup of the extrusion equipment

As previously emphasized, maintaining an appropriate temperature within the cylindrical barrel is crucial for ensuring the effective impregnation of carbon fibers with PLA, consequently influencing the overall filament quality and printability. To achieve the desired temperature control for this specific component, two cylindrical copper resistors, are strategically positioned around the cylindrical barrel, as seen in figure 3.10. The temperature regulation is accomplished through the implementation of two PID controllers, with each controller responsible for governing the corresponding resistor. These controllers are housed within a rectangular container, as illustrated in figure 3.11b, which will henceforth be referred to as the "control box." The PID controller associated with the left digital display is responsible for regulating the temperature of the upper resistor, while the controller aligned with the right display governs the temperature of the lower resistor.

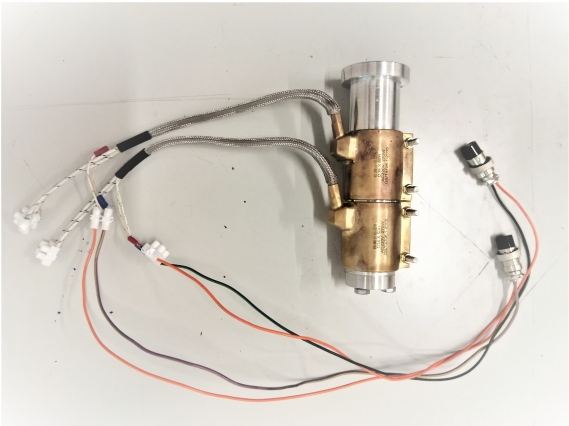

Figure 3.10: Extruder and corresponding resistors.

The choice to build the extruder barrel out of aluminium becomes much clearer, as good thermal conductivity is required to transmit the heat provided by the resistors to the barrel, namely its inner walls. Its cylindrical shape was also adopted to fit the cylindrical resitors, which allowed for efficient heating and easy temperature control, facilitating the setup of the installation.

Nevertheless, there existed a concern regarding the potential disparity between the actual temperature within the barrel and the set value on the controllers. To address this issue, thermal image classification was conducted by employing a thermographic camera, as depicted in figure 3.11a, to capture images of specific zones within the barrel. Subsequently, a correlation analysis was performed to establish a relationship between the set temperature and the actual temperature as observed through the thermographic measurements. However, the obtained results revealed a significant discrepancy between the two temperature values.

The temperature inside the cylindrical barrel varied from 98ºC to 160ºC on its end and middle sections, respectively, for a set temperature value of 280ºC on the controller. As such, an attempt to reduce the heat losses due to convection by isolating the extruder with glass fiber woven fabric was made, as exhibited in figure 3.12a. To evaluate the proposed idea's effectiveness a thermografic analysis was yet again performed. The temperatures measured by the camera corresponded to the

(a) (b)

Figure 3.11: (a) FLIR thermographic camera [44]. (b) PID controllers' housing box.

temperature at the middle section of the barrel's inner wall and the temperature at the die (final section of the barrel), and are displayed in figure 3.12b.

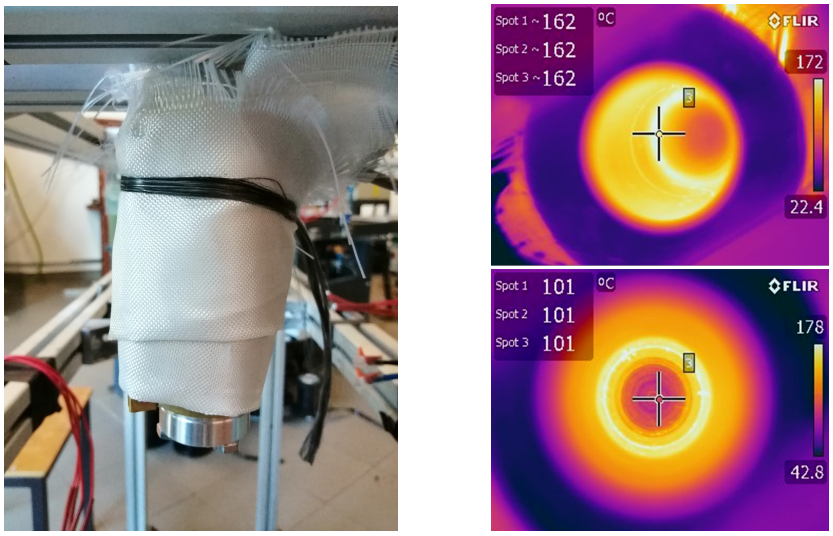

(a) (b)

Figure 3.12: Insulation experiment. (a) Extruder wrapped in glass fiber cloth. (b) Infrared images of the inner wall's middle section (top) and die (bottom).

As seen, the temperature at the middle section of the barrel had a value of about 160ºC, for a set temperature on the controller of 280ºC. As for the temperature at the end stretch of the barrel, where the die is situated, it showed a value of 100ºC, which might also be beneficial for the cooling process of the filament exiting the extruder. This indicates that the insulation wasn't very effective, as it only induced a 2ºC temperature increase in the barrel. This could ultimately mean that the conductive heat losses outweighed the convection heat losses, not allowing the insulation to have a considerable impact on the thermal state of the installation. Thus, the insulation idea was abandoned as it proved to be ineffective.

It should also be noted that the referred temperatures are susceptible to change when the material is deposited on the barrel. As the polymer starts to fill the inner walls of the cylindrical barrel,

the air space decreases and is replaced with material at high temperature, contributing to a raise in the overall temperature inside the barrel. This was later experimentally confirmed, as the thermographic analysis showed that the temperature inside the melt PLA filled barrel was very nearly identical to the set temperature on the controllers (figure 3.13), which were set to a temperature of 190ºC (figure 3.13a). Yet again, the filament of extruded material at the die's exit appeared to be at a temperature approximately 10ºC below the setpoint, at 180ºC (figure 3.13b).

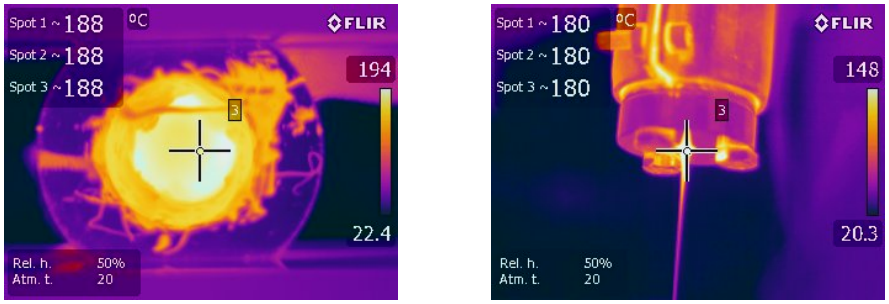

(a) (b)

Figure 3.13: Infrared images of the barrel's middle section (a) and die (b), with their respective temperature values.

To better understand the polymer and subsequently the composite material's ideal flowing conditions with respect to its temperature, several experiments were conducted in which PLA pellets were introduced in the extruder's barrel and the flowing behaviour was analyzed at different temperatures on each of the two resistors. The attempted experiments sought to create a temperature gradient on the extruder's cylindrical barrel by having the bottom resistor at a slightly lower temperature the top one, which in itself hovered around the melting point of the PLA polymer. This would help material gain the consistency and viscosity needed for it to maintain the die geometry after exiting said component.

Prior to establishing the extrusion setup and initiating the PLA extrusion tests, there was apprehension regarding the potential die-swelling behavior of the material at the exit of the die. However, upon extruding the first PLA samples, it was observed that no significant swelling occurred around the exit orifice. This observation can ultimately be attributed to the dominance of contraction phenomena over the die-swelling effect. In other words, this meant that factors such as low PLA viscosity, low fiber content and high and unstable pulling speeds outweighed the factors contributing to the occurrence of the die-swell phenomenon. It is noteworthy that the numerical simulations did not account for the thermal contraction phenomenon, which may explain the differences found between the numerical and experimental approaches.

3.2.3 PID Controller

As previously mentioned, the temperature control mechanism present in the extruder installation would be performed by a PID or Proportional Integral Derivative controller. A PID controller is an instrument used in industrial applications to regulate temperature, flow, pressure, speed and other process variables. It does so by using a control loop feedback mechanism to keep the actual output from a process as close to the target or setpoint output as possible, which grants it the title of the most accurate and stable controller type on the market [79].

To better understand these controllers, one must first understand their working principle. What determines how close to the set value the output of the controller is and how stable that output signal is, are the three formerly mentioned proportional, integral and derivative terms. The way these parameters are individually adjusted or tuned is what ultimately defines the difference between the set and output values, through the calculation of correction factor based on that difference which is then applied to the input. Note that the output value is read with a thermocouple or "thermoelectrical thermometer" embebbed in the controllers themselves. With that said, three distinct tuning actions are performed for each of the three main terms [80]:

- **Proportional tuning** - involves correcting a target proportional to the difference between the target and output values, also known as "error". As such, the target value is never achieved because as the difference approaches zero, so too does the applied correction.
- **Integral tuning** - Counteracts the proportional tuning by by effectively cumulating the error result from the "P" action to increase the correction factor. For instance, if the temperature of a device we were attempting to control, such as an oven, remained below temperature, the "I" term would increase the heat delivered. But rather than stopping when the target value is reached, "I" would attempt to nullify the cumulative error, causing an overshoot.
- **Derivative tuning** - tries to minimize the overshoot by slowing the correction factor applied as the set value is approached.

Nowadays, most PID controllers are "plug and play", meaning that they possess the ability to automatically tune the three aforementioned terms to better suit the control application in question. The controller used in this particular extruder setup also happens to be able to auto-tune the "P", "I" and "D" terms to find the optimal control combination for this specific temperature control application. Note that process dynamics such as mass and size of the material/equipment, as well as noise from electrical interference influence the control process, so any major changes in these elements will require a repeat in the tuning process to find the required constants for optimal control [81].

As previously explained, the extruder installation in question made use of two separate PID controllers situated besides one another in the control box. After both of the referred controllers performed their auto-tuning procedure, the results in table 3.3 were obtained for each of the control terms:

PID Controller	P	I	D	|SV-PV|
Left	81	39	9	1
Right	76	39	9	1

Table 3.3: PID Controller parameters after tuning

3.3 Filament production

3.3.1 Initial experimental tests

With a deeper comprehension of the preferred flow conditions and the overall spatial configuration for the extrusion setup, the filament production tests were set to commence. In order to fabricate fiber-reinforced PLA utilizing the developed extrusion arrangement, the carbon fibers were initially drawn through the extruder barrel, followed by passage through the die orifice. Subsequently, the polymer material was introduced into the cylindrical barrel, allowing for an assessment of the resulting impregnation level and geometric properties. However, due to equipment and time unavailability at that particular instance, the filaments had to initially be manually pulled through the extruder's die. This meant that a constant pulling velocity was not yet achievable, and ultimately compromised the validity of the initially obtained samples and hindered the experimental process as a whole. Despite this, the tests that took place and are registered in the present chapter still remain as an indicator of the process' shortcomings and accomplishments, setting the path for the optimization of the installation and production method.

For the initial tests, a die diameter of 2mm was employed, while the extruder temperature was set to 190ºC and 180ºC for the top and bottom resistors, respectively. The resulting filament is visually depicted in figure 3.14.

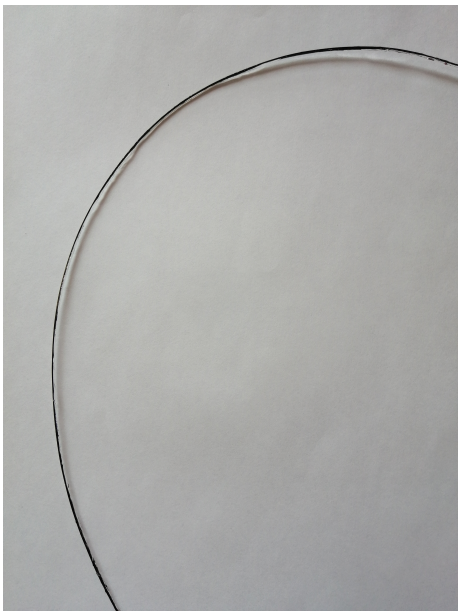

Figure 3.14: CF/PLA filament produced with the first extrusion setup, using a 2mm die

The produced filament exhibited inconsistent cross-sectional geometry throughout its length, and after visual inspection the level of impregnation appeared to be notably low. In particular, the filament displayed poor homogeneity in terms of fiber distribution, with the polymer appearing to wrap around the fibers rather than achieving proper impregnation.

While the inadequate impregnation may not significantly impact the overall quality of the filament, given that it will undergo reheating during its utilization in 3D printers and primarily experience traction loads, the issue of inconsistent geometry poses a more significant concern. To ensure proper functioning within FDM printers, where the filament needs to fit precisely between the gear and roller and be accurately guided to the printer's nozzle, maintaining a consistent cross-sectional geometry is strongly recommended. One potential contributing factor to the occurrence of inconsistent geometry in filament production can be attributed to the nature of the chosen material for the die, specifically 2014 aluminum-copper alloy. The use of this die material can result in a certain level of grip between its surface and the extrudate due to its higher surface friction. Consequently, variations in the filament's cross-sectional geometry may arise. This circumstance elucidates the rationale behind the common adoption of brass nozzles in 3D printers. Brass, being a cost-effective alternative, is specifically chosen to mitigate this particular issue associated with inconsistent geometry. The utilization of a brass nozzle alleviates concerns related to surface friction, as brass possesses a low coefficient of friction. Moreover, brass exhibits high thermal conductivity, which further enhances its suitability for this application.

To determine the fiber content of the filament in terms of its mass, multiple samples measuring 20mm in length were cut from a 1.5m produced filament and later weighed. By knowing the linear weight of the fibers [tex] (grams per 1000 meters) and the total mass of each filament sample, along with its length, it is possible to calculate the mass percentage of fibers present in the filament. After measuring the mass of four filament samples, an **average fiber mass fraction of 15% was obtained**. The obtained value of 15% for the fiber mass fraction is relatively low compared to other commonly used carbon fiber/thermoplastic composites. This characteristic can be seen as a double-edged sword. On one hand, the low fiber ratio contributes to easier processing of the composite without encountering significant issues. However, on the other hand, the mechanical properties of the composite may be compromised.

Typically, higher carbon fiber mass ratios in composites result in enhanced strength and stiffness. However, this may come at the cost of increased material expenses and additional challenges during processing. Therefore, finding the right balance between the fiber mass ratio, mechanical properties, cost, and processability is essential when developing carbon fiber/thermoplastic composites.

Along with its cross sectional geometry, the filament's diameter change along its length was also measured and evaluated. Measurements were taken from specific length values along the 20mm samples, namely around the 5, 10, 15 and 20 mm marks. These measurements found that the filament suffered significant contraction at the exit of the extruder, as the average filament diameter clocked in at about **1.4mm**. This meant that a **reduction of 30%** was verified on the composite filament. While the previously enumerated limitations regarding the technology and methodology involved in these experimental tests may play a big part in the occurrence of this particular phenomenon, specially the inconsistent pulling velocity due to manual pulling, the factor deemed as the main cause for this particular issue was the slow thermal contraction seen at the die's exit.

It is also worth noting that the production method was replicated with a die orifice diameter of 4mm to evaluate the filament quality, mass distribution, and geometric consistency at a larger die diameter, and the resulting product is displayed in figure 3.15. This variation in die diameter would lead to a lower fiber mass ratio in the filament, allowing for an assessment of the effects on the aforementioned factors. Following the same methodology as for the previous experiment, results revealed an **average fiber mass ratio of 7%**, along with an **average diameter of 2.5mm**, which equates to a **reduction of 37.5%**. Due to the formerly described reasons, this particular filament suffered from the same minor geometrical inconsistencies that plagued the previous experiment.

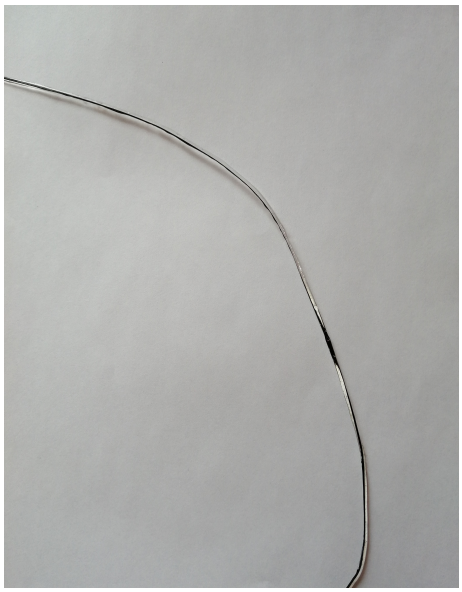

Figure 3.15: CF/PLA filament produced with the first extrusion setup, using a 4mm die

As such, cooling at the specified exit area was to be tested and the process and obtained results were to be registered and analyzed in the following subsection of this experimental chapter.

It is also worth noting that all the filament diameter and mass measurements, for this particular initial setup are registered in **Appendix C**.

3.3.2 Assessment of the impact of water cooling and constant pulling speed on filament quality

The previous experiment managed to prove the feasibility of the developed installation for the production of carbon fiber reinforced PLA filaments. However, filament consistency and overall quality still posed as compromising factors in terms of their applicability to current FDM printing devices.

Furthermore, expert advice from experienced operators in the field of 3D printing emphasized the importance of material properties such as high elasticity for optimal performance. Based on these recommendations, the decision was made to use the 4mm die for the subsequent filament production. This choice resulted in higher polymer quantities incorporated into the filaments and yielded an average diameter that was closer to the recommended 2mm for compatibility with FDM printing devices. The selection of the 4mm die aligns with the objective of producing filaments that meet the desired material properties and are suitable for successful 3D printing applications.

To address the aforementioned challenges, modifications were made to the installation, including the addition of a cooling tank and a pulling motor. The cooling tank was constructed using a plastic container, repurposed from a water bottle due to time constraints. A cylinder was inserted into the width of the container using a threaded connection. This cylinder served to guide the exiting filament, preventing cuts and potential water leaks from the bottom of the container. The pulling motor utilized in the setup was sourced from a nearby pultrusion installation that was not currently in use. It was controlled through computational software, providing precise control over the filament pulling process. An illustration of the described setup can be seen in figure 3.16.

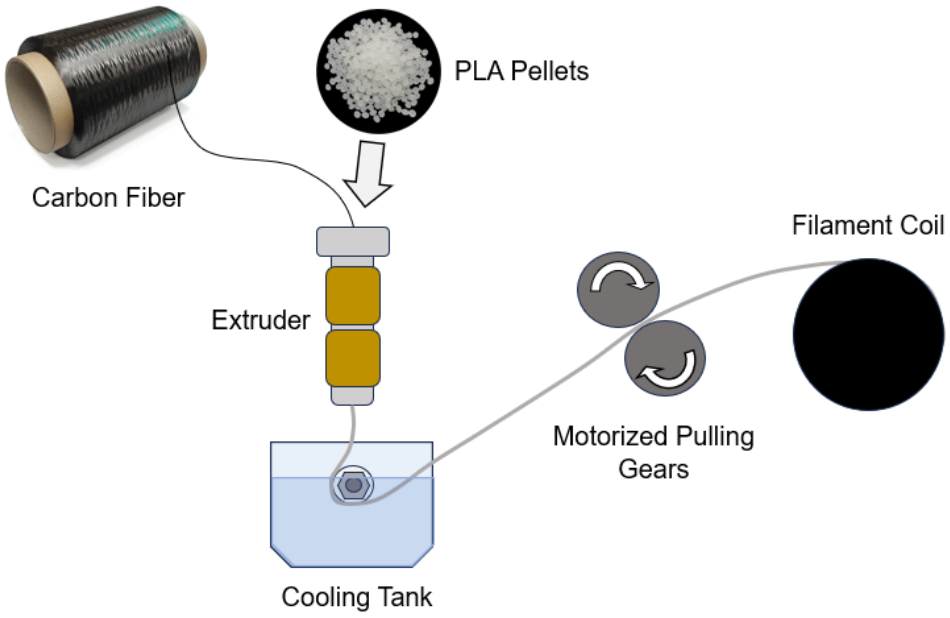

Figure 3.16: Second version of the developed extrusion installation

The possibility of adding a pressing system to aid the extrusion of the material out of the die was also evaluated, but ultimately wasn't implemented given the lack of impurities and air in the resulting filament, as well as the satisfactory filament flow through the pulling system.

Following the modifications to the installation, the production of filament resumed with a pulling speed set at 0.5m/min. The resulting filament, which incorporated carbon fiber reinforcement in PLA (figure 3.17), was extracted and subjected to a preliminary analysis. Initial observations indicated a significant improvement in the consistency and definition of the filament's geometry and diameter along its length. This improvement was further supported by diameter measurements, which revealed a notably more uniform diameter throughout the entire length of the sample see **Appendix C**. Moreover, a comparative analysis with previously produced filaments clearly demonstrated that the most recent sample exhibited a significantly enhanced circular cross-sectional geometry, indicating improved overall quality and consistency.

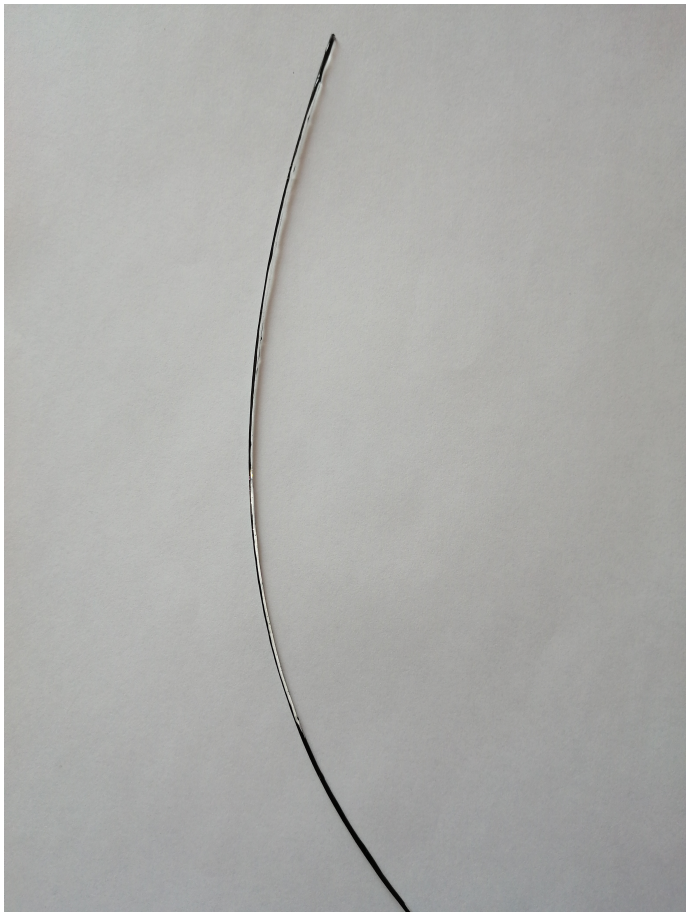

Figure 3.17: Second version of the developed extrusion installation

To further validate the achieved enhancements to the extrusion installation, the various filament samples' cross sections were evaluated under magnifying glass lenses.

3.3.3 Optical Filament Analysis

Despite the successful production of filament samples through two iterations of the setup, the information obtained about their composition and fiber distribution was primarily based on direct visual observations. However, to obtain a more detailed understanding of the filaments' structure and fiber distribution, a closer examination using a magnifying glass was recommended.

Considering that the PLA material used for the experimental tests was highly transparent and exhibited a strong contrast with the dark carbon fibers, magnifying glass analysis was deemed suitable for the intended basic microstructural analysis, rendering the use of microscopy unnecessary.

The previously produced 20cm samples were yet again cut into smaller 4cm segments, and the obtained images were expected to provide valuable insights into potential further adjustments that could be made to the installation, as well as offer valuable information about the overall quality and suitability of the filaments for additive manufacturing.

All previously produced samples underwent evaluation using a 40x magnifying glass lens, using an Olympus BX61 Motorized Brightfield Darkfield Microscope (figure 3.22) and the following results were observed:

- 2mm filament sample with no cooling and inconstant pulling speed

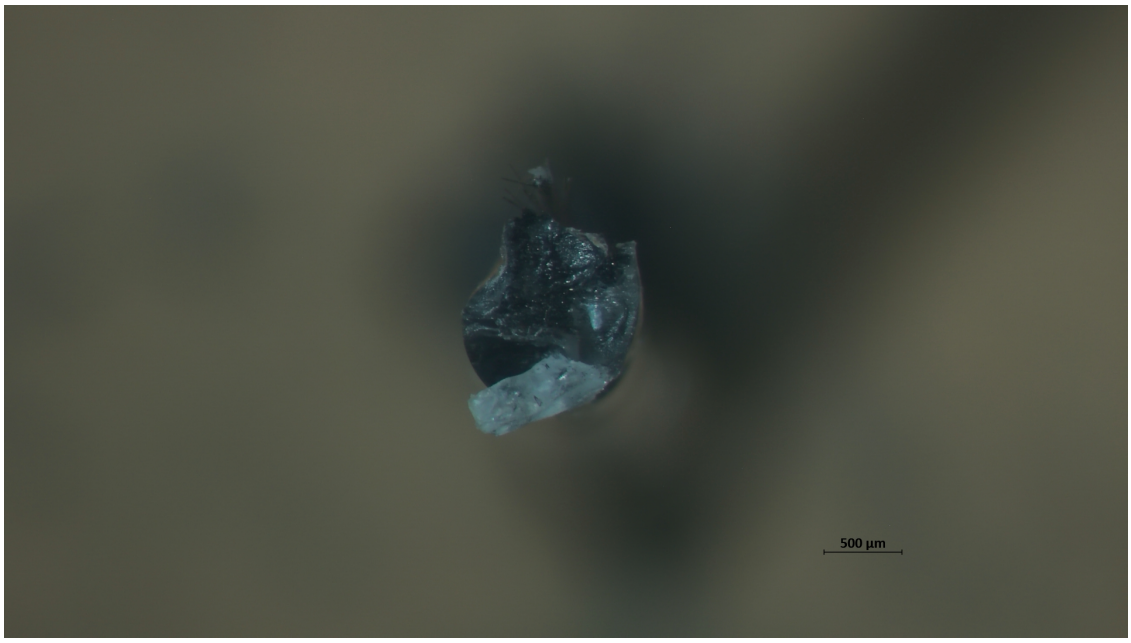

Figure 3.18: 40x cross section image of a 2mm sample.

- 2mm filament sample with water cooling and constant pulling speed

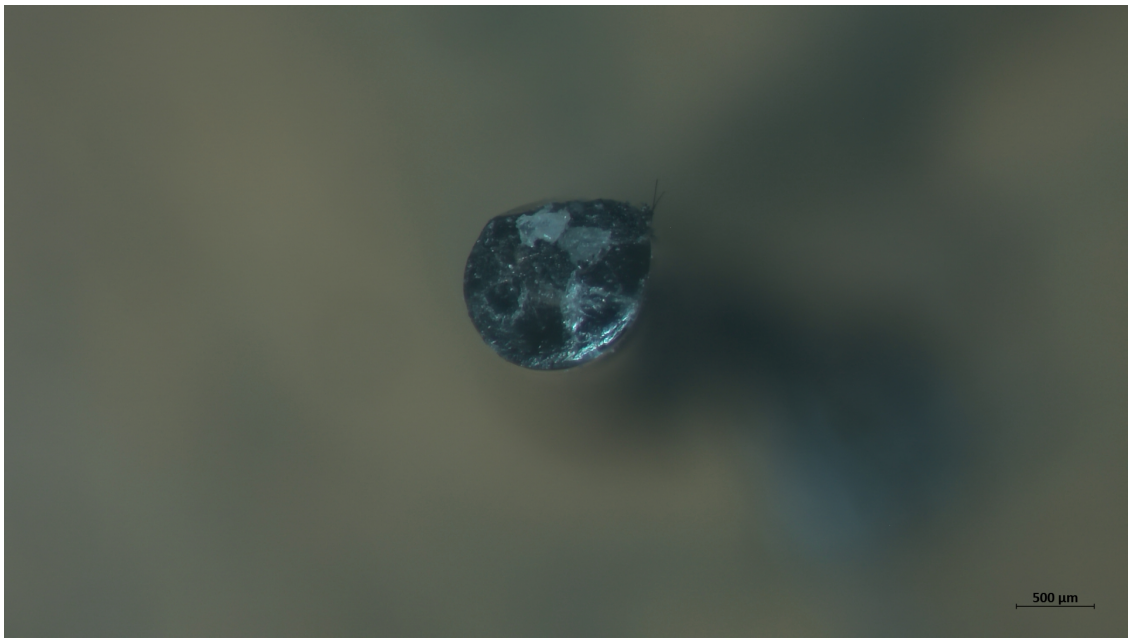

Figure 3.19: 40x cross section image of a 2mm sample produced with water cooling and constant pulling speed.

- 4mm filament sample with no cooling and inconstant pulling speed

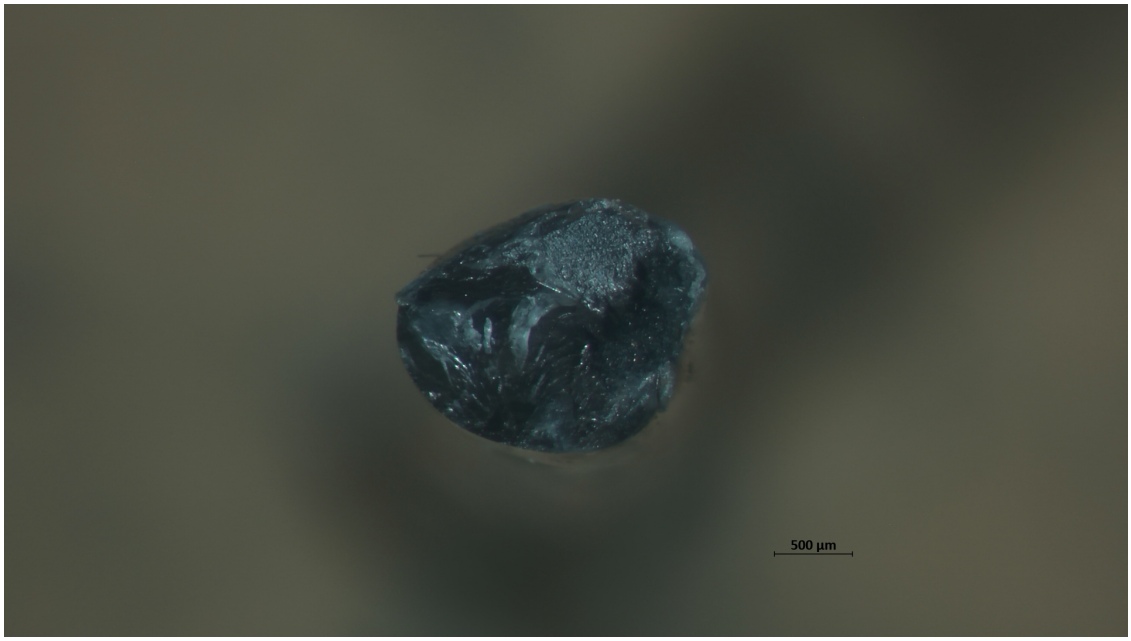

Figure 3.20: 40x cross section image of a 4mm sample.

- 4mm filament sample with water cooling and constant pulling speed

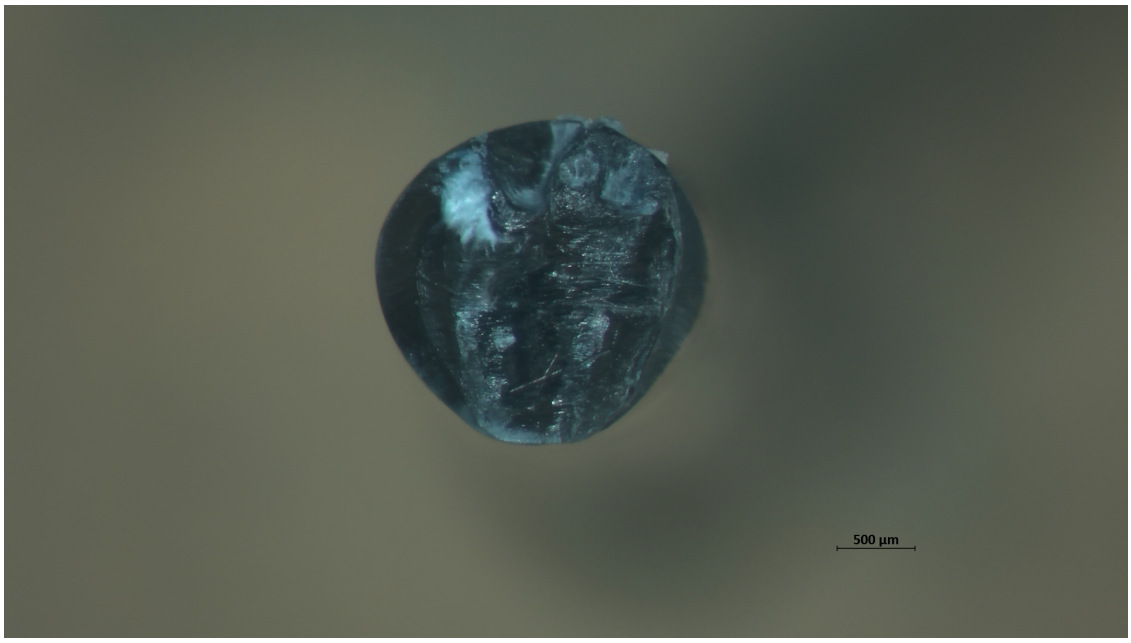

Figure 3.21: 40x cross section image of a 4mm sample produced with water cooling and constant pulling speed.

Figure 3.22: Olympus BX61 Motorized Brightfield Darkfield Microscope w/ Laser Autofocus Pred BX63 [45].

Upon comparing Figure 3.18 with Figure 3.19, a notable improvement can be observed in the latter, characterized by enhanced fiber distribution and a more circular cross-sectional geometry. Similarly, when examining Figure 3.20 and Figure 3.21, it becomes evident that the latter also exhibits improved fiber distribution and a more consistent circular cross-sectional geometry. These

comparisons provide visual evidence of the positive effects resulting from the modifications made to the extrusion installation, reinforcing the assertion of enhanced filament quality achieved in the second iteration.

3.3.4 Filament implementation on FDM 3D printing devices

Having accomplished filament production of several samples with respectable quality, it was time to put their applicability in 3D printing to the test. The filaments were introduced in a Prusa i3 mk3s+ 3D printer (figure 3.23), and the following conclusions were reached:

- the filaments obtained with the 2mm die successfully engaged with the printers' gear and roller, beginning the extrusion process with relative ease. However, upon entering the nozzle area, the filament ended up fraying and was ultimately unable to undergo proper extrusion. One of the reasons as to why this might have happened may lie on the fact that a nozzle size of 0.4mm was too small to allow the correct passage of the fibers. Another factor limiting the printing process was the low flexibility shown by these particular filaments.
- The filaments produced using the 4mm die, despite showing better flexibility than their 2mm die counterpart (due to their higher polymer content), proved to be unable to correctly fit in between the roller and gear, as their diameter exceeded the spacing between the two components.
- To address the encountered issues, the production of CF reinforced PLA filaments with a die diameter of 2.75mm or 3mm was recommended. This adjustment would help achieve the optimal filament diameter of 1.75mm or 2mm, ensuring compatibility with the spacing between the roller and gear in the 3D printer. By selecting a slightly larger die diameter than 2mm, it was anticipated that the filaments would maintain their flexibility while also facilitating successful extrusion and proper fit within the printer components.

Figure 3.23: Prusa i3 MK3S+ 3D Printer kit [46].

Consequently, the recommended approach was implemented, and composite filaments were produced using the specified die, resulting in an intermediate diameter that fits the 3D printing

equipment more effectively (see Figure 3.24). Furthermore, the standard 0.4mm nozzle commonly found in most 3D printers was replaced with a 0.8mm nozzle. It is worth noting that this adjustment may not have been necessary if the carbon fibers used in the composite filaments had a lower tex value, reducing their overall diameter.

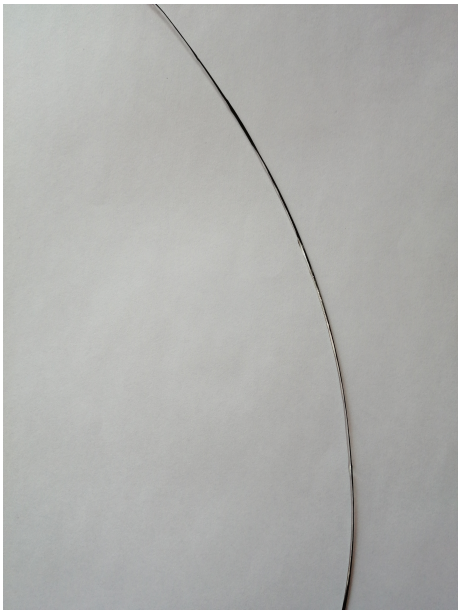

Figure 3.24: CF/PLA composite filament produced with the second extrusion setup, using a 3mm die.

These changes would have an immediate impact on the printing procedure, allowing for the extrusion of the material seen in figure 3.25, although not without its issues. The extruded material appeared to yet again suffer from fraying, but to a much lesser extent to what was experienced with the 0.4mm nozzle. In this instance though, the fibers seemed to retain their alignment and it was the polymer that presented a rough texture and an extremely irregular geometry. This was most likely due to the temperature inside the printer (near the nozzle) exceeding the optimal value, as the polymer in the extruded filament seemed to flow at a much higher pace relatively to the fibers. This also directly contradicts the recommended printing temperature present in the datasheet (see Appendix A), which stands at a value of 220ºC.

As such, yet another study aiming to find the optimal flowing temperature of the already produced filament was conducted. The study consisted of feeding the previously obtained PLA filaments in 3.2.2 into the printer and experimenting with different temperatures in order to reach satisfactory polymer viscosity and flowability. The iterative study's results revealed an optimal processing temperature of 190 ºC.

The printing process was yet again attempted under the recently found recommended temperature. The extruded material resulting from this experiment, visually depicted in figure 3.26, showed a more consistent geometry and texturing throughout its entirety, validating the effectiveness of the conducted study.

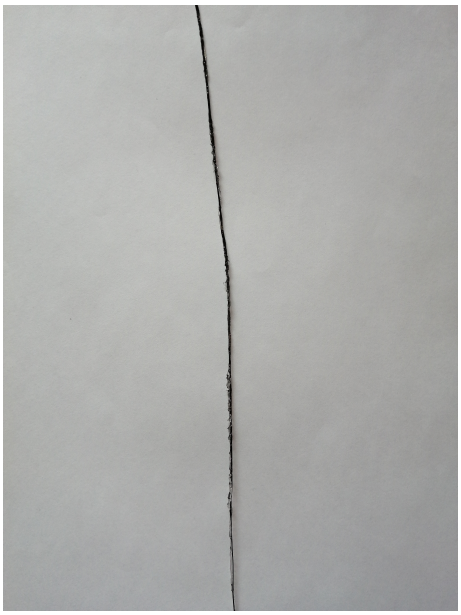

Figure 3.25: CF/PLA filament after printing

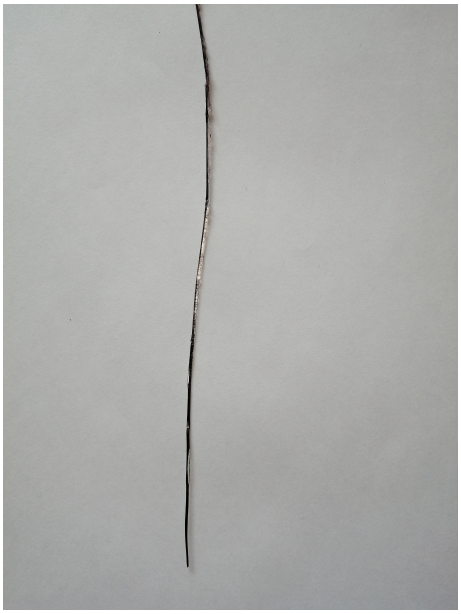

Figure 3.26: CF/PLA filament printed after the thermal study

The filament produced through the extrusion installation presented in this study was nearing the point of full compatibility with FDM printing devices, requiring only a few adjustments. However, it is important to note that there are still complexities associated with 3D printing processes involving composite filaments. Further research on continuous fiber reinforced composites' printing, especially its pre- and post- processing areas should be conducted in order to obtain the best possible quality for the printed pieces.

Moreover, it should be emphasized that this type of printing requires specialized slicer software capable of creating a continuous path for the printed material, as well as specialized printing

devices that can support this specific procedure.

Looking ahead, it is recommended that specific mechanical test specimens be produced, tested, and analyzed to further advance the technology and understand the necessary changes to be applied in the production and printing processes to achieve optimal quality and performance. A practical approach to contribute to the advancement of this concept would be to print ring test specimens and conduct a split disk test, following the ASTM D2290 standard. This method provides a simple, cost-effective, and efficient means of obtaining the circumferential tensile properties of the material, which can provide valuable insights for its characterization and performance evaluation.

Chapter 4

Discussion of results and Conclusions

In light of the escalating armed conflicts and persistent occurrence of natural disasters, there is a pressing need for a portable and deployable shelter solution that can cater to displaced individuals. Extensive research has highlighted the primary limitations and challenges associated with the development of such structures, as well as the complexities involved in the manufacturing methods, particularly 3D and 4D printing.

This research aimed to build upon previous dissertations conducted at FEUP on the same topic, with the objective of addressing the main structural limitations identified in those works. Following the recommendations put forth in those previous studies, the production and implementation of Shape Memory Polymer Composite (SMPC) filaments for 4D printing were pursued, with future Fused Deposition Modeling (FDM) device utilization in sight. The core focus of this research involved the development of a composite filament extrusion system capable of producing carbon fiber reinforced PLA filaments that are compatible with 3D printing technology.

Given the lack of technical knowledge on the acquired polymer material, further thermal and mechanical characterization was conducted. MFI and TGA tests were performed in order to get a better grasp of the PLA's flowability and thermal degradation, respectively. The results obtained from these tests were consistent with those reported in existing literature for other PLA materials. These findings provided valuable insights into the flow behavior and thermal stability of the PLA used in the study, contributing to a comprehensive characterization of the material.

Before commencing the experimental endeavours that sought to obtain composite filaments for 3D printing, a numerical simulation was conducted to perceive the effect and magnitude of die-swelling and pressure drop phenomena existing in the extruder machine. Numerical results for the shear rate, pressure and velocity fields were obtained, which consequently led to the analytical determination of the pressure drop and die-swell in the extruder die. The results indicated that these phenomena had no significant impact on the extrusion process, and the values obtained were consistent with those reported in the existing literature. Subsequent extrusion experiments using only polymer material confirmed the initial deductions, as no visible die-swelling was observed.

The initial extrusion installation comprised a cylindrical liquefier barrel where the carbon fibers would impregnate with the deposited PLA material. Subsequently, the impregnated mixture

would be extruded through the central orifice of a cylindrical die. Following the extrusion process, the filaments were manually pulled and wound around a coil. This setup successfully demonstrated the equipment's viability in producing reinforced PLA filaments with a significant production rate and satisfactory quality. However, challenges related to inconsistent cross-sectional geometry and filament diameter were observed, indicating the need for further modifications to the installation in order to address these issues.

In the second iteration of the installation, several modifications were introduced to address the observed issues. A water cooling system was incorporated, which involved a water tank with a specially designed 3D printed cylinder spanning its width. This addition aimed to enhance the rapid consolidation of the filament at the extruder exit, with the intention of preserving the desired circular cross-sectional geometry within the die.

Furthermore, a motorized filament pulling system was integrated into the installation, repurposed from a previous retired production setup. This inclusion served two purposes. Firstly, it aimed to ensure a more consistent filament diameter along its entire length. Secondly, it provided the flexibility to experiment with different pulling speeds, allowing for further fine-tuning of the filaments' properties.

The implementation of the modifications in the second iteration of the installation yielded significant improvements in the quality of the filament samples compared to those produced with the original production setup. The desired effects of the changes were clearly and immediately observed. The filaments exhibited a more consistent circular cross-sectional geometry and diameter throughout their entire length, resulting in enhanced overall quality. These improvements would hopefully increase the compatibility of the filaments with existing 3D printing devices, expanding their potential applications.

The effectiveness of the implemented changes in the extrusion installation was further validated through magnifying glass imaging of the cross-sectional profiles of the filament samples. A comprehensive evaluation and comparison of all the samples produced in both iterations of the production setup were conducted. The findings confirmed the initial observations, as they demonstrated notable improvements in fiber distribution, cross-sectional geometry, and overall consistency of the filaments. These results provided additional evidence of the positive impact of the modifications made to the initial extrusion installation.

Finally, the feasibility of implementing the filaments in 3D printing processes, which represented a critical milestone towards achieving the ultimate objective of the dissertation, was assessed. Initial testing revealed the need for further adjustments in filament production due to encountered extrusion issues in the FDM 3D printing device. Consequently, production was resumed using a die diameter of 3mm, resulting in CF/PLA filaments with an average diameter of 1.75mm, which was deemed optimal to ensure proper fitting between the printer's guiding roller elements. To further enhance the printing process, the printer's nozzle was replaced with a larger nozzle of 0.8mm in diameter. However, the obtained filament still exhibited inconsistency and rough texture, particularly in the PLA zones of the printed filament. In order to address this issue, a thermal study was conducted to determine the optimal printing temperature for this specific

PLA material. It was concluded that a temperature of 190ºC would significantly improve the extrusion process. After correcting the printing temperature, the textural and geometric consistency improved. The experimental work would then stagnate due to the unavailability of printing equipment capable of performing continuous fiber 3D printing with composite filaments. Future production of mechanical test specimens was recommended in order to gather valuable insights for material characterization and performance evaluation.

(*blank page*)

Chapter 5

Final remarks and future works

5.1 Final remarks

The present study, while unable to achieve a scaled-down prototype of a self-assembling and easily transportable shelter or validate the shape memory behavior of the printed material, has made significant contributions in the development of a simple yet innovative extrusion installation capable of producing SMPC filaments for 3D printing. Various constraints, such as time limitations, unavailability of equipment, limited information on the subject matter, and a constrained budget, hindered the project's progress and prevented the attainment of the final objective.

Nevertheless, the foundational knowledge presented throughout this dissertation, coupled with the advancements made in this specific research and the rapid evolution of 3D printing technology, provide a promising outlook for the future of this technological concept. Despite the challenges faced, the groundwork laid in this work sets the stage for further exploration and advancements in the development of self-assembling shelter solutions using shape memory polymer composites and 3D printing techniques.

5.2 Future works

Though significant progress was achieved with this particular work, the main goal of reaching a structurally stable self-deploying and easily transportable shelter solution was not accomplished. As such, the following set of recommendations aims to provide guidance to potential future works on the same topic and with similar equipment/techniques:

i Test the shape memory effect of the PLA or any other SMP acquired for the same purpose;

ii Further production parameter optimization (feeding rate, die size, temperature control, pulling speed) to improve filament consistency and quality, consequently improving its applicability in FDM printing;

iii Optimize the die geometry to further reduce the pressure drop at the extruder exit and improve the filament's flowability;

iv Characterize the obtained SMPC material mechanically.

v Test the effect of creep/relaxation on the shape memory process of the produced SMPC;

vi Define a definitive shelter design, directly utilizing one of the previously developed models or even studying the viability of shape optimization for this particular problem;

vii Simulate the shape memory effect of the shelter concept, to define the ideal minimum dimensions for the contracted and activated states;

viii Perform structural numerical simulations on the shelter model with the experimentally obtained material inputs, and validate the results by comparing them with the analytical threshold set by the EUROCODE (also calculated in previous FEUP works);

ix Estimate the durability of the SMPC shelter solution;

x Develop a small-scale shelter model and analyze its shape memory and structural behaviour;

xi Study the economic viability of the production process and compare it to current production solutions;

xii Print identical parts using both stock polymer filaments and continuous fiber reinforced composite filaments, characterize them mechanically and compare the obtained results;

xiii Create a full-scale shelter prototype and validate it experimentally.

Bibliography

[1] United Nations High Commissioner for Refugees. Refugee statistics, 2023. Accessed February 2023. Available at https://www.unhcr.org/refugee-statistics.

[2] L. A. C. Henriques. 4d structures for rapid construction of a shelter in crisis situations. Master's thesis, University of Porto, June 2019.

[3] Ana Silva. "structural analysis of a temporary shelter with shape memory effect.". Master's thesis, University of Porto MSc thesis, September 2020.

[4] L.Raposo. Development of an emergency shelter using 4d printing. Master's thesis, University of Porto, July 2021.

[5] Santos A. "finite element analysis of shape memory polymers.". Master's thesis, University of Porto MSc thesis, September 2021.

[6] I. F. o. R. C. Societies and R. Crescent. Transitional shelters - eight designs. Geneva, 2011.

[7] IFRC. Shelter kit. Accessed in March 2023. Available at https://itemscatalogue.redcross.int/relief--4/shelter-and-construction-materials--23/shelter-and-construction-kits--104/shelter-kit--KRELSHEK02.aspx.

[8] Domehome standardized family tents. Accessed in March 2023. Available at https://www.nrsrelief.com/products/domehome/.

[9] Designboom. "designnobis' tentative provides shelter in post-disaster situations.", 2015. Accessed in March 2023. Available at https://www.designboom.com/design/designnobis-tentative-post-disaster-shelter-07-11-2015/.

[10] Piotr Pańczyk Damian Granosik, Jakub Kulisa. Skyshelter.zip: Foldable skyscraper for disaster zones. Accessed in March 2023. Available at https://www.evolo.us/skyshelter-zip-foldable-skyscraper-for-disaster-zones/.

[11] G. Gardiner. "composites in tornado shelters". Accessed in March 2023. Available at https://www.compositesworld.com/blog/post/composites-in-tornado-shelters.

[12] Christian Dela Cruz. Shelter, Sep 2022. Accessed in March 2023. Available at https://bettershelter.org/shelter-effects/.

[13] Life cube rapid deployment. Accessed in March 2023. Available at http://www.redhawksurvival.com/lifecube3.html.

[14] European Space Station (ESA). Additive manufacturing process. Accessed in April 2023. Available at https://www.esa.int/ESA_Multimedia/Images/2014/04/Additive_Manufacturing_process.

[15] Zhizhou Zhang, Kahraman G. Demir, and Grace X. Gu. Developments in 4d-printing: A review on current smart materials, technologies, and applications. *International Journal of Smart and Nano Materials*, 10(3):205–224, 2019.

[16] Yuliang Xia, Yang He, Fenghua Zhang, Yanju Liu, and Jinsong Leng. A review of shape memory polymers and composites: Mechanisms, materials, and applications. *Advanced Materials*, 33(6):2000713, 2020.

[17] Madhubhashitha Herath and Jayantha Epaarachchi. Shape memory polymer composites and their smart structural applications. *Composite Materials*, page 581–610, 2021.

[18] Anum Azam, Kate E. Laflin, Mustapha Jamal, Rohan Fernandes, and David H. Gracias. Self-folding micropatterned polymeric containers. *Biomedical Microdevices*, 13(1):51–58, 2010.

[19] Kate Malachowski, Joyce Breger, Hye Rin Kwag, Martha O. Wang, John P. Fisher, Florin M. Selaru, and David H. Gracias. Stimuli-responsive theragrippers for chemomechanical controlled release. *Angewandte Chemie*, 126(31):8183–8187, 2014.

[20] Qi Ge, Amir Hosein Sakhaei, Howon Lee, Conner K. Dunn, Nicholas X. Fang, and Martin L. Dunn. Multimaterial 4d printing with tailorable shape memory polymers. *Scientific Reports*, 6(1), 2016.

[21] Hongqiu Wei, Qiwei Zhang, Yongtao Yao, Liwu Liu, Yanju Liu, and Jinsong Leng. Direct-write fabrication of 4d active shape-changing structures based on a shape memory polymer and its nanocomposite. *ACS Applied Materials & amp; Interfaces*, 9(1):876–883, 2016.

[22] Robert J. Morrison, Scott J. Hollister, Matthew F. Niedner, Maryam Ghadimi Mahani, Albert H. Park, Deepak K. Mehta, Richard G. Ohye, and Glenn E. Green. Mitigation of tracheobronchomalacia with 3d-printed personalized medical devices in pediatric patients. *Science Translational Medicine*, 7(285), 2015.

[23] Shida Miao, Haitao Cui, Margaret Nowicki, Lang Xia, Xuan Zhou, Se-Jun Lee, Wei Zhu, Kausik Sarkar, Zhiyong Zhang, Lijie Grace Zhang, and et al. 4d bioprinting: Stereolithographic 4d bioprinting of multiresponsive architectures for neural engineering (adv. biosys. 9/2018). *Advanced Biosystems*, 2(9):1870081, 2018.

[24] Shida Miao, Wei Zhu, Nathan J. Castro, Margaret Nowicki, Xuan Zhou, Haitao Cui, John P. Fisher, and Lijie Grace Zhang. 4d printing smart biomedical scaffolds with novel soybean oil epoxidized acrylate. *Scientific Reports*, 6(1), 2016.

[25] Shunsuke Yamamura and Eiji Iwase. Hybrid hinge structure with elastic hinge on self-folding of 4d printing using a fused deposition modeling 3d printer. *Materials & Design*, 203:109605, 2021.

[26] Aslan Miriyev, Kenneth Stack, and Hod Lipson. Soft material for soft actuators. *Nature Communications*, 8(1), 2017.

[27] Qi Ge, H. Jerry Qi, and Martin L. Dunn. Active materials by four-dimension printing. *Applied Physics Letters*, 103(13):131901, 2013.

[28] Jheng-Wun Su, Xiang Tao, Heng Deng, Cheng Zhang, Shan Jiang, Yuyi Lin, and Jian Lin. 4d printing of a self-morphing polymer driven by a swellable guest medium. *Soft Matter*, 14(5):765–772, 2018.

[29] Skylar Tibbits, Carrie McKnelly, Carlos Olguin, Daniel Dikovsky, and Shai Hirsch. 4d printing and universal transformation. *Proceedings of the 34th Annual Conference of the Association for Computer Aided Design in Architecture (ACADIA)*, 2014.

[30] Yiqi Mao, Kai Yu, Michael S. Isakov, Jiangtao Wu, Martin L. Dunn, and H. Jerry Qi. Sequential self-folding structures by 3d printed digital shape memory polymers. *Scientific Reports*, 5(1), 2015.

[31] Ying Liu, Brandi Shaw, Michael D. Dickey, and Jan Genzer. Sequential self-folding of polymer sheets. *Science Advances*, 3(3), 2017.

[32] Joanne Teoh, Jia An, Xiaofan Feng, Yue Zhao, Chee Chua, and Yong Liu. Design and 4d printing of cross-folded origami structures: A preliminary investigation. *Materials*, 11(3):376, 2018.

[33] Quan Zhang, Kai Zhang, and Gengkai Hu. Smart three-dimensional lightweight structure triggered from a thin composite sheet via 3d printing technique. *Scientific Reports*, 6(1), 2016.

[34] Jiangtao Wu, Zeang Zhao, Xiao Kuang, Craig M Hamel, Daining Fang, and H Jerry Qi. Reversible shape change structures by grayscale pattern 4d printing. *Multifunctional Materials*, 1(1):015002, 2018.

[35] H. M. Herath, J. A. Epaarachchi, M. M. Islam, and J. Leng. Carbon fibre reinforced shape memory polymer composites for deployable space habitats. *Engineer: Journal of the Institution of Engineers, Sri Lanka*, 52(1):1, 2019.

[36] Fengfeng Li, Liwu Liu, Xin Lan, Xiaojun Zhou, Wenfeng Bian, Yanju Liu, and Jinsong Leng. Preliminary design and analysis of a cubic deployable support structure based on shape memory polymer composite. *International Journal of Smart and Nano Materials*, 7(2):106–118, 2016.

[37] Tian Chen and Kristina Shea. An autonomous programmable actuator and shape reconfigurable structures using bistability and shape memory polymers. *3D Printing and Additive Manufacturing*, 5(2):91–101, 2018.

[38] Ayesha Kausar, Ishaq Ahmad, M. H. Eisa, Malik Maaza, and Hamdullah Khan. Manufacturing strategies for graphene derivative nanocomposites—current status and fruitions. *Nanomanufacturing*, 3(1):1–19, 2023.

[39] Anna Bellini, Selc¸uk Gu¨c¸eri, and Maurizio Bertoldi. Liquefier dynamics in fused deposition. *Journal of Manufacturing Science and Engineering*, 126(2):237–246, 2004.

[40] Dynisco. Lmi4000. Accessed in May 2023. Available at https://www.dynisco.com/polymer-evaluation/polymer-evaluation-legacy-products/legacy-melt-flow-indexers/LMI4000.

[41] Rupinder Singh, Ranvijay Kumar, and Inderpreet Singh Ahuja. Thermal analysis for joining of dissimilar polymeric materials through friction stir welding. *Reference Module in Materials Science and Materials Engineering*, 2017.

[42] MatWeb - The Online Materials Information Resource. Accessed in May 2023. Available at https://www.matweb.com/search/DataSheet.aspx?MatGUID=ab96a4c0655c4018a8785ac4031b9278&ckck=1.

[43] Dong Xie, Yang Zhao, Yuan Li, Anna Marie LaChance, Jinqing Lai, Luyi Sun, and Junjia Chen. Rheological, thermal, and degradation properties of pla/ppg blends. *Materials*, 12(21):3519, 2019.

[44] Teledyne FLIR LLC. Flir e4.

[45] IMEB Inc. Olympus bx61 microscope (refurbished), Jun 2023. Accessed in June 2023. Available at https://www.imebinc.com/product/olympus-bx61-microscope/.

[46] Josef Prusa. Original prusa i3 mk3s+ 3d printer kit: Original prusa 3d printers. Accessed in June 2023. Available at https://www.prusa3d.com/product/original-prusa-i3-mk3s-3d-printer-kit/.

[47] Joamin Gonzalez-Gutierrez, Santiago Cano, Stephan Schuschnigg, Christian Kukla, Janak Sapkota, and Clemens Holzer. Additive manufacturing of metallic and ceramic components by the material extrusion of highly-filled polymers: A review and future perspectives. *Materials*, 11(5):840, 2018.

[48] Global internal displacement database. Accessed in February 2023. Available at https://www.internal-displacement.org/database/displacement-data,.

[49] S. Krishnan and Y. Liao. *"Integrating Shelter Design and Disaster Education in Architectural Curriculum"*. in 126th Annual Conference and Exposition - American Society for Engineering Education, 2019.

[50] A. Bashawri, S. Garrity, and K. Moodley. "an overview of the design of disaster relief shelters". in 4th International Conference on Building Resilience, Salford Quays, 2014.

[51] N. D. Temmerman and L. A. Mira. Deployable scissor arch for transitional shelters. *Automation in Construction*, 2014.

[52] Wohlers, Terry, and Tim Gornet. History of additive manufacturing. *Wohlers Report 2014*, 2014.

[53] Joamin Gonzalez-Gutierrez, Santiago Cano, Stephan Schuschnigg, Christian Kukla, Janak Sapkota, and Clemens Holzer. Additive manufacturing of metallic and ceramic components by the material extrusion of highly-filled polymers: A review and future perspectives. *Materials*, 11(5):840, 2018.

[54] Manufacturing Guide. Stereolithography, sla. Accessed in April 2023. Available at https://www.manufacturingguide.com/en/stereolithography-sla.

[55] MakerVerse. Laser powder bed fusion (l-pbf). Accessed in April 2023. Available at https://www.makerverse.ai/technologies-lpbf.

[56] Ben Redwood. What is dimensional accuracy in 3d printing and how do you achieve it? Accessed in April 2023. Available at https://www.hubs.com/knowledge-base/dimensional-accuracy-3d-printed-parts/#variables.

[57] Skylar Tibbits. "the emergence of "4d printing". TED conference, 2013.

[58] Farhang Momeni, Seyed M.Mehdi Hassani.N, Xun Liu, and Jun Ni. A review of 4d printing. *Materials & amp; Design*, 122:42–79, 2017.

[59] Xiaozhou Xin, Liwu Liu, Yanju Liu, and Jinsong Leng. Mechanical models, structures, and applications of shape-memory polymers and their composites. *Acta Mechanica Solida Sinica*, 32(5):535–565, 2019.

[60] Patrick T. Mather, Xiaofan Luo, and Ingrid A. Rousseau. Shape memory polymer research. *Annual Review of Materials Research*, 39(1):445–471, 2009.

[61] Carlos Alejandro Garcia Rosales, Hoejin Kim, Mario F. Garcia Duarte, Luis Chavez, Mariana Castañeda, Tzu-Liang Bill Tseng, and Yirong Lin. Characterization of shape memory polymer parts fabricated using material extrusion 3d printing technique. *Rapid Prototyping Journal*, 25(2):322–331, 2019.

[62] Shuai Liu and Qing-Sheng Yang. Finite element analysis of shape-memory polymer mast. *International Journal of Smart and Nano Materials*, 10(4):285–299, 2019.

[63] Yonglin Chen, Junming Zhang, Zefu Li, Huliang Zhang, Jiping Chen, Weidong Yang, Tao Yu, Weiping Liu, and Yan Li. Manufacturing technology of lightweight fiber-reinforced composite structures in aerospace: Current situation and toward intellectualization. *Aerospace*, 10(3):206, 2023.

[64] Helena N Chia and Benjamin M Wu. Recent advances in 3d printing of biomaterials. *Journal of Biological Engineering*, 9(1), 2015.

[65] Ferry P.W. Melchels, Marco A.N. Domingos, Travis J. Klein, Jos Malda, Paulo J. Bartolo, and Dietmar W. Hutmacher. Additive manufacturing of tissues and organs. *Progress in Polymer Science*, 37(8):1079–1104, 2012.

[66] Saeed Fathi, Phill Dickens, Khosrow Khodabakhshi, and Marianne Gilbert. Microcrystal particles behaviour in inkjet printing of reactive nylon materials. *Journal of Manufacturing Science and Engineering*, 135(1), 2013.

[67] Evren Yasa and Kıvılcım Ersoy. Additive manufacturing of polymer matrix composites. *Aircraft Technology*, 2018.

[68] Roger I. Tanner. A theory of die-swell revisited. *Journal of Non-Newtonian Fluid Mechanics*, 129(2):85–87, 2005.

[69] Ryszard Steller. Determination of the first normal stress difference from viscometric data for shear flows of polymer liquids. *Rheologica Acta*, 55(8):649–656, 2016.

[70] Guilong Wang, Dongmei Zhang, Gengping Wan, Bo Li, and Guoqun Zhao. Glass fiber reinforced pla composite with enhanced mechanical properties, thermal behavior, and foaming ability. *Polymer*, 181:121803, 2019.

[71] AIP Precision Machining. Understanding heat deflection temperature (hdt) of plastics, Jun 2021. Accessed in May 2023. Available at https://aipprecision.com/understanding-heat-deflection-temperature-plastics/.

[72] Mr. Gaurav Malhotra. Uses of mfi test method in plastic industries. Accessed in May 2023. Available at https://www.prestogroup.com/blog/uses-of-mfi-test-method-in-plastic-industries/.

[73] Amina Sarfraz, Asif Hassan Raza, Mojtaba Mirzaeian, Qaisar Abbas, and Rizwan Raza. Electrode materials for fuel cells. *Encyclopedia of Smart Materials*, page 341–356, 2022.

[74] ELTRA. Thermogravimetric analyzer tga thermostep. Accessed in May 2023. Available at https://www.eltra.com/products/thermogravimetric-analyzers/tga-thermostep/.

[75] A. W. Coats and J. P. Redfern. Thermogravimetric analysis. a review. *The Analyst*, 88(1053):906, 1963.

[76] Lu Cui, Lan Yi, Yating Wang, Yunchong Zhang, Péter Polyák, Xiaofeng Sui, and Béla Pukánszky. Rheology of pla/regenerated cellulose nanocomposites prepared by the pickering emulsion process: Network formation and modeling. *Materials & Design*, 206:109774, 2021.

[77] İbrahim Savaş DALMIŞ, Ümit GÜLER, Alper KARAKOCA, and Sait Özmen ERUSLU. An experimental and theoritical study on the pressure drop of fluid at extrusion process. *EJOVOC Electronic Journal of Vocational Colleges*, 5(4):70, 2015.

[78] Nor Aiman Sukindar, M. K. Ariffin, B. T. Baharudin, Che Nor Jaafar, and Mohd Idris Ismail. Analyzing the effect of nozzle diameter in fused deposition modeling for extruding polylactic acid using open source 3d printing. *Jurnal Teknologi*, 78(10), 2016.

[79] OMEGA Engineering inc. Accessed in May 2023. Available at https://www.omega.co.uk/prodinfo/pid-controllers.html.

[80] OMEGA Engineering inc. Accessed in May 2023. Available at https://www.omega.co.uk/prodinfo/how-does-a-pid-controller-work.html.

[81] Automation Direct. Pid autotuning. Accessed in May 2023. Available at https://www.automationdirect.com/microsites/clickplcs/click-help/Content/247.htm.

Appendix A

Smartfil PLA Technical Data Sheet

Physical Properties	Typical Value	Test Method
Material Density	1,24 g/cm^3	ISO 1183
Chemical Name	Polylactic Acid	

Mechanical Properties	Typical Value	Test Method
Tensile Strength	MD 110 MPa	ASTM D882
	TD 114 MPa	ASTM D882
Tensile Modulus	MD 3309 MPa	ASTM D882
	TD 3861 MPa	ASTM D882
Elongation at Break	MD 160%	ASTM D882
	TD 100%	ASTM D882
Elmendorf Tear	MD 15 g/ml	ASTM D1922
	TD 13 g/ml	ASTM D1922

Thermal Properties	Typical Value	Test Method
Heat Deflection Temperature B	65 ºC	ASTM D1505
Vicat Softering Temperature	85º C	ASTM D1525

Printing Properties	Typical Value
Print Temperature	220±20 ºC
Hot Pad	0-60 ºC
Fan Layer	On (100%)

Size	Net W.	Gross W.	Diameters	Packaging Characteristics
S	330 g	348 g	1'75 mm	SmartBag, security seal
M	750 g	975 g	1'75 / 2'85 mm	SmartBag, security seal
L	1000 g	1256 g	1'75 / 2'85 mm	SmartBag, security seal
XL[1]	3300 g	3864 g	1'75 / 2'85 mm	SmartBag, security seal
XXL[1]	5600 g	6346g	1'75 / 2'85 mm	SmartBag, security seal
XXXL[1]	8000 g	8746 g	1'75 / 2'85 mm	SmartBag, security seal

(1)XL, XX and XXL son fabricados bajo demanda. Plazo de entrega entre 1 y 5 semanas.
XL, XX and XXL spools are made under order. Delivered term between 1 and 5 weeks.

Colores Disponibles / Available Colours

Color	Name	Colour
Natural	Natural	Natural
Blanco	Ivory White	White
Negro	True Black	Black
Amarillo	Orinoco	Yellow
Naranja	Sunset	Oranje
Coral	Coral	Coral
Rojo	Ruby	Red
Brilla en la Oscuridad	Smart Glow	Glows in the Dark
Marrón	Mahogany	Brown
Verde	Chlorophyll	Green 1
Verde 2	Emerald	Green 2
Verde 3	Jade	Green 3
Verde 4	Olive	Green 4
Azul 1	Sapphire	Blue 1
Azul 2	Cobalt	Blue 2
Fluor Yellow	Neo Yellow	Fluor Yellow
Violeta 1	Wisteria	Violet 1
Violeta 2	Aubergine	Violet 2
Rosa	Hillier Lake	Pink
Gris	Antracite	Grey
Dorado	Gold	Gold
Plateado	Silver	Silver
Cambio de Color	Mix	Colour Transition
Rosa Fluor	Neo Pink	Fluor Pink

Appendix B

Teijin Tenax Carbon Fiber Technical Data Sheet

Teijin Tenax® J HTS40 E13 3K 200tex Poly-acrylonitrile Carbon Fiber

Material Notes: HTS40 is a family of high strength/standard modulus aerospace grade carbon fibers made in Japan (E13- sized products) and Germany (F13-sized product) for use as reinforcement in high performance composites. These fibers are produced from poly-acrylonitrile (PAN) precursor and are surface treated to promote adhesion to organic matrix polymers. Sizing materials are designed to aid in handling. The -J HTS40 E13 3K/6K and the -E HTS40 F13 12K fibers have been qualified to the NMS 818 dry fiber specification. This allows manufacturers to call out an industry standard, PCD-controlled, aerospace-grade carbon fiber without the expense of writing and maintaining their own in-house specifications. Information provided by Teijin Carbon America, Inc

Physical Properties	Metric	English	Comments
Density	1.77 g/cc	0.0639 lb/in³	
Filament Diameter	7.0 µm	7.0 µm	

Mechanical Properties	Metric	English	Comments
Tensile Strength	4400 MPa	638000 psi	
Elongation at Break	1.9 %	1.9 %	SACMA SRM16
Tensile Modulus	230 GPa	33400 ksi	SACMA SRM16

Descriptive Properties			
Density		203 tex	Linear density without sizing
Sizing level (%)		1.3	

Appendix C

Experimental diameter and mass measurements

Die diameter [mm]		First Installation iteration				
		Filament Diameter [mm] at x length				Filament mass [g]
		x=5	x=10	x=15	x=20	
2	sample 1	1.46	1.37	1.34	1.42	0.2945
	sample 2	1.22	1.29	1.41	1.51	0.2401
	sample 3	1.41	1.51	1.39	1.43	0.2734
4	sample 1	2.55	2.62	2.44	2.57	0.5689
	sample 2	2.50	2.39	2.48	2.54	0.5667
	sample 3	2.32	2.47	2.56	2.55	0.5688
	Second installation iteration					
4	sample 1	2.56	2.50	2.46	2.49	0.5682
	sample 2	2.48	2.52	2.51	2.50	0.5685
	sample 3	2.51	2.52	2.48	2.53	0.5687